3D Display System Using Scanning LED Array Modules

by

Murat Sayınta

A Thesis Submitted to the
Graduate School of Engineering
in Partial Fulfillment of the Requirements for
the Degree of

Master of Science
In
Electrical & Computer Engineering

Koç University

July, 2008

Koc University

Graduate School of Sciences and Engineering

This is to certify that I have examined this copy of a master's thesis by

Murat Sayinta

and have found that it is complete and satisfactory in all respects,
and that any and all revisions required by the final
examining committee have been made.

Committee Members:

_____

Hakan Urey, Assoc. Prof (Advisor)

_____

Murat Tekalp, Prof. Dr.

_____

Arda Yalcinkaya, Asst. Prof..

Date: 10.07.2008

ABSTRACT

3D displays seem to be the next step in the evolution of displays from monochrome to color and high definition displays in the era of "digital revolution" and leading to the ultimate display that can create perfect illusion of reality that cannot be separated from its true copy. In this research, a novel three-dimensional (3D) display concept is introduced and various aspects of the system design are studied. The 3D display method is based on creating multiple light emission directions from each screen pixel using 2D array of scanning LED modules behind a diffuser screen. The resultant image source points appear to emanate from virtual points in 3D space. The system architecture is scalable and higher resolution displays can be easily generated by increasing the number of scanning modules. The display provides a possibility of solving or relieving the accommodation-vergence rivalry which is the major problem with today's conventional auto-stereoscopic display technologies when multiple views can be provided to each eye pupil.

The main building block of the modular display is a printed-circuit-board (PCB) based scanner that carries 1D array of LEDs and imaging lens on the scanning platform. A unique feature of the system is the integration of LEDs with PCB electronics and magnetic actuation directly on the scan modules. The scan modules are fabricated using the low-cost standard PCB fabrication techniques and can achieve large rotation angles to address large number of screen pixel positions. Using LEDs is quite advantageous as they are available at various pitch sizes, colors and have high light efficiency. Proof-of-concept experimental demonstrations using few modules and custom LED drive electronics are discussed.

Keywords: 3D displays, quasi-holographic displays, electromagnetic actuation, polymer scanners, LED arrays, LED Drivers

ÖZET

Üç Boyutlu (3D) Ekranlar, renksiz ekranlardan günümüzde yaşanmakta olan“dijital devrim” çağında renkli ve yüksek çözünürlüklü (HD) ekranlara varmış olan ekranların evrimleşme sürecinin bir sonraki adımını oluşturacak ve gerçeğinden ayırt edilemeyecek kadar mükemmel bir görüntü yaratacak ekranlara doğru giden yolda öncülük edecek gibi gözükmektedir. Bu tez çalışmasında, yeni bir üç boyutlu ekran tanıtılmakta ve ilgili sistem tasarımı çeşitli boyutları ile incelenmektedir. Bu yeni üç boyutlu ekranın temel prensibi, gelen ışığı yayabilen bir ekranın arkasına iki boyutlu bir dizi halinde yerleştirilmiş olan tarayıcı LED modülleri kullanarak, ekranın her bir pikselinden birbirinden bağımsız olarak kontrol edilebilir birden çok ışık yayılım yönü yaratılması üzerine kurulmuştur. Görüntüyü oluşturan noktalar, göz tarafından üç boyutlu uzay içinde bulunan zahiri noktalardan ışık yayıyormuş gibi algılanır. Sistem mimarisi ölçeklenebilirdir ve tarayan modüllerin sayısının arttırılmasıyla daha yüksek çözünürlüklü ekranlar kolayca elde edilebilir. Tek bir göze birden fazla görüntü göndermek şartıyla, bu üç boyutlu ekran, günümüzün oto-stereoskopik ekranların temel problemi olan akomodasyon ile verjans arasındaki uyumsuzluğu giderebilme ihtimali sunmaktadır.

Modüler ekranın ana elemanı baskı devre yapımında kullanılan temel malzeme olan FR4’dan yapılan, üzerinde tek boyutlu LED dizisi ile görüntüleme lensi taşıyan tarayıcı modüllerdir. Sistemin özgül özelliği LED dizisinin, baskı devre elektroniği ve elektromanyetik tahrikleme ile birlikte direkt olarak tarayıcı platformun üzerinde entegrasyonudur. Tarayıcı modülleri düşük maliyetli standart baskı devre üretim tekniği ile üretilmişlerdir ve bu tarayıcılar kullanılarak yüksek sayıda piksel adreslemek için gerekli geniş dönme açıları elde edebilir. LED’leri kullanmak, çok çeşitli renklerde, büyüklüklerde bulunabildiklerinden ve yüksek ışık verimine sahip olduklarından çok avantajlıdır. Çalışma

prensibini ispatlayan, birkaç modül kullanılarak yapılan deneysel gösterimler ve bu sistem için geliştirilmiş olan LED sürme elektroniği de bu çalışmada tartışılmaktadır.

Anahtar kelimeler: Üç boyutlu ekranlar, holografiye benzeyen üç boyutlu ekranlar, elektromanyetik tahrikleme, polimer tarayıcılar, LED dizileri, LED sürücüleri

ACKNOWLEDGEMENT

First of all, I would like to express my utmost gratitude to my advisor Dr. Hakan Ürey for his continuous support throughout my research. His broad vision of technology, excitement and ingenuity in developing novel ideas and especially his trust and encouragement made me feel the same excitement, be motivated and have fun during this period.

I also would like to sincerely thank Prof. Murat Tekalp and Prof. Arda Yalçınkaya for kindly taking part in my thesis committee.

I acknowledge 3DTV NoE and the Network of Excellence in Micro-Optics (NEMO) for supporting this project. I also acknowledge OSRAM for providing the LEDs that are used in preparation of the sample devices.

I would like to thank all my colleagues in OML. It was a great chance to have the same habit of working at night in the laboratory with Çağlar Ataman. I am grateful to him for his invaluable help in many steps of my research. I would like to thank Sven Holmstrom for those long and enjoyable hours spent together in the clean room with the same fear of HF. Many thanks go to Serhan Isikman for his help in the FR4 mechanical designs. Special thanks to Onur Ferhanoğlu who was my constant mate to study for the exams. I would also like to thank Fatih Toy for his helpful ideas for every kind of problem and question I was confronted with.

I sincerely thank my managers in Vestek Electronics for their patience, support and understanding. They always gave me time whenever I needed to focus on my thesis. I would especially like to thank Ali Sayinta, as both my manager and brother for his invaluable help, support and wisdom in all aspects of my life.

I also thank to my friends Necmiye Genç from Vestek Electronics, Serbulent Aydinoglu and Sercan Kibar from Vestel Defense & Security for their help with LED driving circuitry

design and integration. Many thanks go to Engin Ufuk Temoçin from Aselsan Inc. for his help with wire bonding.

Last but not least, I thank my mom, my dad, my sister and Tuğba for always being there when I needed them most, and for supporting and encouraging me through all these years. None of these would be possible without you.

TABLE OF CONTENTS

LIST OF TABLES

LIST OF FIGURES

Chapter 1 INTRODUCTION

3D displays seem to be the next step in the evolution of displays from monochrome to color and high definition displays in the era of "digital revolution" and the sine qua non leading to the ultimate goal of creating perfect illusion of reality that cannot be separated from its true copy. The vital deficiencies of today's 2D displays stem from expressing the real world on a 2D plane without taking into consideration the fact that human beings experience their environment through two eyes. However, with the incredible developments in the digital video processing and visualizing technologies, first commercial 3D display products are already available in the market to overcome the deficiencies of current 2D Displays. Today, with quickly increasing interest and investment from industry, the impact of 3D display systems will be available in many application areas from computer-aided design (e.g. car interior design) to data visualization (e.g. molecular modeling) and from medical systems to entertainment (e.g. computer games).

1.1 Main Contributions of the Thesis

This thesis mainly introduces a novel 3D display system using array of LEDs mounted on rotating scanner modules, trying to solve some major problems of auto stereoscopic displays. The main contributions of this thesis are:

- Conception and design of a novel 3D display system architecture
- Developed specifications for the display system,
- Designed FR4 scanner modules housing LEDs and the LED driver circuitry

- Designed optical system and performed numerical simulations to validate performance
- Demonstrated proof-of-concept sub-system using 2-scanning modules with integrated LEDs.
- Presented 2 conference papers, submitted one journal paper to IEEE J. Displays (under review, see Appendix A), second journal paper is in preparation for OSA journals, and filed one PCT patent application with WPO (see Appendix B)

1.2 Thesis Outline

Section 1.3 gives a brief history of 3D photography up to today's relatively developed 3D display systems. Chapter 2 gives a detailed description of the psychology *and* physiology behind 3D perception together with a general classification of the existing 3D display systems and positioning of the developed 3D display system in the big picture constituted by the classification effort. Chapter 3 focuses on system design of scanning LED array based 3D display and working principles of the system both on system and sub module level. Chapter 4 discusses optical performance analysis of the system including both the imaging and photometric calculations.

1.3 Brief History of Stereoscopy (3D Photography)

It is quite surprising to learn that the idea of stereoscopy – 3D photography, actually preceded the idea of photography and the history of 3D visualization is as old as its 2D counterpart. People have been aware of binocular disparity since Ancient Greeks. Euclid at about 300 B.C. noted that each eye sees a slightly different image. One of the greatest artists of history, Leonardo Da Vinci was very interested in depth perception and produced many paintings showing a deep understanding of 3D cues such as texture, shading and viewpoint projection. He was also aware of the vital importance of binocular vision in

experiencing reality through the pictures. He stated this clearly in his words: "*that a painting though conducted with the greatest art and finished to the last perfection, both with regard to its contours, its lights, its shadows and its colors, can never show a relief equal to that of natural objects, unless these natural objects be viewed at a distance and with a single eye*" **[1]**, **[2]**. In terms of Euclid's studies, at the beginning of 17th century French physicist Giovanni Battista Della Porta developed an interesting theory and explained the reason behind a single image perception although each eye receives slightly different image from the other one receives as the perception with one eye and then the other one successively **[3]**. He was also able to sketch the first stereoscopic image. However, history of stereoscopy was mostly accepted to start with Charles Wheatstone's presentation of his paper named "*the importance of the binocular vision in the perception of the distance, depth and relief of object in Nature*" in the British Royal Society on the scarcely known phenomenon binocular vision **[1]**. As an application of his presented theories, Wheatstone invented in 1838 a mirror device named "stereoscope" that has enabled the viewer to see the slightly different drawings of the same scene at the same time, resulting in compelling three-dimensional perception **[4]**. The invention of Wheatstone was further improved into more practical apparatus by the contributions of different scientists including Sir David Brewster and as a result the popular Victorian 'parlor stereoscope' has appeared. Viewing of stereoscopic still images of timely subjects, popular people and natural views became a popular pastime in both the U.S. and Europe and Brewster's stereoscope became a commercial success of his time, selling more than 250.000 in a short period. 20th century's greatest artists including Salvador Dali could not stay apart from the popularity of 3-D photographing and produced amazing stereoscopic image pairs.

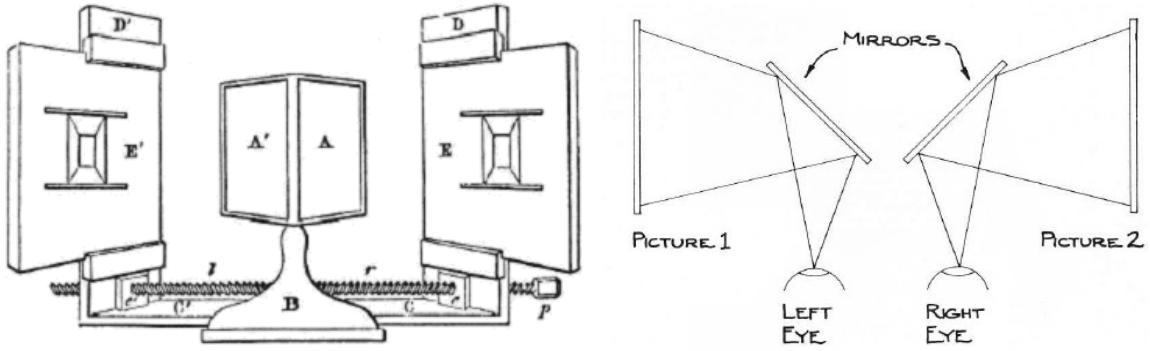

Figure 1-1 The mirror device stereoscope developed by Charles Wheatstone

Advent of motion pictures decreased the popularity of stereoscopy for a while but stereoscopic cinema and television concepts were already present at the first appearance of their monoscopic counterparts. The first full length 3D film "The Power of Love" was shown to a large group of audiences in 1922 **[5]**.

In spite of these early successes of 3D cinema, Hollywood tried to launch 3D cinema as the "next big step in cinema history" only after 1950s because of economical reasons rather than artistic, to protect the popularity of cinema against the new emerging technology, television **[5]**. The great success of 3D featured film "*Bwana Devil*" in 1952 ignited a 3D craze and between 1952 and 1954, more than sixty five 3D feature films including famous films such as Alfred Hitchcock's "*Dial M for Murder*" were produced by Hollywood. However, after this overwhelming start, 3D cinema could not fulfill the great expectations because of photographic inexperience with the new emerging technology, inadequate quality control in the laboratories and unsuccessfully operated projection systems in theaters together with the headaches, eyestrain caused after a few hours of 3D experience **[4]**.

This negative reputation of stereoscopy could not discourage the television industry from paying attention in 3D Technologies. Both in U.S. and Europe there have been successful and unsuccessful 3D stereoscopic broadcasting attempts **[6]**.

With the fast developments both in 3D software and hardware technologies, the dream of 3D displays seem to be realized in the following decade. Stereoscopy already has been utilized in many application areas from computer-aided design (e.g. car interior design) to data visualization (e.g. molecular modeling) and from medical systems to entertainment (e.g. computer games).

Chapter 2 3D VISION AND 3D DISPLAYS

2.1 3D Perception Psychology and Physiology

Human beings perceive the world in three dimensions (3D), although the inputs to the visual system are only two-dimensional retinal images. The visual system infers the depth information from a variety of visual sources of information - cues in these two-dimensional images. These visual cues are generally grouped into two categories as 'monocular' cues and 'binocular' cues **[7]**, **[8]**.

2.1.1 Monocular (Pictorial) Cues

Monocular cues are obtained from just a single retinal image. The effectiveness of monocular cues can be realized by the considerable depth perceived with a single eye. The pictures depicting four of the monocular cues:

- *Interposition (Occlusion)*: Occlusion of objects by some other objects leads to depth perception as occluded objects are perceived further than the occluding objects as illustrated in Figure 2-1(a). This monocular cue is a weak one as it provides only 'a depth ordering' between different objects but no information about actual distances of the objects **[8]**, **[9]**.
- *Aerial (Atmospheric) Perspective*: Light is scattered as it travels long distances in the atmosphere due to different reasons such as fog, rain and particles. As a result of the scattering, colors loose saturation, contrast of the objects decrease, sharp edges

are softened and color hue is shifted towards blue as blue color having a shorter wavelength can penetrate more than the other visible colors **[9]**, **[10]**.

- *Linear Perspective*: Parallel lines, such as railroad tracks converge as the lines go further away from the observer as depicted in Figure 2-1(b). At infinity the lines meet on a 'vanishing point'. In the same way, objects become smaller as they move away. The link between size and perceived depth stems from the fact that the retinal image size decreases with the increasing distance from the observer's position **[7]**, **[9]**.
- *Texture Gradients*: Fineness of detail or 'texture' decreases gradually with the increasing distance from the observer as shown in Figure 2-1(c). In other words, texture gradient is a surface pattern that gives information to the visual system about the distance and shape of objects. Texture is more dense and smaller in a distant object than a closer object. A sharp change in texture implies an instant variation in depth **[11]**.
- *Shading and Shadowing*: Light amount illuminating surface of an object decreases with the increasing distance from the light source. Hence, objects become darker as they move away from the light source, which provides depth and shape information. As it is biologically assumed that there is only one light source coming from above, when the bottom part of a shape is lighter than the top, the shape is perceived as a concave – holes and when the top part is lighter than the bottom, the shape is perceived as a convex as illustrated in Figure 2-1(d). Shadows cast by one object on another (shadowing) also give cues about relative position and size **[8]**, **[11]**.

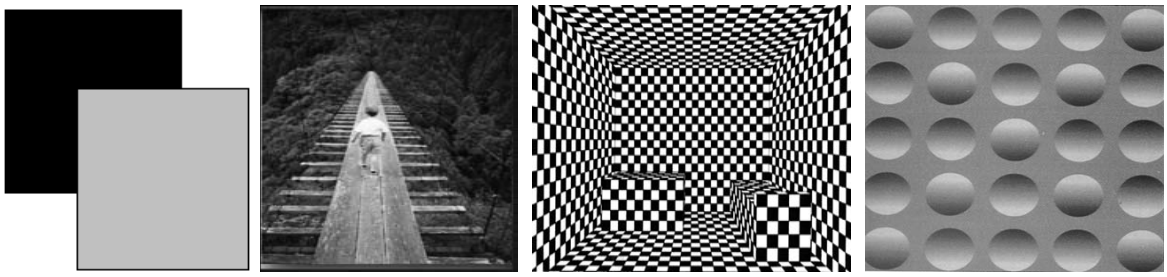

Figure 2-1 Monocular Depth Perception Cues (a) Occlusion. (b) Linear Perspective. (c) Texture Gradient. (d) Shading and Shadowing [6], [9]

- *Motion Parallax*: Motion Parallax is a powerful cue for the visual system. It is simply the position change of an object relative to its stationary background as seen by an observer when either the observer or the object moves. These movements cause motion parallax by which nearby objects change position faster than the distant objects in retinal image which result in depth perception. For instance, the observer moving with a vehicle sees the closer objects passing faster in a blur while distant objects moving slightly **[9]**, **[10]** and **[12]**.

2.1.2 Binocular Cues

Binocular cues are extracted by processing both right and left eye retinal images. As the inter pupilar distance is approximately 6.5 cm apart, the left and right eye retinas have slightly different projections of the same 3D scenery as illustrated in Figure 2-2. This slight difference is called *binocular disparity* and it is easy to notice that closer objects have a larger disparity **[13]**. The visual system infers depth information by processing the binocular disparity and creates the sensation of depth known as stereopsis – solid seeing.

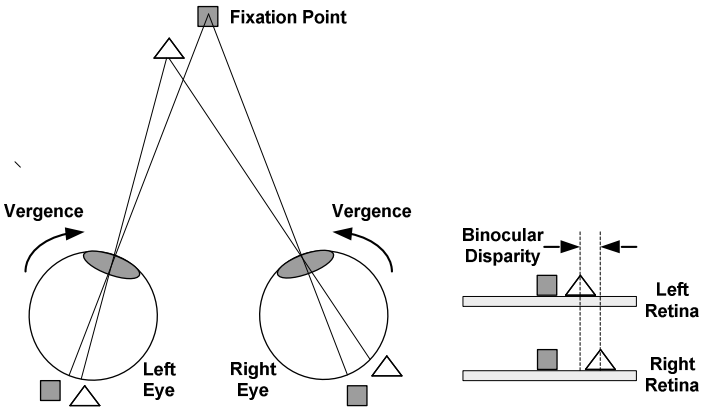

Figure 2-2 Binocular Disparity and Vergence Mechanism [13]

Vergence and accommodation are two physiological mechanisms of the visual system helping it to obtain and process the binocular disparity. Vergence is simply, the inward rotation of the right and left eye to the object of interest and fixates the left and right eye visual axes to a certain point named vergence or fixation point **[9]**, **[13]**. The vergence point is imaged to the same point in left and right eye retinas which means it has no binocular disparity. Accommodation is the focal length adjustment to see the object of interest and objects close to it in focus. Vergence and accommodation mechanisms work synchronously.

Binocular cues provide important advantages to the visual system in depth perception when they are compared with the monocular cues **[7]**, **[9]**:

- The depth information of objects can be inferred directly from binocular disparity
- The capability of focusing on objects placed at a specified depth and ignoring the objects on the other depth levels.
- The camouflaged objects in a scene can be detected more easily which is a probable evolutionary reason behind the development of binocular vision.

2.2 Classification of 3D Displays

It is helpful to classify 3D displays for a better understanding of their development trend. A possible classification can be **[14]**:

- Holographic displays
- Volumetric displays
- Auto stereoscopic displays

The display system developed during this thesis research can be classified as holoform display (quasi-holographic display) under the auto stereoscopic display category which is quite different than the conventional multi view displays. This type of displays is investigated as another sub section. In the following subsections, each type of 3D displays as classified above will be studied.

2.2.1 Holographic Displays

The name holography comes from the Greek words 'holo' & 'graph' and means the complete information. Holography technique was firstly developed by the Hungarian scientist Denis Gabor in 1947 **[15]** and the main advances in the field start with the invention of laser in 1960. Holography Technique is the only technique that can record and reproduce the light waves diffracted by or scattered from a natural object completely as it records both the phase difference and the amplitude information of the waves diffracted by or scattered from the which makes holography a nearly ideal free viewing 3D technique **[16]**, **[17]**. The critical problem with holography is the loss of natural shading existing in the original scene due to laser illumination. The developments in electronic sensor and spatial light modulator technologies helped to realize holography in digital domain where storage and transmission of the holographic data is more likely. A typical hologram recording and reconstruction setup in digital domain can be seen in Figure 2-3.

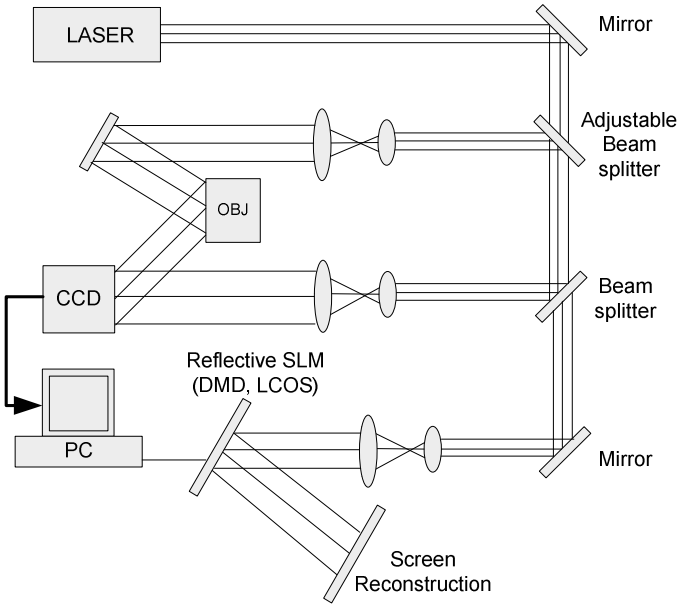

Figure 2-3 A typical setup for digital holography recording and reconstruction using reflective SLM [18]

The recording step of digital holography is quite similar to recording on holographic films. The output of a laser source is first split into two ways by a beam splitter, one for the reference wave and the other one for illuminating the object. The reference beam directly illuminates the CCD with a normal angle to the plane of sensor array and constitutes interference pattern with the wave front scattered and diffracted from the object. The interference pattern is conducted to the SLM as electronic signal and the object is reconstructed by the illumination of the SLM with the reference wave **[18]**, **[19]**. There are some other alternative recording and reconstruction methods such as optical scanning holography (OSH) where the information is recorded by single 2D scanning. It is also possible to obtain only horizontal parallax holograms using OSH techniques to reduce the amount of information a typical hologram carries **[20]**.

However, digital video-based holographic techniques are still in their infancy. An ideal full-color holographic display with large area, full parallax and caption, transmission of the data that would be displayed on such a holographic display require developments in many different branches of technology **[14]**. First of all, there should be dramatic improvements in VLSI and interconnection technologies in order to build multi-million pixel spatial light modulators (SLM) with pixel sizes on the order of 1 μm. Such dramatic improvements could not be realized before a decade period if the "Moore's Law" would still apply **[21]**. Today's available SLM technologies are liquid crystal displays (LCDs), acousto-optic (AOs) displays and digital micro devices (DMDs). The main disadvantage of these technologies is their small space-bandwidth product (SBP – product of the pixel frequency and device dimension). The SBP of current SLMs is one tenth of SBP of a conventional hologram with 3000 line-pair/mm and a size of 20 cm^2. Fabricating SLMs with larger SBP values decreases speckle size in the reconstructed object and enables smaller distances between the SLM and the reconstructed object which results in higher intensity levels at the reconstructed image [12]. Secondly, compact and safe laser sources or LEDs with sufficient coherence and power should be fabricated for each primary wavelength together with a method of color combining such as color mixing or time-division multiplexing for generating high quality colorful holograms **[22]**, **[23]**. The synthesis of computer generated holograms (CGH) fast enough for real time applications with high refresh rates and efficient compression of them for storage and transmission purposes needs developments in video processing technologies **[24]**, **[25]**.

2.2.2 Volumetric Displays

In volumetric displays, images are formed in a physically three-dimensional (3D) volume rather than on a static two-dimensional (2D) display screen. There are light

emitting, scattering or absorbing units – i.e., volume elements (voxels) with specific location in the physical volume of the display **[26]**. Volumetric displays have a variety of approaches which can be divided into two basic groups:

- Real image methods applying static or moving displays
- Virtual image methods applying movable or deformable lenses or mirrors

Moving display type volumetric displays applying the real image methods display the slices of the 3D scenery on a moving display which is sweeping the physical volume of the display. A good commercial example to this type of displays is Perspecta^{TM} developed by Actuality Systems **[27]**. It has a rotating disc rotating at 900 rpm on which 200 2D radial slices of the 3D scenery with resolution of 768 x 768 are projected sequentially at 30 Hz refresh rate. The physical volume of the display is a 20-inch dome as shown in Figure 2-4.

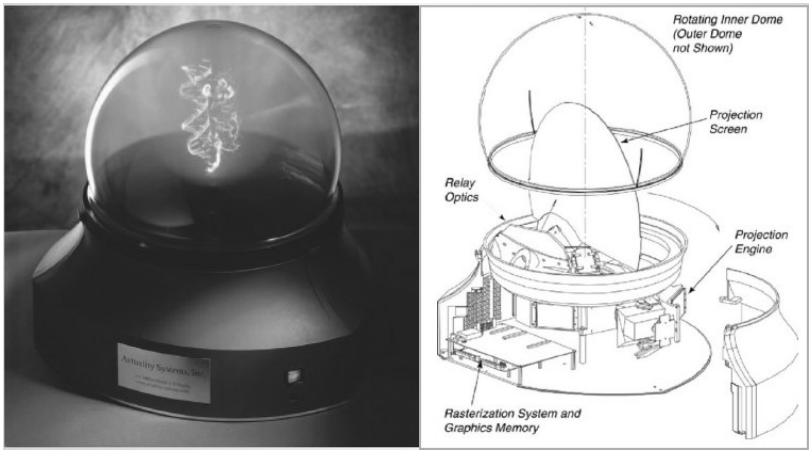

(a) (b)

Figure 2-4 Perspecta Spatial 3D Display [24], [25]

In static display type volumetric displays, 3D scenery is generated on stationary voxels in the physical volume of the display. DepthCube volumetric display developed by Lightspace Technologies is a good example to static display type volumetric displays as

illustrated in Figure 2-5 **[27]**. 2D planar slices of 3D scenery are projected into a multi-planar optical element successively by a high speed digital projector. Each planar optical element can be either in transparent or light scattering state **[26]**. The planar optical element which the projector will project on the corresponding 2D image slice is updated into light scattering state, while all the other planar optical elements are updated into transparent state.

In virtual image methods, mirrors or lenses with varying focal lengths are used to generate images at different depth levels corresponding to the slices of the 3D scenery. An earliest volumetric display example applying the virtual image method uses a mirror with a varying focal length to display images at different depth levels. A method like this, changing the curvature of the mirror to change the image depth needs smaller movements than a moving display realizing the same effect **[26]**.

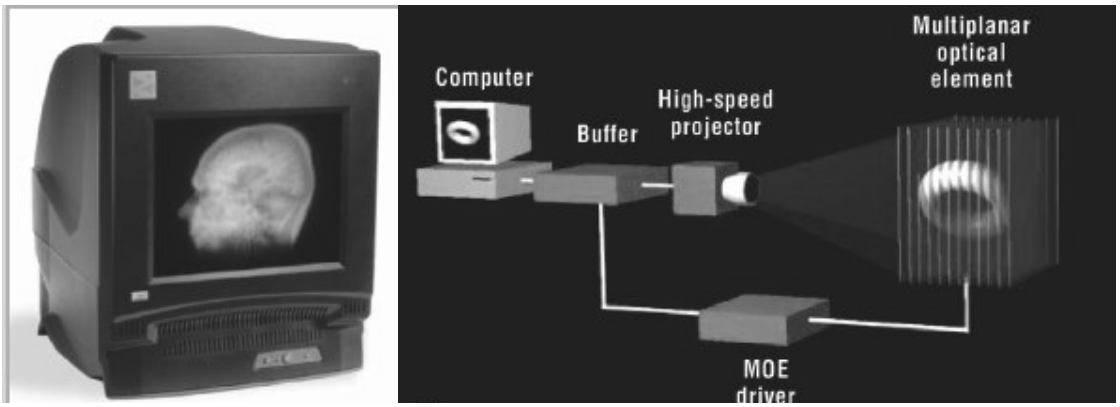

(a) (b)

Figure 2-5 Depth Cube Volumetric 3D Display by Lightspace Technologies [26], [28]

The volumetric displays naturally provide the depth cues such as binocular disparity, motion parallax and accommodation-vergence synchronism **[28]**. Many of them provide unrestricted viewing position. The volumetric displays have the vital drawback of

transparency. It means that objects that should be behind some other objects, are not occluded by the front object and seen by the viewer which cause a confliction in viewer's 3D perception. Another drawback with volumetric displays is their incapability of displaying surfaces having non-Lambertian intensity distributions resulting in unnatural images. Another difficulty with volumetric displays arises in building up large scale displays **[14]**, **[26]**, and **[29]**.

2.2.3 Auto-stereoscopic 3D Displays

The term "auto-stereoscopy" is used for type of 3D displays which does not need any viewing aid like special glasses to view in 3D. Although holographic and volumetric 3D displays are also auto-stereoscopic displays by definition, this term is used for a specific group of 3D displays which provide two or multiple numbers of 2D discrete views side by side in the FOV of the display. These displays can be categorized as **[14]**, **[30]**:

- Two view – binocular displays which only provides single stereo image pair
- Multiple view displays which provide more than two discrete views in FOV
- Holoform displays which provide high number of discrete views enough to constitute hologram like appearance with smoother motion parallax and better accommodation-convergence synchrony.

Binocular displays are the simplest auto-stereoscopic displays and provide single image pair by using various technologies such as cylindrical lenses – lenticular sheet, parallax barrier or holographic optical elements **[31]**, **[32]** and **[33]**. Parallax barrier technology is probably the oldest known auto-stereoscopic display technique which is simply a vertical, periodical slit array placed in front of the display **[31]**, **[32]**. For binocular displays, there is a slit in front of each pair of vertical pixel stripes and by properly aligning the slits, one of the vertical pixel stripe is perceived by the left eye while the other one is perceived by the

right eye. In displays with lenticular sheets, cylindrical lenses are placed vertically similar to the parallax barrier or with slight inclination (slanted lenticular sheet) onto the focal plane of the LCD display pixels **[34]**. Similar to binocular displays with parallax barrier, a single cylindrical lens covers a pair of vertical pixel stripes. The pitch of each cylindrical lens or the distance between adjacent slits is slightly smaller than the pitch of the vertical pixel stripe pair and the amount of the slight difference determines the distance to the display of the optimum viewing zones.

The stereo image pair are formed on fixed viewing zones that repeat within the FOV of the display as illustrated in Figure 2-6(a) and the viewer should place his/her head to the right position to view the 3D stereo image pair. However, if the viewer places his/her head to wrong zones (e.g. his left eye to the right eye zone and right eye to the left eye zone stemming from repeating zones), the viewer will see pseudoscopic images as shown in Figure 2-6(a) resulting in eye discomfort **[30]**. By using head tracking systems the position of the stereo image pair can be changed according to the viewer's position in the FOV in order to prevent viewer from placing his/her head to wrong position.

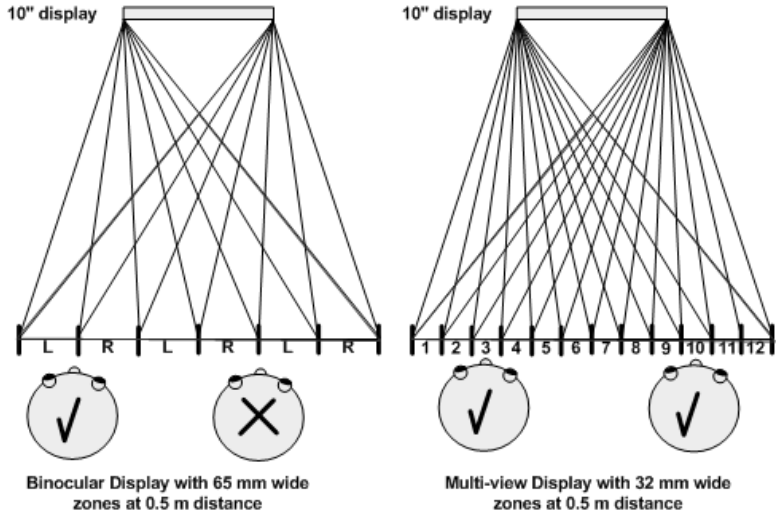

Figure 2-6 Binocular and Multi view Auto-stereoscopic displays

Increasing the number of views is another solution to the viewing position rigidness of the binocular displays. In multiple view displays more than two discrete views are displayed across the FOV and the viewer is free to place his/her head anywhere within the FOV as described in Figure 2-6(b). Multiple view displays use 3D generation methods similar to that of binocular displays such as lenticular sheet, parallax barrier or holographic optical elements **[30]**, **[31]** and **[32]**. The difference stems from the pitch of the cylindrical lenses or the distance between slits on the parallax barrier. The number of display pixels behind a single vertical cylindrical lens or vertical slit specifies the number of multi views as illustrated in Figure 2-7. The slightly smaller pitch of a vertical lens or vertical slit than the total width of the LCD pixel array the lens is covering specify the optimum distance of the viewing zones similar to the binocular displays.

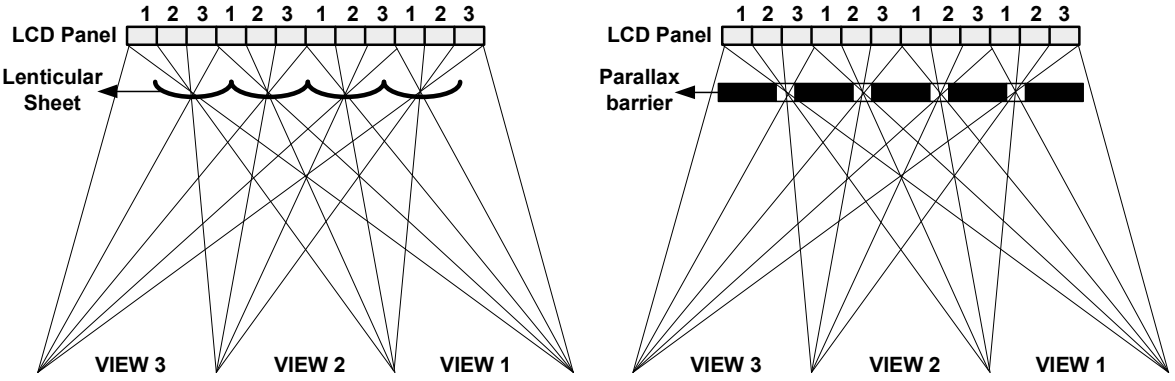

Figure 2-7 Lenticular Sheet and Parallax Barrier Methods

Philips nine-view display **[34]** using slanted lenticular sheet or Sanyo four-view display **[7]**, **[9]** using parallax barrier technology are some of the commercial examples of the auto-stereoscopic multi-view displays. In Sanyo's Display both the image display and the parallax barrier image splitter are realized by using LC technology. There are two image

splitters one in front of the image display, the other one behind the display in order to reduce the cross-talk **[7]**, **[9]**.

It should be mentioned that increasing the number of views decrease the resolution of each view for a specific display resolution. For vertically placed lenticular sheets and parallax barrier technology, the resolution is lowered only in horizontal direction but by placing the lenticular sheet with slight inclination distributes the resolution lowering between vertical and horizontal directions **[34]**. There are common problems of both binocular and multi-view auto-stereoscopic displays. These problems include accommodation-convergence rivalry causing eye fatigue, image quality difference between different viewing regions, decreased 3D visualizing quality stemming from Moiré fringes and decrease in image brightness due to optical plates especially in parallax barrier **[31]**, **[32]** and **[33]**. In multi view displays, the number of views is not sufficiently large to provide smooth motion parallax and apparent jumping occurs between the neighbor views **[32]**, **[33]**. A further step in increasing the number of multi-view displays in order to provide smoother motion parallax and solve or relieve the accommodation-convergence rivalry is the Holoform displays. The Holoform name is used as these types of displays are claimed to provide similar properties to holograms such as continuous motion parallax and harmony between accommodation and convergence mechanisms of the eye.

The display system developed during this thesis research falls under Holoform type displays. There are different names denoting Holoform type auto stereoscopic displays such as quasi-holographic and high density directional displays. Quasi-Holographic classification name will be used for these types of displays and for the novel display proposed in the following sections.

2.2.4 Quasi-Holographic 3D Displays

Quasi-holographic displays can potentially generate larger number of views compared to auto-stereoscopic multi view displays and as a result can provide smoother motion parallax in the horizontal direction. If the number of views is increased to a point where at least two viewing zones are generated within one eye pupil, then such a display system is functioning in a new region called Super Multi-view (SMV) Region and it is claimed that displays working in SMV region can provide truly continuous motion parallax and solve the accommodation and convergence rivalry **[33]**, **[35]**, and **[36]**.

In conventional auto-stereoscopic multi-view displays, the viewer adjusts the vergence mechanism to the point where the 3D object point appears according to the properly tuned binocular disparity as illustrated in Figure 2-8(a). However accommodation mechanism that should work in synchronization with the vergence mechanism cannot focus to the point where the viewer's eyes are converging because each pixel (L_1 and R_1 in Figure 2-8) constituting the 3D object point is on the display not on the position of the 3D object point. This synchronization problem is called accommodation -vergence rivalry.

However, for a display working in SMV region as shown in Figure 2-8(b), at least two different views enter from each eye pupil which means that a 3D object point is represented by two pixels for each eye (L_1, L_2 for left eye R_1, R_2 for right eye). The viewer tunes his/her vergence mechanism to the location where 3D object point appears to be similar to the conventional multi view display case. However, this time the viewer may focus to the plane of the 3D object because when he/she focuses to the display instead of the 3D object plane, then two different points (L_1 and L_2 or R_1 and R_2) will be perceived by viewer's each eye for a single 3D object point resulting in unnaturalness as described in Figure 2-9 **[35]**, **[36]**.

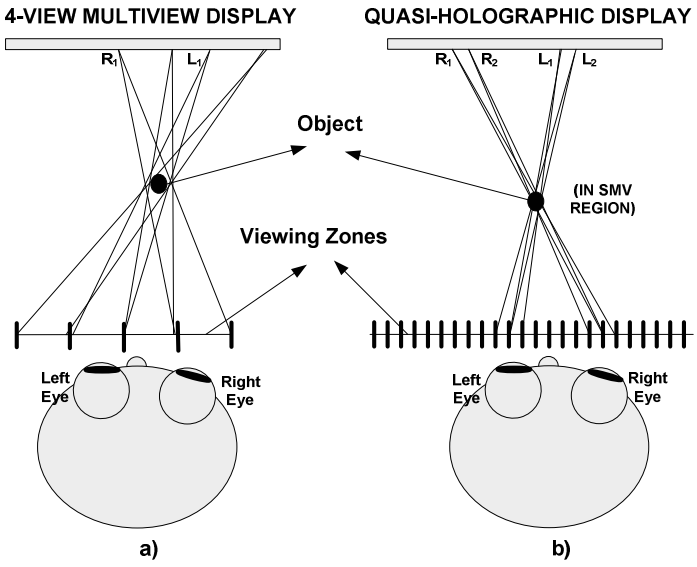

Figure 2-8 Viewer looking to an object by a 4-view multi-view display and by a quasi-holographic display in SMV region [35]

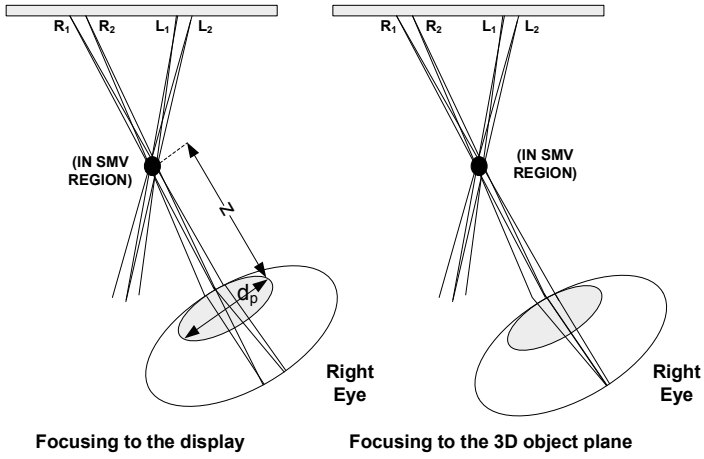

Figure 2-9 The accommodation mechanism for a display working in SMV region [35], [36]

The necessary angular resolution for the quasi-holographic display to work in SMV region can be easily calculated by

$$R_A = \arctan(\frac{d_p}{z}) \quad (2.1)$$

- R_A: Angular Resolution of the Display
- d_p: the eye pupil diameter (varies between 2 mm and 8 mm according to the brightness conditions)
- z: the viewer distance to the virtual 3D point

The Figure 2-10 shows the necessary angular resolution for realizing a quasi-holographic display working in SMV region. The distance axis in Figure 2-10 starts from 300 mm, the nearest viewing distance in average.

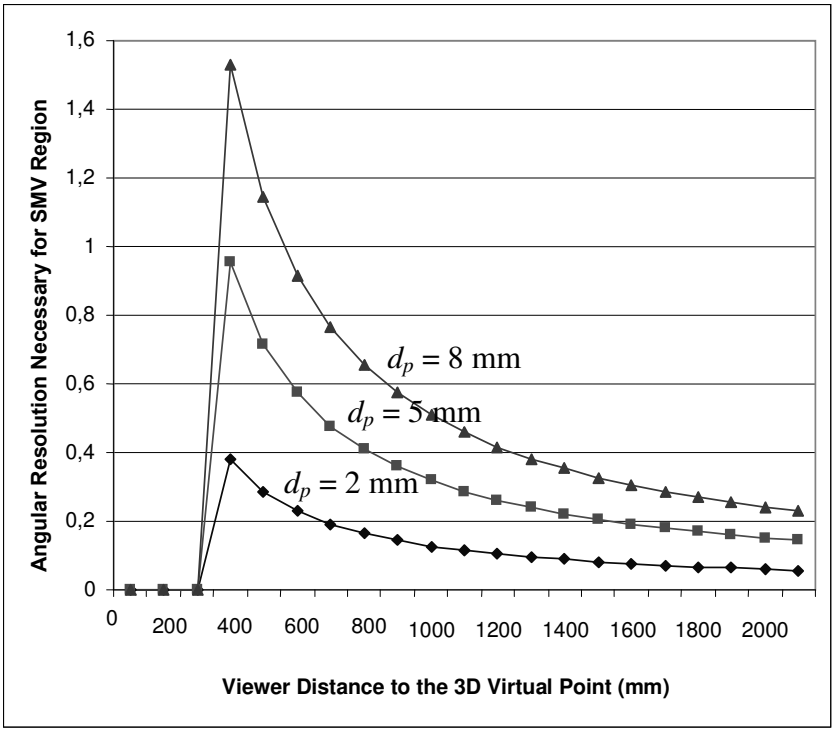

Figure 2-10 The necessary angular resolution to work in SMV region for 2, 5 and 8 mm eye pupils according to the viewing distance [35]

The basic concept of quasi-holographic displays can be interpreted as a two dimensional (2D) display where display pixels – multi-view pixels can emit light with different color and intensity to many different directions as illustrated in Figure 2-11. There are various quasi-holographic displays using different technologies such as collimated light source together with micro display array **[38]** – **[40]**, a laser or array of laser diodes together with 2D scanners **[35]** - **[37]**.

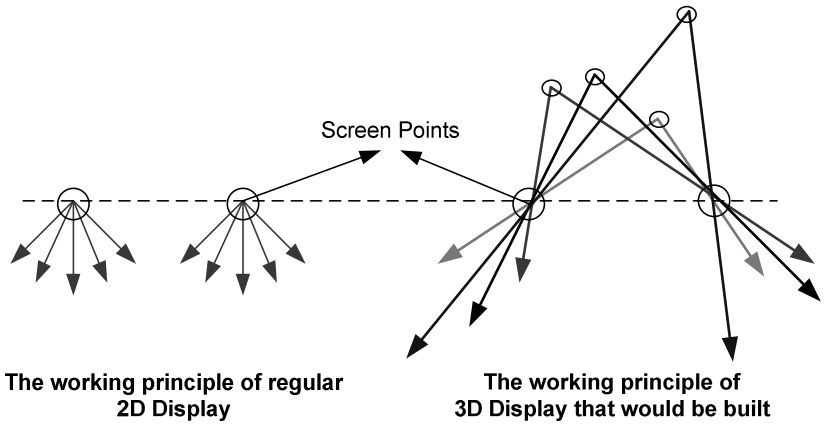

Figure 2-11 The basic difference between a 2D and 3D Display

The focused light array (FLA) concept developed by Y. Kajiki et al. **[36]**, **[37]** as illustrated in Figure 2-12 basically forms the multi-view pixel by focusing a laser diode array placed on a horizontal arc with a specific angular distance 0.5º to the center of the arc. The generated multi-view pixel the center of the arc is collimated by a collimating lens and is scanned both in the vertical and the horizontal directions. The collimated and the 2D scanned light is focused by an imaging lens to a screen where it is vertically diffused to increase the field of view (FOV) in the vertical direction as illustrated in Figure 2-12**.**

In another quasi-holographic display, a 2D array of 2D micro displays is used together with a lens and aperture array in front with one to one correspondence as shown in Figure

2-13 **[35]**. It should be mentioned that horizontal location of each micro display is different from the others to increase the number of different views in horizontal direction. The parallel light modulated through each micro display is focused by the lenses in front to the focal plane of the lenses where it is filtered by the aperture to limit the ray directions from each focal point. This focal plane also constitutes the focal plane of another relatively large lens enough to cover all the micro displays. As each micro display is in a different horizontal location than the others, the light modulated by each micro display is also focused to a different horizontal location and then collimated to a different direction by the larger lens. The display is placed to the location where all these different directions are overlapping. The light is vertically diffused in the display plane to increase the FOV in vertical direction.

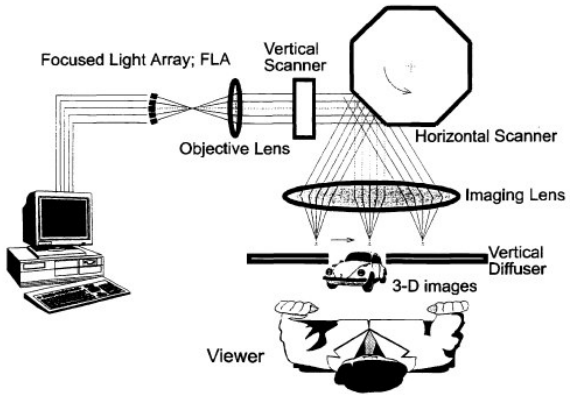

Figure 2-12 Working principle of Focused Light Array (FLA) concept [36]

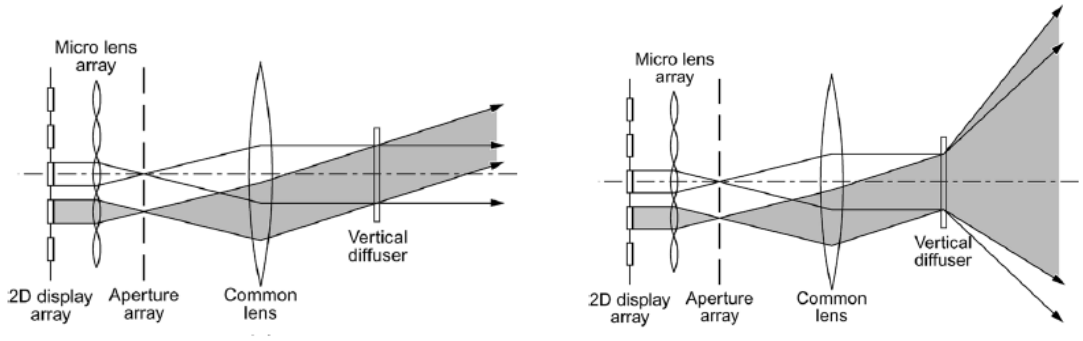

Figure 2-13 Vertical and Horizontal cross-sections of the High-Density Direction Display [33]

Another quasi-holographic display concept is HoloVizio developed by Holografika **[38]**-**[40]**. The display consists of numerous 2D micro displays in the horizontal directions, which are illuminated by collimated light. The micro displays are controlled according to the 3D image information. Each pixel of the modulated light is then transmitted in different directions to different screen points by the lens system present in front of each 2D micro display, as illustrated in Figure 2-14. Each screen point receives light from a specific number of modules that is equal to the number of different directions from the screen point. By the help of a diffuser screen, the modulated light beams are asymmetrically diffused to the viewing zone. The modulated light is diffused with a narrow angle in the horizontal direction and with a wide angle in the vertical direction to enlarge the vertical field of view (FOV). One of the most important advantages of such a system is its capability to be produced by integrating identical sub blocks side by side in a modular fashion. The 3D display volumetric size is scalable in a way similar to LEGO™ blocks.

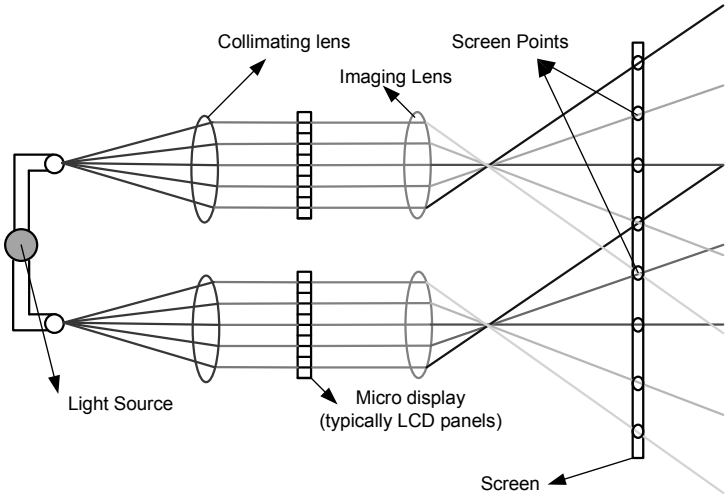

Figure 2-14 The basic unit of HoloVizio Display concept [38]

Chapter 3 SCANNING LED ARRAY BASED 3D DISPLAY SYSTEM AND DESIGN

One of the main contributions of this research is the alternative system configuration proposed for the HoloVizio 3D Display system (2.2.4). The external light sources illuminating the 2D micro displays, collimating optics, 2D micro displays, and the lens system on each arm of the HoloVizio 3D display concept illustrated in Figure 2-14 are replaced with a 1D vertically oriented LED array with an imaging lens in front rotating together on a polymer scanner. Individual modules appear as rotating horizontal lines of light emanating from the LED light sources, providing different emission angles. Rotational movement gives the freedom of converting 2D spatial multiplexed system into a 1D time multiplexed system. The use of the LEDs is a key advantage as they are widely available in different colors at low-cost and modulatable at several MHz rates.

A one-dimensional (1D) LED array per color and the LED driver IC integrated on a scanning module as can be seen in Figure 3-1(a), constitutes the basic functional unit of the proposed display system. Scanner is made on FR4 substrate, a fiber-glass epoxy composite, using standard PCB technology **[41]**. Depending on the number of LEDs per module, the driver IC can be mounted ON or OFF the moving platform. 2D array of such modules are tiled behind a special screen for full system operation **[42]**.

Each scan module creates a horizontal scan line by way of electromagnetic actuation **[43]**. The electromagnetic actuation is realized by the help of a permanent magnet that is mounted onto the back side of the scanner. The magnet interacts with the magnetic field from a properly aligned external electro-coil driven with alternating sinusoidal current signal as illustrated in Figure 3-2.

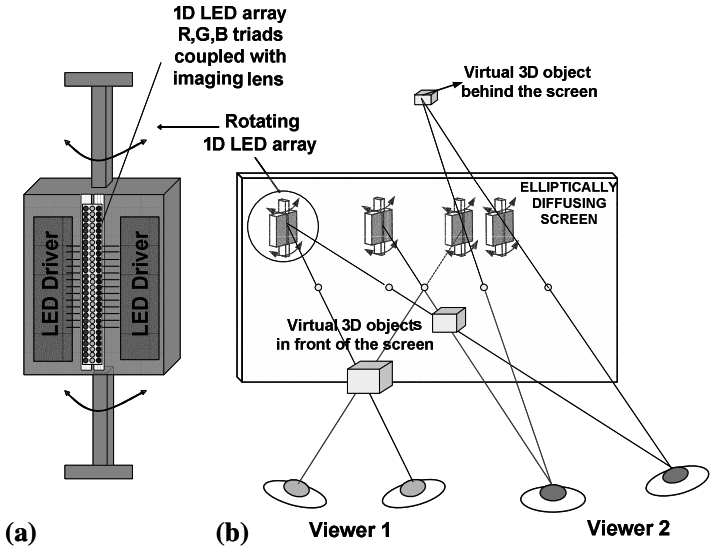

Figure 3-1 (a) 1D LED arrays in RGB colors and driver IC mounted on FR4 scanner platform; (b) Scanner modules as the basic unit of the 3D display.

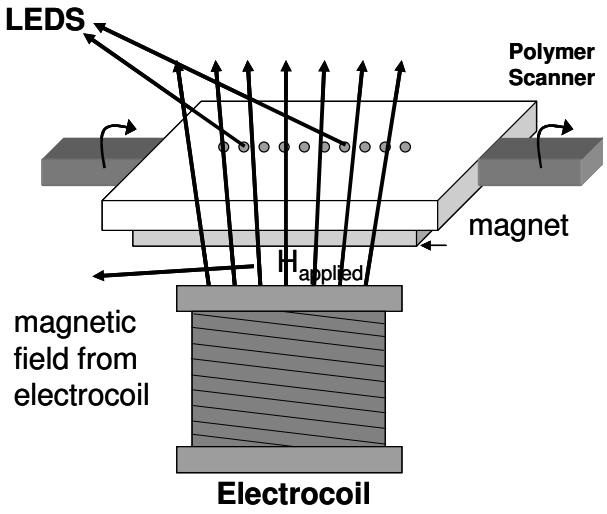

Figure 3-2 The scanners are electromagnetically actuated in torsion mode by an external electro coil interacting with the magnet mounted onto scanner

In order to realize the screen capable of emitting different color and intensity light to different directions from its pixels, red, green, and blue LEDs are modulated individually during scan. As R, G, B 1 D LED arrays are slightly shifted on the scan module, their images on the screen are also shifted by a few screen pixels. However, the images for each color LED can be overlapped on the screen by introducing slight time-shifts in between R, G, B LED drive signals during the scan. As an example, if we assume a spatial shift of 3 pixels in between R, G, B LEDs, while the middle color LED is fed with the information of pixel N, the other color LEDs on either side will be fed with the information of pixels N+3 and N-3. There will be also slight angular displacement between ray angles of different color LEDs illuminating the same pixel on the screen and generating the same ray angle. However, the angular displacement is small enough to ignore (~0.02º for 0.1 mm distant LEDs illuminating a screen at 250 mm distance from the LED arrays). Synchronization of modules to each other can be done but not essential. Each module should complete a full rotation within the frame time and the video data fed to each module need to be synchronized with the position of the scanner. The position feedback is obtained using the back-emf signal from the rotation of the magnet mounted on the scanner. The back-emf coil is simply machined on the FR4 scanner using standard PCB technology.

As illustrated in Figure 3-1(b), each module addresses an array of pixels on the special screen and provides different particular ray angles for each screen pixel. Screen pixels are illuminated by a number of such scan modules with different ray angles to convert them into pixels capable of emitting different color and intensity light to different directions. The number of pixel emission directions is equal to the number of modules illuminating the pixel. Placing mirrors at the sides of the display would create virtual modules and create the missing illumination directions for the screen pixels near the edge of the display as illustrated conceptually in Figure 3-3. A module can behave as at the most two different virtual modules one at the left side and one at the right side according to its relative

position with both left side and right side mirrors. A virtual source point or voxel is perceived at the intersection of two properly modulated ray bundles received by the left and right eyes of a viewer.

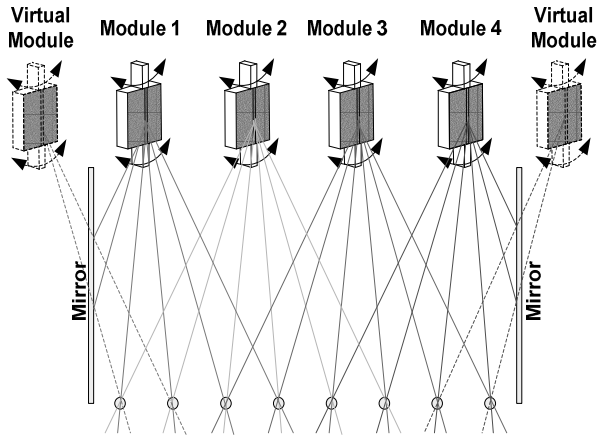

Figure 3-3 Every pixel on the screen is illuminated by different modules whose number is equal to the number of different emission directions from the pixel

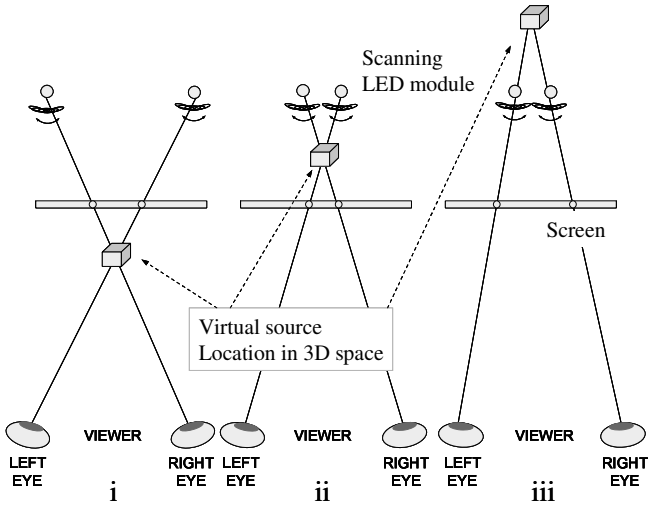

Figure 3-4 Voxels rendered (i) in front of the screen, (ii) between the screen and the LED modules, (iii) behind the LED modules.

Voxels can be rendered at different depths, in front of the screen, between the screen and the modules, or behind the modules as illustrated in Figure 3-4. Note that the viewer's focus and vergence may be in coordination and different for each voxel depth and the binocular rivalry may be eliminated by working the system in super-multi view region

Two viewers observing from two different horizontal positions would see different virtual source positions and perceive different 3D images. The Figure 3-5 depicts the working principle of the display in more detail. Both viewers in the figure receive light rays from different LED arrays through different pixels on the elliptical diffusing screen with different angles. At the intersection point of two ray bundles coming to right and left eye of the viewers, the viewers think that there are objects. The viewer 1 realizes that object 3 is behind object 1 as the ray bundle coming to his right eye from object 3 is occluded by object 1.

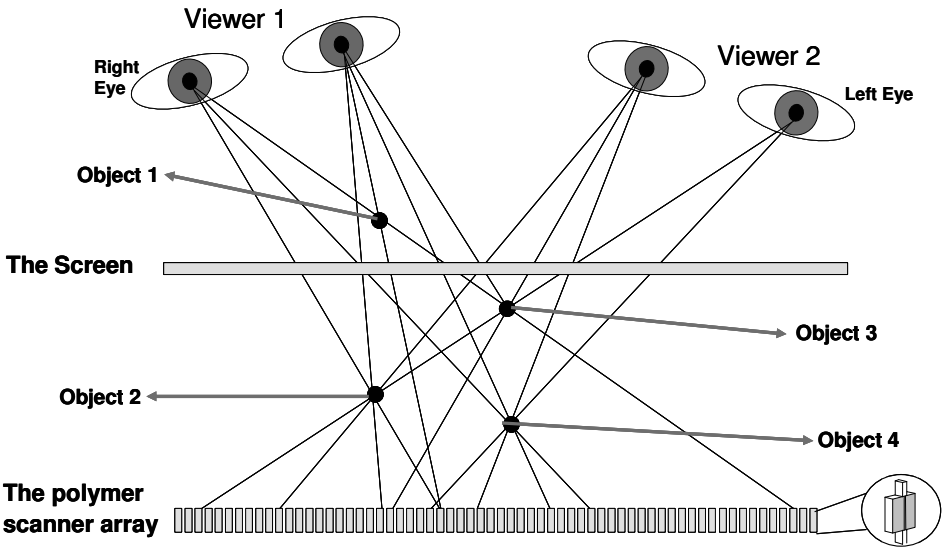

Figure 3-5.. The working principle of the 3D quasi-holographic volumetric display [38]

The screen is capable of diffusing light into a narrow angle in the horizontal direction and into a wide angle in the vertical direction – i.e., elliptically diffusing screen. A narrow

angle is required in the horizontal direction as each pixel on the display should emit light with different color and intensity to separate horizontal directions with neither any crosstalk nor unlit region between neighboring directions. The wide angle in the vertical direction is required as the display is designed to provide motion parallax only in the horizontal direction (i.e., the same image is received by the viewer at the same horizontal position and different vertical positions of the eye pupils.)

The full system requires 2D array of 1D LED scanners behind the diffuser screen as illustrated in Figure 3-6. The number of scanners needed both in horizontal and vertical directions together with some other critical parameters of the display are calculated in 3.1.

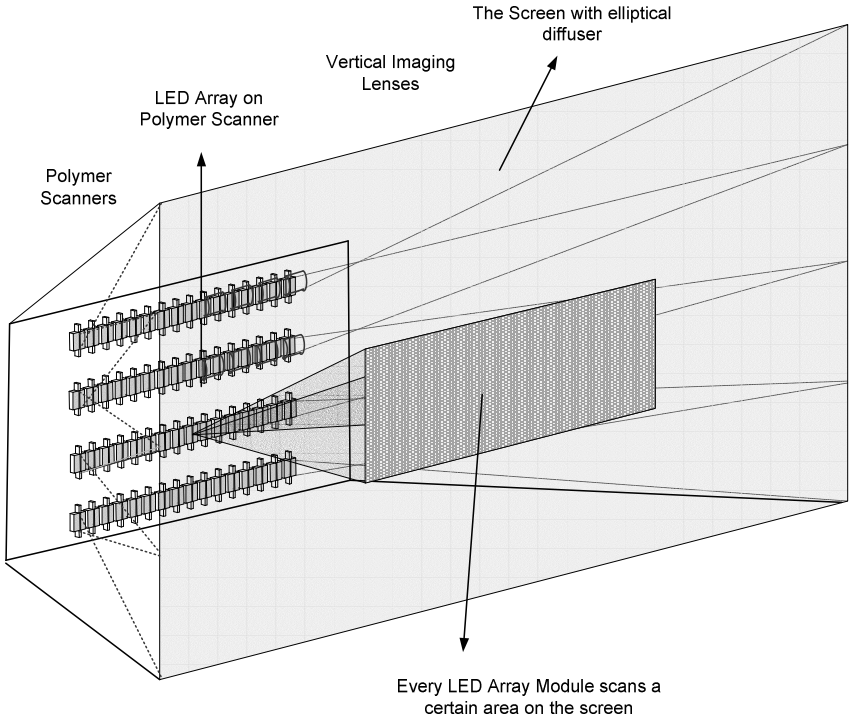

Figure 3-6 The Illustration of Complete Scanning LED Array Based 3D Display

3.1 System Design and Resolution Tradeoffs

The number of different views for the display is the same with the number of independently controllable horizontal emission directions from the screen pixels. Actually the number of screen pixels in horizontal and vertical direction gives the resolution of each view the viewer will perceive. As an example, there are 40 different views using 1º divergence for each emission direction and 40º scan angle. When mirrors are assumed on the sides of the display as illustrated in Figure 3-3, the resolution of the display – the resolution of each view can be calculated using the following relationship:

$$N_H = \frac{n_h \; x \; p}{r} \tag{3.1}$$

$$N_V = n_h \; x \; l \tag{3.2}$$

- N_H , N_V: number of screen pixels in the horizontal and vertical directions,
- n_h, n_v: number of scanner modules in the horizontal and vertical directions,
- p: number of horizontal screen pixels addressed by each scanning module
- r: number of different ray directions through each screen pixel
- l: number of LED color triads on a line in each scanner module

In Figure 3-3, $n_h = 4$, $p = 6$, and $r = 3$, resulting in $N_H = 8$ using Equation 3.1. It should be mentioned that equation 1 should be treated together with the subsequent equations to result in a reliable display system. Number of voxels-perceived-by-a-single-eye is equal to the number of screen pixels. However, unlike FPDs, the voxels are not perceived on the screen, they would appear to come from a virtual source point when combined with the view of the other eye. The total number of voxels (N_T) is defined as a product of voxels-perceived-by-a-single-eye and the number of views:

$$N_T = N_h \, N_v \, r \tag{3.3a}$$

Equivalently, N_T can also be calculated by the product of total number of LEDs and p using the total number of screen pixels and ray directions:

$$N_T = n_h\, n_v\, l\, p \tag{3.3b}$$

Table 3-1 provides an exemplary system design parameters for 2 million, 20 million and 65 million voxels with two different display depths.

Voxels	$2x10^6$	$2x10^6$	$20x10^6$	$20x10^6$	$65x10^6$	$65x10^6$
N_H	240	240	720	720	1440	1440
N_v	160	160	576	576	900	900
n_h	80	48	240	144	480	288
n_v	5	5	18	18	30	30
P	150	250	150	250	150	250
L	32	32	32	32	30	30
r	50	50	50	50	50	50
FOV	50	50	50	50	50	50
Display Thickness	160 mm	268 mm	160 mm	268 mm	160 mm	268 mm

Table 3-1 Exemplary system design parameters for 2 Million, 20 Million and 65 Million voxels in 3D space for two different system sizes.

The table implies that the resolution of the system can be increased by increasing the number of scan modules without altering the scan module design or the screen depth, resulting in a scalable architecture.

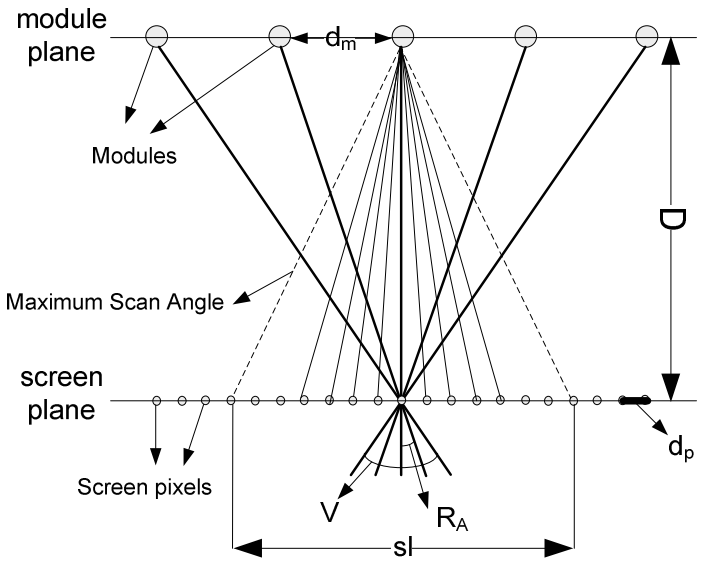

Figure 3-7 The basic parameters of the system

System configuring methodology for a specific vertical and horizontal display resolution and given pixel size is as follows:

The basic system parameters that will be used in the below calculations are illustrated in Figure 3-7 The number of modules that should be placed behind the screen in horizontal direction is determined by the horizontal resolution of the display, center to center distance of the distance of two modules (d_m), and screen pixel pitch (d_p):

$$n_h = \frac{d_p N_H}{d_m} \tag{3.4}$$

For a specific number of ray directions through each screen pixel, using the number of modules calculated from Equation 3.4, the total number of necessary scan angles from each scanner module is easily calculated from Equation 3.1. Using the above relations, it can be easily observed that decreasing the module sizes also decrease the number of pixels

addressed by each scanner module (p) as illustrated in Figure 3-8. The limit in decreasing the modules sizes and the distance between neighbor modules is placing a scanner module onto each pixel's position ($d_m = d_p$; $N_H = n_h$).

The scan line length of each scanner on the display screen can be easily calculated by multiplying pixel pitch with the number of intervals between pixels addressed by each scanner as each scanner should illuminate all the pixels along the length of its scan line (sl):

$$sl = d_p\ (\mathrm{p} - 1) \cong d_p\, p \tag{3.5}$$

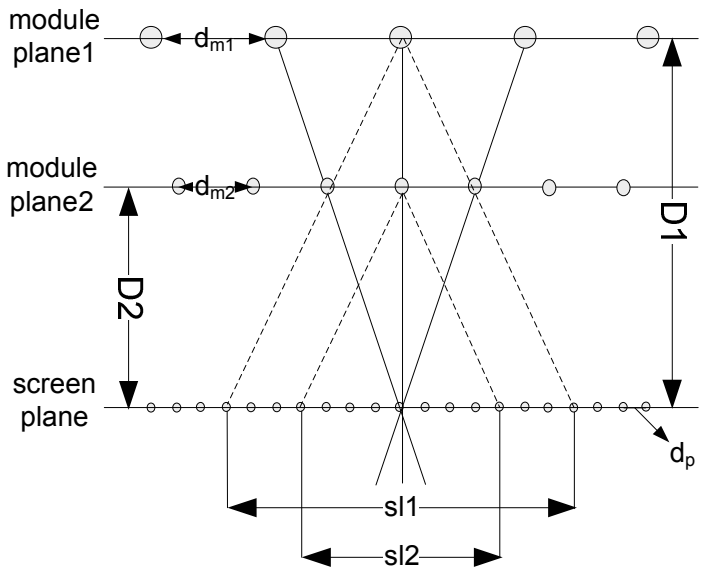

Figure 3-8 Decreasing d_m value, results in a thinner display and less addressed pixels by the scanners

Field of View (FOV) of the display – the total light emission angle through each screen pixel is equal to the total optical scan angle (TOSA) of the scanners. The distance of the 2D

scanning module array to the display screen (the depth of the display) is calculated by using the following relationship:

$$D = \frac{sl}{2\tan(\frac{V\pi}{2x180})} \tag{3.6}$$

- D: the distance of 2D scanning modules to the display
- V: Field of View (FOV) of the display

The distance between 2D scanner module array and display screen calculated from Equation 3.6 directly determines the angular resolution of the display pixels (the angle between two neighbor light emission directions from a single display pixel). Two neighbor emission directions from a single display pixel are generated by illumination of the pixel by two neighbor modules in the horizontal direction. The relation between the distance of modules to the screen and the angular resolution of the display (R_A) can be shown as follows by assuming that D >> d_m:

$$R_A = \frac{180\,d_m}{\pi D} = \frac{180\,d_m\,2\tan(\frac{V\pi}{2x180})}{\pi\, sl} = \frac{360\tan(\frac{V\pi}{360})}{\pi\, d_p\, p} = \frac{360\tan(\frac{V\pi}{360})}{\pi\, r} \tag{3.7}$$

The optics for the system is rather simple and illustrated in Figure 3-9 . Each scan module has a lens that rotates together with the module and provides imaging of LEDs onto the screen with some magnification. The focal length of the lenses and the distance of the lenses to the LEDs are determined by the distance of the screen to the scanners and the emission area of the LEDs. The vertical cross section of the display shows an array of 1D LED arrays and the horizontal cross section shows an array of single LEDs. Each LED on a module provides illumination to a fraction of one row of the screen in a light efficient manner by turning the LED ON only while traversing a screen pixel.

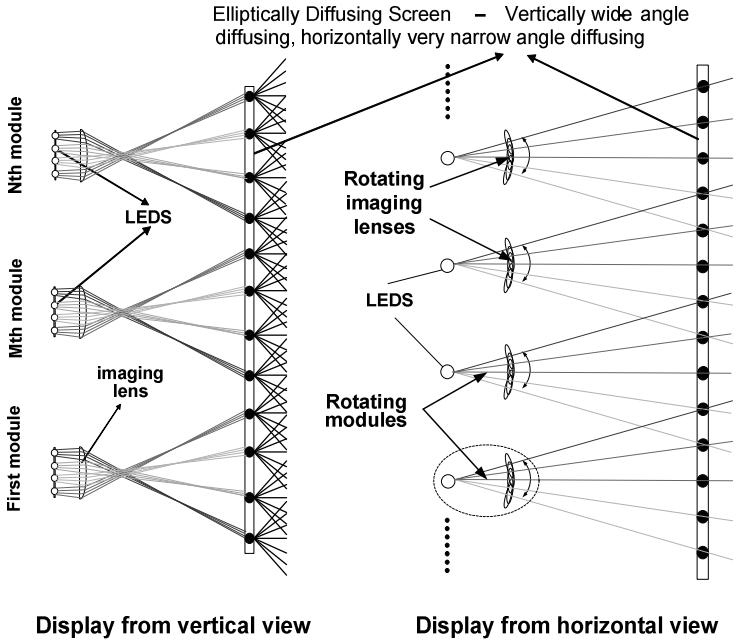

Figure 3-9 The optical behavior of the system in vertical and horizontal directions.

The elliptical diffuser constituting the display screen should diffuse the light in the horizontal direction such that there should be neither any crosstalk nor unlit regions between the two neighboring emission directions of the same pixel. This restriction on the diffuser means that the diffusing angle from a screen pixel for each emission direction should be equal to the angular resolution R_A of the display. The diffusing angle in horizontal direction is:

$$A_H = AD_H + L_H \tag{3.8}$$

- A_H: Horizontal emission angle from a screen pixel for each emission direction
- AD_H: Horizontal diffusing angle of the diffuser
- L_H: The emission angle of the imaged light bundle from the display pixel for a single direction

As it is illustrated in Figure 3-10, the crosstalk between two neighbor ray directions for a single pixel is closely related to the diameter of the imaging lens. When the imaging lens diameter is exactly one screen pixel (d_p) less than the distance between two neighbor modules (d_m) then there will be constant crosstalk region having pixel size length. If the lens diameter is increased, the crosstalk region will not be constant anymore and start to diverge with a constant angle:

$$\alpha \cong \frac{180\left| d_p - (d_m - d_L) \right|}{\pi D} \tag{3.9}$$

- d_L: Imaging lens diameter
- α : crosstalk/unlit region diverging angle

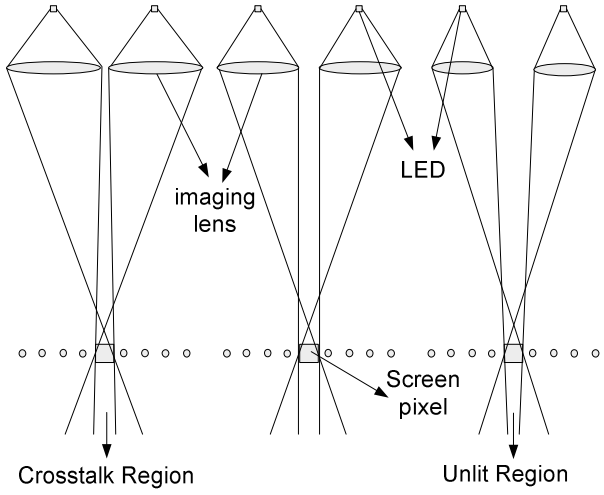

Figure 3-10 The divergence angle from the pixel according to the diameter of the imaging lens

When the lens diameter is decreased, the same α angle will give this time diverging angle of the unlit region. The equation 10 shows that the lens diameter is critical and it should have an upper limit to prevent the constant crosstalk between two neighbor emission

directions from a pixel. When the lens diameter is smaller than this limit, there will be necessity for the horizontal diffuser. However, the amount of the necessary diffusing could be very small and could be ignored. For a display design from Table 3-1, D = 268 mm, d_m = 5 mm, d_L = 3.8 mm, and d_p = 1 mm, $\alpha = 0.04°$ less than ten percent of the angular resolution (R_A) of a display with 0.5° R_A.

3.2 Scanner Design

Magnetic actuators have been widely used in different areas such as optical communications, display and imaging applications, biomedical applications. Magnetic actuators can provide relatively large forces over large distances **[43]**. They can make use of the Lorentz force, magneto-static force with moving permanent magnets, or magnetic anisotropy torque with high-permeability thin films. Combination of electromagnetic actuation technique with polymer scanners that have relatively low resonant frequencies is especially useful to obtain large rotation angles to produce wide scan lines at low power levels which are desired features for the scanners in the Scanning LED Array Based 3D Display concept **[44]**.

Fire Resistant 4 (FR4) which is the most widely used material for printed circuit board (PCB) is a very good candidate for fabricating the polymer scanners. It offers good electrical, mechanical, and thermal properties. In addition to its common usage in the field of electronics, micromechanical devices can as well be fabricated with high-precision and low-cost on PCBs **[41]**. FR4 has recently been adapted for board level optical interconnects that integrate micro-optics and optoelectronics on PCBs. FR4 provides fast and low-cost design and fabrication as well as a high degree of flexibility compared to conventionally used materials such as silicon micro-electro-mechanical systems (MEMS) devices or conventional scanners. The fabrication is fully realizable with standard PCB

machinery. Copper coils for actuation are printed on both sides of a thin FR4 substrate, which can then be tailored into the desired device shapes by cutting. In another implementation, NiFe or other magnetic films are plated on FR4 for electromagnetic actuation with an external coil. A permanent magnet can also be placed directly on top of the scanner to actuate with an external electro coil as in the case of scanners used in the proposed 3D Display concept. Different FR4 scanner designs are shown in Figure 3-11.

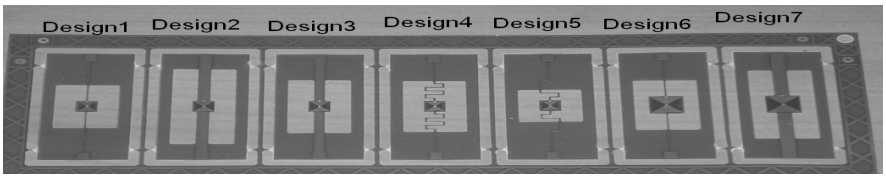

Figure 3-11 Different FR4 Scanner Designs with Copper Coils for actuation

FR4 scanner module carrying wirings to drive 10 LEDS independently through its flexures (6 wires from each flexure – 5 for LEDs cathodes and 1 for common anode connection) is designed using FEMLAB for 3D demonstrators. There is a common anode line on the FR4 polymer scanner in the middle to mount LEDs on it from their bottom surfaces. The cathode contacts of the LEDs are wire bonded to separate cathode connections on the scanner as illustrated in Figure 3-12. The LEDs are controlled independently by changing the voltage level at these cathode connections. The voltage level of all the cathode connections are controlled by the output pins of the FPGA via the driving circuitry. The voltage level of the common anode connection is controlled by the external DC voltage source. The cathode and anode connections are carried to the LEDs through the flexures of the scanner. The scanner has a rectangle frame with 13 mm X 13.5 mm area and flexures with 3.95 mm length, 1.85 mm width with 2 different thickness values (200 microns and 350 microns). It is designed to place a permanent magnet onto the backside and actuate with an external electro-coil.

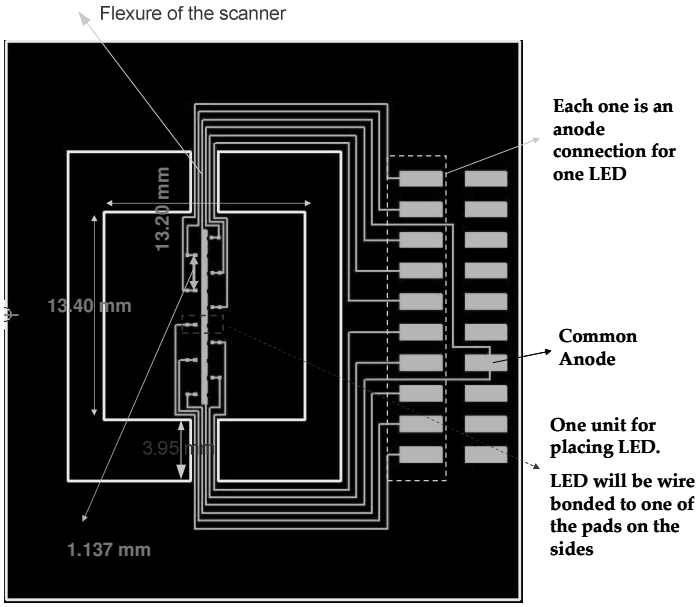

Figure 3-12 ORCAD PCB Layout of the Designed Scanner with wirings for driving 10 LEDs independently

The torsion mode is predicted to be at 69.0 Hz for 200 micron thick design in FEM analysis which is suitable for a display concept with typical 60 Hz refresh rate. As shown in Figure 3-13, the lens and the optomechanics are not included in the simulation, but the permanent magnet that is used for magnetic actuation is taken into account.

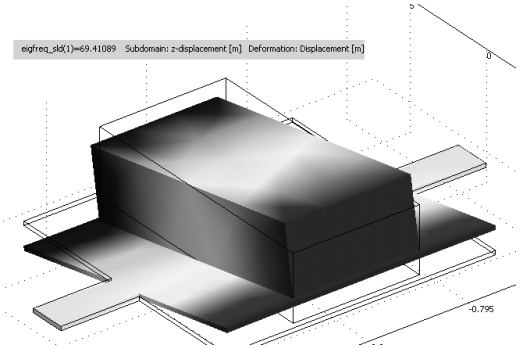

Figure 3-13 FEM analysis of the FR4 scanner with the moving magnet

3.3 LED Driver Circuit Design

An external LED driving 4-layer PCB circuitry with a Field Programmable Gate Array (FPGA) is designed for driving the LEDs on each module as can be seen in Figure 3-14. FPGA board design and PCB layout are drawn using Altium's Protel DXP.

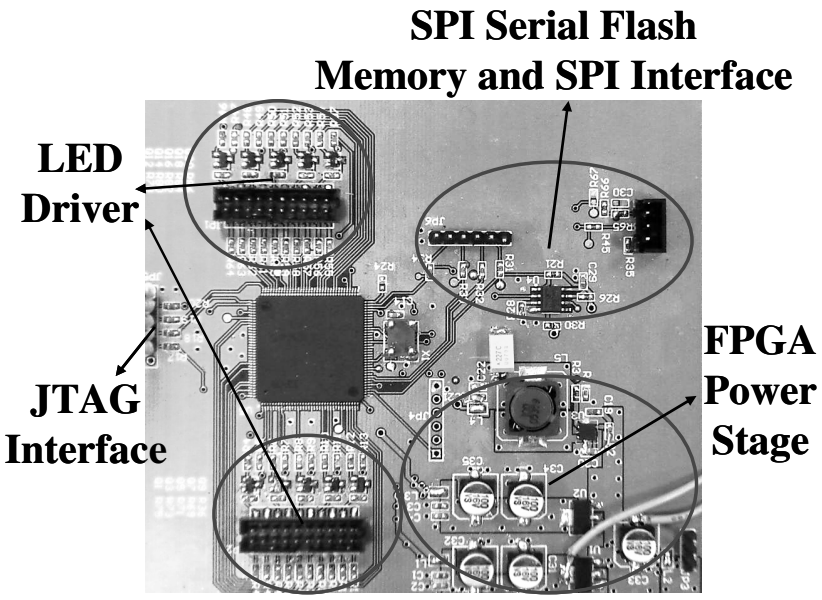

Figure 3-14 LED driving circuitry with Spartan 3E FPGA

The FPGA on the external driving circuitry is XC3S100E device from Xilinx Spartan-3E FPGA family having 108 pins available as user I/Os. The PCB circuitry can be divided into three parts.

- The first part is the FPGA power stage. This part takes 5 volt as input voltage and regulates it with 3 different regulators to three different voltages, VCCO = 3.3 V, VCCAUX = 2.5 V and VCCINT = 1.2 V which are supply voltages of the FPGA. VCCINT is the internal core supply voltage and supplies all the internal logic including the block RAMs, block multipliers and configurable logic blocks (CLBs).

VCCAUX is the auxiliary supply voltage and supplies digital clock managers (DCMs) and JTAG programming interface. VCCO supplies the I/O voltages of the FPGA.

- The second part is the FPGA configuring stage. The circuitry provides two different methods of programming the FPGA. The first method is programming in boundary scan mode through the Joint Test Action Group (JTAG) interface and the second method is programming through serial peripheral interface (SPI) from an SPI serial flash. In this circuitry, 4 mega-bit flash memory "25P40" from ST Company is used.
- The third part is the LED driver, which is outside the scan module, and is capable of driving 40 LEDs from 40 different output pins of the FPGA. Two different driving circuits illustrated in Figure 3-15 are tried for the prototypes. 20 LEDs are directly driven from the output pins through 100Ω resistors. The other 20 LEDs are driven through a general purpose NPN BJT transistor – 2N3904. The output pins of FPGA are connected to the bases of the transistors through 2.2 kΩ resistors. All LED cathodes are connected to the collectors of the transistors through 100Ω resistors while anodes are connected to a controllable DC voltage source in order to control the amount of current conducting through the LEDs. The emitter of the transistor is connected to the ground. When the output pin of the FPGA is set to zero, the transistor and the LED are off. When the FPGA is set to 3.3V, LED conducts current according to the voltage level of the controllable DC voltage source. The I/O pins of Spartan 3E family devices are capable of driving maximum 16 mA so that the above configuration prevents damage to the I/O pins of the FPGA from excessive current flow and as a result increase the current flow limitation through the LED from 16 mA to 200 mA, the maximum rating for the collector current of the transistor.

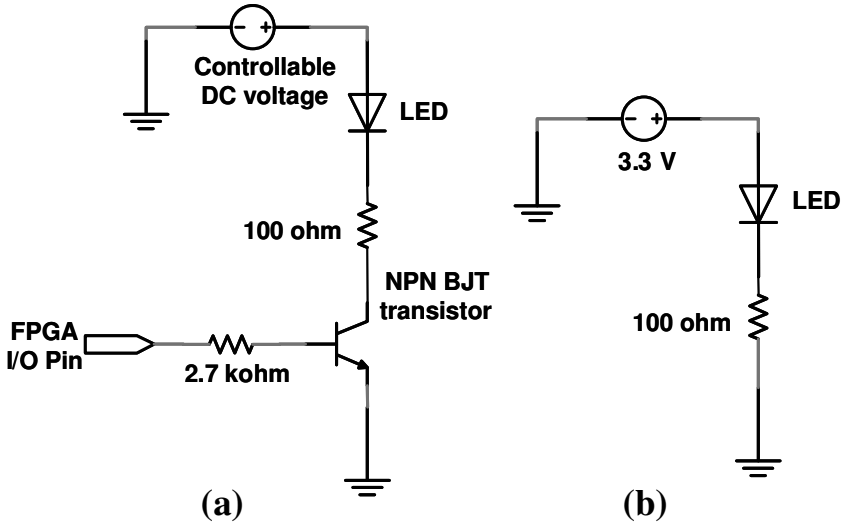

Figure 3-15 Two different configurations to drive LEDs (a) using NPN inverter stage, (b) directly from the FPGA

The LEDs are driven by pulse width modulation (PWM) method. N bit depth level PWM provides 2^N different intensity levels. A counter is synthesized within FPGA which is incremented periodically and is reset when its value becomes 2^N-1. The counter's output value is compared with a reference value for each single output pin and produces PWM LED drive signal as shown in Figure 3-16. N-bit video input determines the LED drive pulse width.

The input video data frequency at which the data will be fed into the FPGA will be:

$$f_V = \frac{3l\,n\,2p\,f_{\mathrm{D}}\,d_{PWM}}{\mathrm{d_w}} \tag{3.10}$$

- f_v: the frequency of the input video data
- l: number of LEDs per color on a line on each scanner module
- n: the number of scanners driven with the same driver
- p: number of horizontal screen pixels addressed by each scanning module
- f_D: display refresh rate

- d_{PWM}: PWM bit depth
- d_w: input video data line width

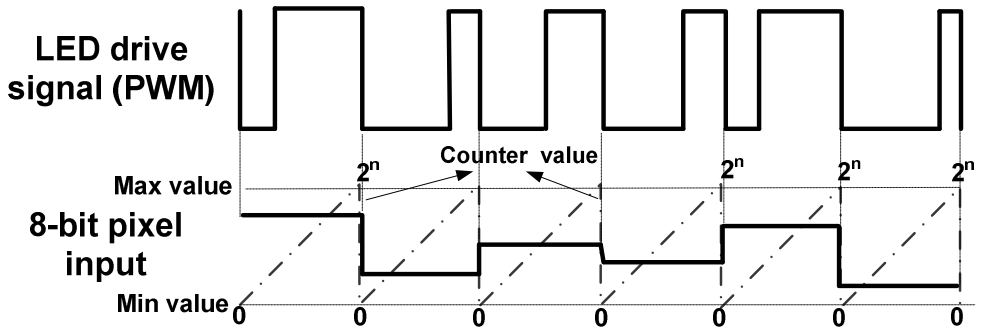

Figure 3-16 LEDs are driven with PWM by using a counter synthesized in FPGA. LED remains ON until dashed-red line reaches the n-bit pixel input level and turned OFF for the rest of the pixel time.

As an example, assume f_D = 60 Hz scan frequency– typical refresh rates of displays and l = 30 (or 90 LEDs per module), dPWM = 10-bit, n = 1 (scanners controlled by each driver), p = 100 pixels/LED (=200 modulations per cycle due to bidirectional scanning). In such a case, if 1 bit per color (d_w = 3) serial input video data is fed into the FPGA then 3.6 MHz clock frequency would be required. Due to the sinusoidal speed variation of the scanner, this average data rate needs to vary by about a factor of 2 from the center to the edge of the scan line. There is a 4 MHz oscillator on the PCB board whose frequency can be modified by FPGA's DCM blocks for different scanner and system designs according to the above calculation.

The other method of driving LEDs will be an LED driving IC placed directly on the backside of the scanner, which is planned to be an FPGA or a complex programmable logic device (CPLD) as illustrated in Figure 3-17. It is better to place an ASIC in the long run as it will be much smaller than an FPGA or CPLD and give the opportunity of designing smaller scanner modules.

Placing the LED driving IC on top of the scanner provides a more compact design and gives the opportunity of increasing the number of LEDs on a single FR4 scanner as fewer electrical signals should be carried through the flexures of the scanner. These signals would be limited, in the case of an FPGA, with the FPGA supply voltages VCCO, VCCAUX and VCCINT, JTAG programming interface signals, 1 bit clock signal and 1 bit serial input data that would modulate the LEDS connected to the FPGA I/O pins as illustrated in Figure 3-17. In this case, the number of the LEDs that can be driven will be limited with the number of I/O pins of the FPGA which can be quiet high; more than four hundred with an I/O optimized FPGA.

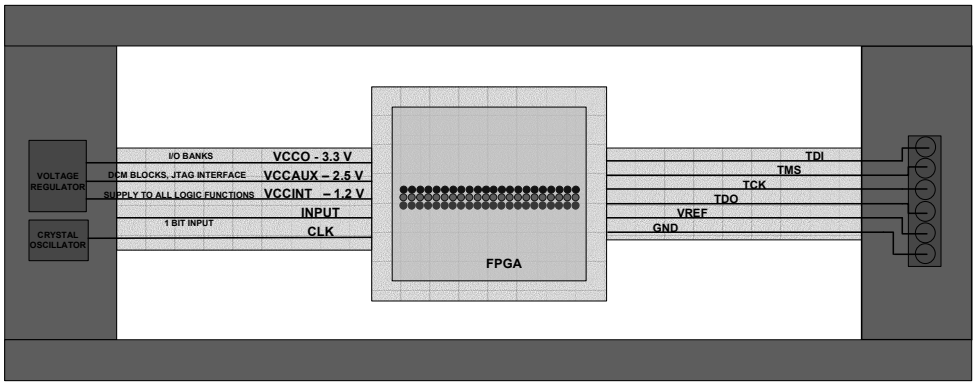

Figure 3-17 The signals carried through the flexures of the scanner when an FPGA is mounted on top of the scanner as the LED driver.

3.4 Software Simulations of the Display Concept

In conventional multi-view auto stereoscopic displays, the different displayed views are perspective projections of a 3D scene from well defined view points in a specific horizontal viewing plane **[36], [37]**. These displays are designed to display these different perspective projections to the regions centered on the corresponding view point locations where the

viewer should place his/her head. However, in the proposed system and in the other quasi-holographic displays directional rays method is used. Directional rays are nearly parallel rays propagating in a certain direction with a quite small divergence. The quasi-holographic displays are capable of displaying different directional ray sets which are orthographic projection of the same 3D scene with very small angular intervals. Actually no pre-defined view points are assumed in generation of directional images. Actually orthographic projection is a hypothetical perspective projection where camera with infinite focal length is located at infinity. Such a displaying methodology results in a retinal image formation different from the retinal image formation of the conventional multi view displays. Each eye receives information from all the directional images at the same time as addition of specific vertical slices of these images side by side. In a system with pixels having emission directions completely parallel to each other, the vertical slices of the directional images received by the viewer will be continuous. It means that all the pixels received from the same directional image should be adjacent to each other both on the directional image and on the screen pixels. However, in the scanning LED array based display concept, there will be discontinuities changing with the viewer's position stemming from the pixel sets having different emission directions as illustrated in Figure 3-18.

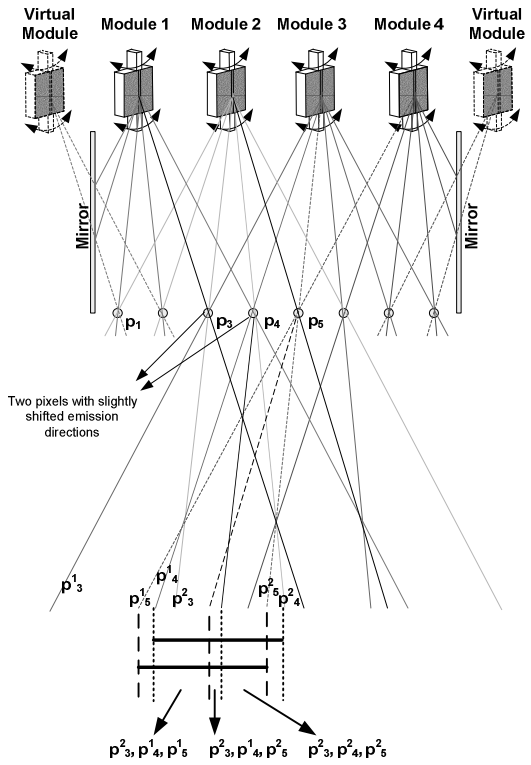

Figure 3-18 Pixels with different emission directions will result in discontinuities in the vertical slices of the images received by the viewer

In Figure 3-18, the pixel 5 (p_5) has first emission direction (p^1_5) with a larger angle than the first emission direction (p^1_4) of the pixel 4 (p_4) so that after a certain distance from the screen, p^1_5 is located at the left of p^1_4 and the diffused region of p^1_5 is located further to the left than the diffused region of p^1_4 although p_5 is located at the right of p_4. This results in a region with discontinuity where the viewer receives light from the second direction of p_3 and p_5 but the first direction of the p_4.

A MATLAB Program is written to model the display together with the side mirrors. The program starts the calculations from the plane of scanner modules. According to the number of pixels on the screen and the number of modules in the system, it positions the

modules behind the screen, sets the display depth and propagates rays from modules to the related pixels. After setting up the system, it finds the rays received by the viewer's left and right eye at any position in front of the display.

For a simple example, a display is set with 500 pixels that can emit to 50 different directions independently. The display is fed with plain gray level from black to white as directional images. Each directional image is a plain gray level, five added to the previous directional image gray level starting with black for the first directional image. A viewer located at center in front of the display (left eye at -32.5 mm and right eye at 32.5 mm), a second viewer at left side (left eye at -215 mm and right eye is -150 mm) and a third viewer at right side (left eye at 150 mm and right eye is 215 mm) at 1000 mm distance from the display will see an addition of specific vertical slices of the directional images a gray level with changing intensity levels according to viewer's position as illustrated in Figure 3-19. The viewer at the left side of the display receives from directions fed with high luminance values – close to white and the viewer at the right of the display receives from directions fed with low luminance values close to black.

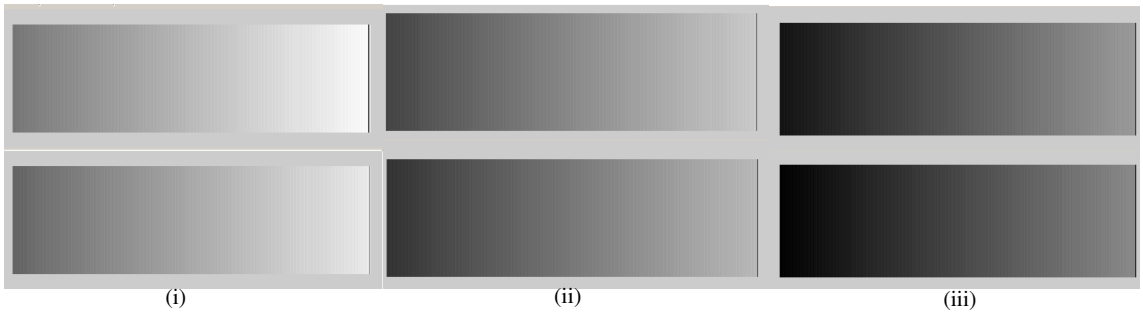

Figure 3-19 The viewer will receive different combination of directional images (i) at left side of the display, (ii) at the center of the display, (iii) at the right side of the display. The above pictures are received by the left eye and the below ones are received by the right eye

A practical visual representation of the emission from each screen pixel to a specific viewer position can be drawing vectors from each pixel having the exact direction of the ray emitted from that pixel to the viewer and having magnitude equal to the luminance value of the ray emitted from that pixel. In the same example above, for the viewers' left eyes located at -215 mm, -32.5 mm and 150 mm, the image received by the viewers' left eye will be as illustrated in Figure 3-20 respectively. According to the position of the viewer, the rays received by the viewer from a specific pixel have different directions and naturally different magnitudes. It can be easily observed from the figures that there is a stepwise increase in the magnitudes from left side to the right side of the display. For a few adjacent pixels, the luminance of the rays emitted is the same which clearly shows that the image received by the viewer is addition of vertical slices of different directional images.

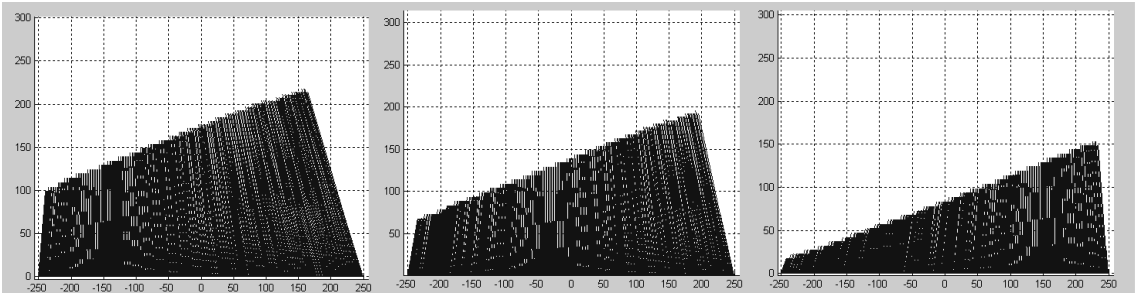

Figure 3-20 The viewer will (i) at left side of the display, (ii) at the center of the display, (iii) at the right side of the display. The above pictures are received by the left eye and the below ones are received by the right eye

As mentioned above, there are discontinuities in the vertical slices by nature of the display concept. Figure 3-21 illustrates clearly the discontinuities in the vertical slices received by the viewer from a specific direction. It can also be observed from the Figure 3-21 that by going further away from the display, the vertical slice received from a specific direction also enlarges.

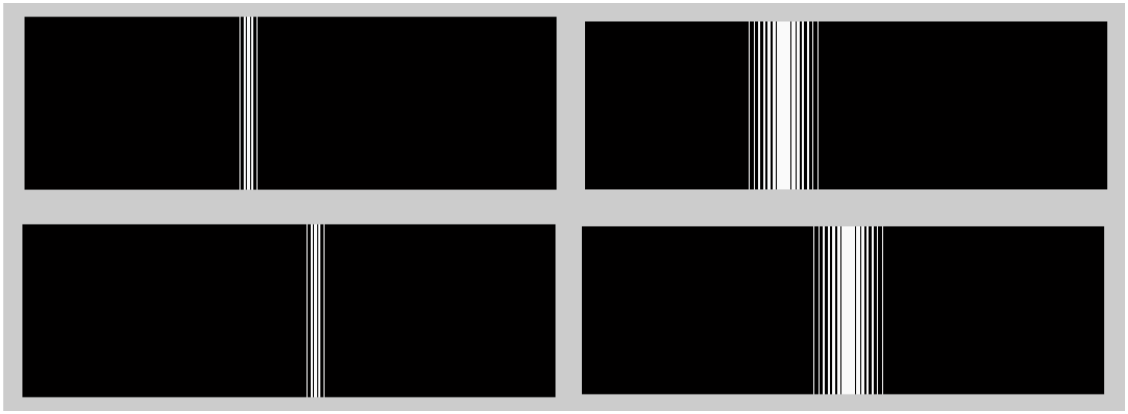

Figure 3-21 The vertical slice received by the viewer located at the center of the display (left eye -32.5 mm and right eye 32.5 mm) from a specific direction (direction normal to the plane of the display), (i) at 500 mm distance (ii) at 2000 mm distance to the display

Chapter 4 OPTICAL SYSTEM ANALYSIS AND MODULE LEVEL OPTIMIZATIONS

The total system can be analyzed in three successive planes, the plane of 2D array of 1D LED arrays, the plane of elliptical diffusing screen and the plane of the viewer as illustrated in Figure 4-1. Both system level and module level simulations are done using non-sequential mode of commercial ray tracing tool ZEMAX^{TM} while lens optimizations are done with sequential mode. The modeling of the LED array, diffusing screen and the viewer planes will be analyzed successively in subsections 4.1 and 4.2.

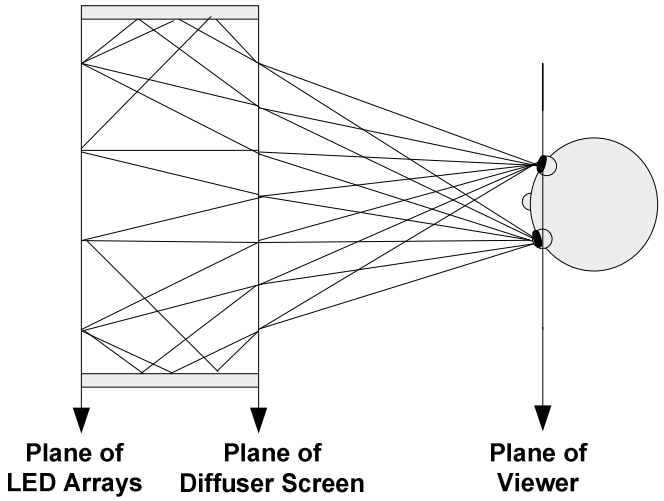

Figure 4-1 The LED Array, Diffuser Screen and Viewer Planes

In 4.1, together with 2D array of 1D LED array plane modeling analysis, the system brightness calculations will also be realized. After modeling the LEDs, diffuser screen and

the viewer, single module lens optimizations will be done in 4.3 to be fully equipped to realize the system level analysis in 4.4.

4.1 Light Source Modeling and Display Brightness

4.1.1 Luminance Calculations

Luminance is the scientific term that is used for "Photopic Brightness" specifying the perceived brightness of an object **[45]**. It is one of the most important parameters in determining the picture quality of a display. The brighter displays are more pleasing to the eye and can be viewed more easily. The frequently used units for luminance are nit (=candela per meter square, cd/m^2) and the British unit foot Lambert (fL). A foot Lambert equals to $1/\pi$ candela per square foot which equals to 3.4262591 nits. For indoor display systems, 250 nits is a good level of luminance while at least 1000 nits are needed for good outdoor display systems. CRT monitors have typical luminance between 50 – 150 units. The other important photometry units are:

- Luminous Intensity: Measure of the light power emitted in a specific direction from a light source weighted according to the wavelength of the light. The weighting is realized according to the standardized sensitivity model of the human eye. Its unit is candela (lumen per steradian) **[46]**.
- Luminous Flux: Measure of the total perceived power of light emitted from a light source. Lumen is the unit of luminous flux. One lumen is the flux produced by a light source emitting one candela of luminous intensity into one steradian solid angle
- Illuminance: Total luminous flux per unit area of surface. Lumen per meter square (Lux) is the unit of illuminance.

Solid angle is another important concept that is widely used in photometry. Solid angle subtended by a surface is the projection area of the surface onto a sphere scaled with the square of the sphere's radius. It is a measure of how big a surface appears to an observer standing at the center of the sphere. A large object far from the observer can subtend the same solid angle with a small object closer to the observer. The solid angle unit is steradian and the maximum solid angle that can be subtended by a surface encircling the center of the sphere is 4π steradian **[46]**, **[47]**. The solid angle is calculated with the following surface integral:

$$\Omega = \iint_S \frac{\hat{n}.da}{R^2} \tag{4.1}$$

- $\hat{n}$: unit vector in the direction of line drawn from the origin – center of the sphere to the infinitesimal surface patch
- da: differential area of a surface patch
- R: the distance from the point to the surface patch

In spherical coordinates, the solid angle can be calculated with the following surface integral:

$$\Omega = \iint_S \sin\phi \, d\theta \, d\phi \tag{4.2}$$

- θ: the spherical azimuth angle in the x-y plane
- φ: the polar angle measured from the z axis

In the LED array based 3D display system, Light Emitting Diodes (LED) are used as the light sources of the display. LEDs together with laser diodes (LD) are non-Lambertian light sources called quasi-homogenous sources while the natural light sources are Lambertian. The LEDs can be most accurately modeled based on the measurement of its emission profile. The LED's emission is measured from all possible angles using a

radiometric ganiometer (i.e. an integrating sphere employing a small entrance aperture and a sensitive photo detector) and LED is modeled according to the collected data **[47]-[50]**. However, the collected data modeling the LED is only valid for that specific LED and cannot be used as a generic LED source. A generic LED can be modeled as an extended light source with light emission varying according to the emission angle with the simplifying constraint that angular distribution of the light emission is the same from all points of the light emitting surface. As a further simplification, the LED can be modeled as a point source if the lateral size of the LED's emission area is smaller than %10 of the distance "R" to the surface of interest which is a valid assumption in the LED array based 3D display system. The approximate relation that is used in ray tracing programs to model point sources with non-Lambertian angular distribution is **[48]**:

$$J = J_0 \cos^n \theta \text{, where n>1} \tag{4.3}$$

- J_0: the luminous intensity at the direction perpendicular to the emission surface
- n = 1 models the Lambertian source

In the above formula, full width half maximum (FWHM) of the source is:

$$\frac{J_0}{2} = J_0 \cos^n \frac{\theta_{FWHM}}{2} \tag{4.4a}$$

$$\theta_{FWHM} = 2\arccos(\sqrt[n]{\frac{1}{2}}) \text{ (120º for n = 1)} \tag{4.4b}$$

n as a function of θ_{FWHM} is:

$$n = \left(-\log_2 \cos(\frac{\theta_{FWHM}}{2}) \right)^{-1} \tag{4.4c}$$

Different half-angle $\theta_{HWHM} = \theta_{FWHM}/2$ and θ_{FWHM} for different integer *n* values can be seen in Table 4-1:

N	Θ_{HWHM}	Θ_{FWHM}
1	60º	120º
2	45º	90º
3	37.5º	75º
4	33º	66º

Table 4-1 θ_{HWHM} and θ_{FWHM} values corresponding to different n values

The solid angle subtended by a circular lens with semi diameter r at a distance d to a point light source as illustrated in Figure 4-2 can be calculated using the following relation **[47]**, **[51]**:

$$\Omega = \int_0^{\arccos(\frac{d_{12l}}{R_{12l}})} \int_0^{2\pi} \sin\phi \, d\theta \, d\phi \tag{4.5a}$$

$$\Omega = -2\pi(\cos(\arccos(\frac{d_{12l}}{R_{12l}})) - 1) \tag{4.5b}$$

$$\Omega = 2\pi(1 - \frac{d_{12l}}{\sqrt{{d_{12l}}^2 + {r_{lens}}^2}}) \tag{4.5c}$$

For small angles, the solid angle can be approximated as:

$$\Omega = \pi {\alpha_{lens}}^2 = \frac{\pi \, {r_{lens}}^2}{{d_{12l}}^2} \tag{4.5d}$$

- d_{12l}: distance from LED array to lens
- R_{12l}: the radius of the sphere the circle is projected

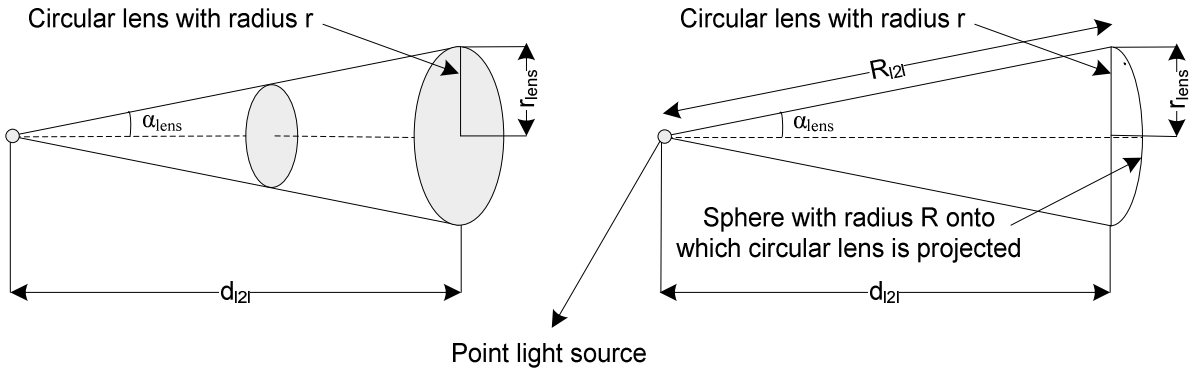

Figure 4-2 Solid angle for a spherical lens

In order to find the flux collected by a circular lens emitted from a non-Lambertian source modeled using the above formula as in the case of "LED Array Based 3D Display Concept", the following surface integral integrating the luminous intensity function of the light source with the solid angle will be used **[47]**, **[48]**, and **[51]**:

$$F_{lens} = \int_0^{\arccos(\frac{d_{12l}}{R_{12l}})} \int_0^{2\pi} J_0 \cos^n(\phi) \sin\phi \, d\theta \, d\phi \tag{4.6a}$$

$$F_{lens} = \frac{2\pi J_0}{n+1}\left[1-\cos^{n+1}(\arccos(\frac{d_{12l}}{R_{12l}}))\right] \tag{4.6b}$$

$$F_{lens} = \frac{2\pi\, J_0}{n+1}\left[1-\left(\frac{d_{12l}}{R_{12l}}\right)^{(n+1)}\right] \tag{4.6c}$$

- J_0: the luminous intensity at the direction perpendicular to the emission surface
- $F_{lens:}$ luminous flux on the screen pixel to a specific direction

The lens will image the luminous flux onto a single pixel area on the screen and the diffuser will diffuse the imaged light into the area according to the vertical and horizontal diffusing angle characteristics. The solid angle subtended by the rectangular shaped output of an elliptical diffuser as illustrated in Figure 4-3 is calculated starting with the surface integral of Equation 4.7a:

$$\hat{n}.da = \cos\phi \, dx \, dy \tag{4.7a}$$

$$R^2 = x^2 + y^2 + d^2 \tag{4.7b}$$

$$\cos\phi = \frac{d_{s2v}}{\sqrt{x^2 + y^2 + d^2}} \tag{4.7c}$$

According to the above values, the surface integral giving the solid angle will be:

$$\Omega = \int_{-a}^{a}\int_{-b}^{b} \frac{d_{s2v}}{(x^2 + y^2 + {d_{s2v}}^2)^{3/2}} \, dx \, dy \tag{4.8a}$$

$$\Omega = 4\arcsin\left(\frac{ab}{\sqrt{(4{d_{s2v}}^2 + a^2)(4{d_{s2v}}^2 + b^2)}}\right) \tag{4.8b}$$

$$\Omega = 4\arcsin(\sin\alpha \, \sin\beta) \tag{4.8c}$$

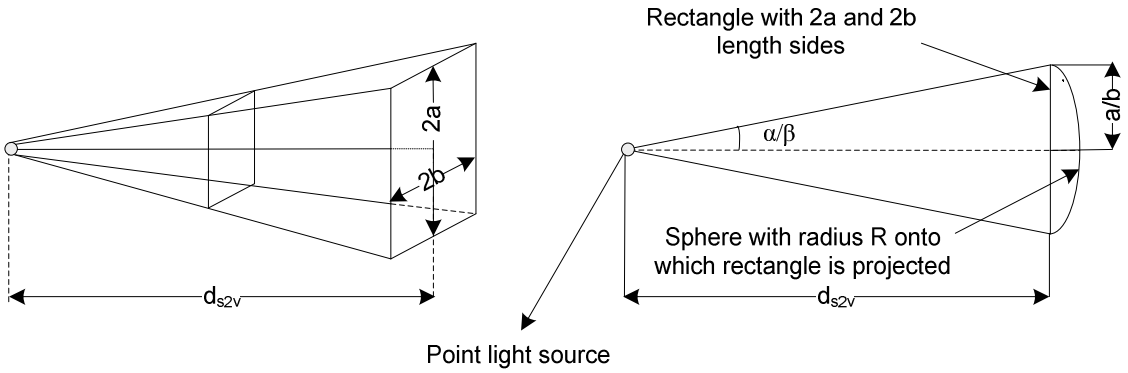

Figure 4-3 Solid angle for the rectangular output of an elliptical diffuser

This calculated solid angle gives the area that the luminous flux imaged to a single screen pixel with a single emission direction on the diffuser screen will be diffused. If the diffuser is uniformly diffusing the light, the eye will collect the amount of the flux according to the solid angle entrance pupil of eye subtends, having 5 mm diameter in average (it varies between 2mm-8mm according to the ambient brightness):

$$F_{eye} = T_{lens}\ F_{lens} \frac{2\pi(1-\frac{d_{s2v}}{R_{eye}})}{4\arcsin(\sin\alpha\ \sin\beta)} \tag{4.9a}$$

$$F_{eye} = T_{lens}\ \frac{2\pi\ J_0}{n+1}\left[1-\left(\frac{d_{l2l}}{R_{l2l}}\right)^{(n+1)}\right]\frac{2\pi(1-\frac{d_{s2v}}{R_{eye}})}{4\arcsin(\sin\alpha\ \sin\beta)} \tag{4.9b}$$

- F_{eye}: luminous flux collected by the eye emitted from a screen pixel to a specific direction
- T_{lens}: transmission coefficient of the lens
- d_{s2v}: distance from screen to the viewer
- R_{s2v}: the radius of the sphere the entrance pupil of the eye is projected on

The luminance of the display can be calculated either from the flux collected by the entrance pupil of the eye or from the flux on the screen:

$$L_{eye} = \frac{F_{eye}}{\mathrm{A}_{\mathrm{eye}}\Omega_{\mathrm{eye}}} = \frac{T_{lens}\ \mathrm{F}_{\mathrm{lens}}\ \frac{2\pi(1-\frac{d_{s2v}}{R_{s2v}})}{4\arcsin(\sin\alpha\ \sin\beta)}}{\pi\ r_{eye}{}^2\ 4\arcsin(\frac{d_p{}^2}{d_p{}^2+4d_{s2v}{}^2})} \tag{4.10a}$$

- Ω_{eye}: solid angle of the eye pupil
- r_{eye}: eye pupil radius

For relatively small values of d_p and r_{lens} when compared with the viewer distance to the screen, the received luminance by the viewer will be:

$$L_{eye} = \frac{T_{lens}\ \mathrm{F_{lens}}\ \dfrac{\pi \dfrac{r_{eye}^{\ 2}}{d_{s2v}^{\ 2}}}{4\arcsin(\sin\alpha \sin\beta)}}{\pi\, r_{eye}^{\ 2}\ \dfrac{d_p^{\ 2}}{d_{s2v}^{\ 2}}} = \frac{T_{lens}\ \mathrm{F_{lens}}}{4\arcsin(\sin\alpha \sin\beta) d_p^{\ 2}} = L_{diffuser} \qquad (4.10b)$$

The luminance calculations for the exemplary display systems proposed in Table with d_m =3 mm, D=160 and d_m =5 mm, D=268 mm, the luminance calculations of the system consisting of 100, 250 and 500 millicandela LEDs. The calculations show that, the more compact display system with d_m =3 mm has better luminance values as the number of screen pixels that should be illuminated by each scanner is less in the compact system design. Both of the systems have promising luminance values. By using 40 milliCandela LEDs, both systems have enough luminance values similar to conventional display systems such as LCDs:

		Design 1			***Design 2***		
lens diameter (r_{lens})	mm	1.25			2		
LED to lens dist. (d_{l2l})	mm	14,6216			24,3694		
display depth (D)	mm	160			268		
Solid Angle of the Lens	steradian	0,02379			0,021034		
T_{lens}	unitless	0.95			0.95		
		LED1	***LED2***	***LED3***	***LED1***	***LED2***	***LED3***
Luminous Intensity at 0º (J_0)	mCandela	10	25	40	10	25	40
LED luminous intensity function		Cos(α)	$Cos^2(\alpha)$	$Cos^3(\alpha)$	Cos(α)	$Cos^2(\alpha)$	$Cos^3(\alpha)$
Luminous flux after (F_{lens})	mLumen	0.2256	0.5628	0.8985	0.1995	0.4978	0.7953
(Screen. To viewer distance) d_{s2v}	mm	500	500	500	500	500	500
Diffusing Angles (H/V)	degree	0.8/60	0.8/60	0.8/60	0.8/60	0.8/60	0.8/60
(Solid Angle of Diffuser) Ω	steradian	0.0140	0.0140	0.0140	0.0140	0.0140	0.0140
(Solid Angle of Eye Pupil) Ω_{eye}	steradian	7,8538 E-05	7,8538 E-05	7,8538 E-05	7,8538 E-05	7,8538 E-05	7,8538 E-05
Ω_{eye} /Ω	unitless	0,00562	0,00562	0,00562	0,00562	0,00562	0,00562
Luminous flux at eye pupil(F_{eye})	mLumen	0.001268	0.003160	0.00506	0.00112	0.002805	0.004473
(Luminance) L_{eye}	*nit*	16155	40311	64376	14287	35658	56956
$L_{diffuser}$	nit	160155	40311	64375	14287	35658	56958
(number of addressed pixels by scanner) p	unitless	150	150	150	250	250	250
(Luminance of the display)L	nit	80,77	201,55	321,87	44.647	111.42	178

Table 4-2 Brightness calculations for two systems with d_m=3, r_{lens}=1.25 mm and d_m=5, r_{lens}=2

4.1.2 Light Source Modeling

The LEDs luminous intensity distributions are modeled as a certain power of cosine function specified according to the FWHM angle of the LEDs as mentioned in Section 4.2.1. However, in these analyses, light sources with Gaussian distribution generally used for modeling laser diodes are used throughout the analysis due to their flexibility for the ray tracing tool. The angular intensity distribution function of the light sources used in the analysis is **[52]**:

$$I(\theta_x,\theta_y) = I_0 \exp\left[-2\left((\frac{\theta_x}{\alpha_x})^{2G_x} + (\frac{\theta_y}{\alpha_y})^{2Gy}\right)\right] \tag{4.11}$$

- α_x, α_y are the divergence angles in XZ and YZ planes respectively
- G_x, G_y are "supergaussian" factors and for a typical Gaussian distribution, they are equal to one

The α_x, α_y values can also be denoted as a function of FWHM angle:

$$\frac{I_0}{2} = I_0 \exp\left[-2(\frac{\theta_x}{\alpha_x})^2\right] \tag{4.12}$$

$$\alpha_x = \frac{\theta_{FWHM}}{\sqrt{2\ln 2}} \tag{4.13a}$$

$$\alpha_x = (0.8493218)\theta_{FWHM} \tag{4.13b}$$

For a light source having FWHM value of 30° (0.524 radian) in both x and y directions, the divergence angles α_x, α_y would be 25.48° (0.445 radian). As it can be seen in Figure 4-4 luminous intensity distributions for the Gaussian and cosine power are very close to each other for the same FWHM angles especially at smaller angles **[52]**.

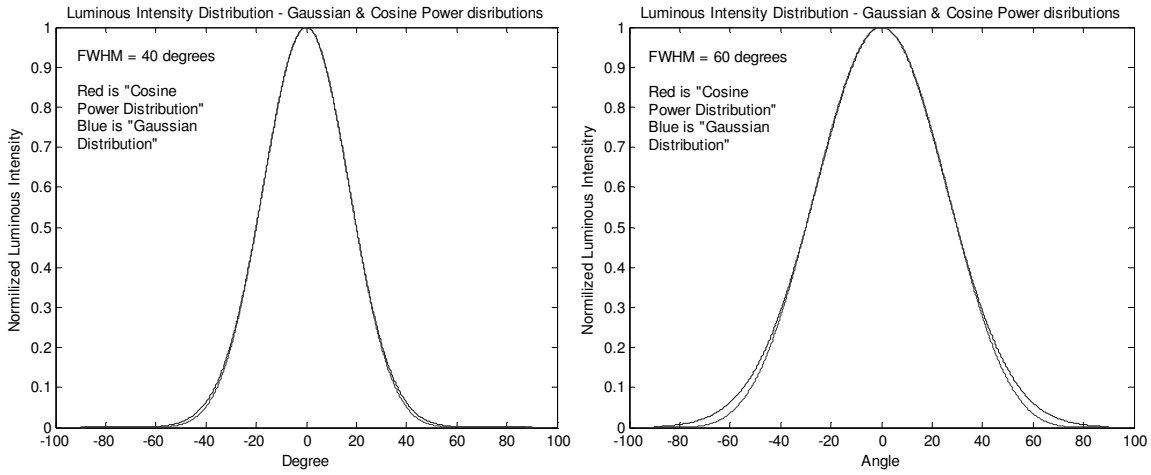

Figure 4-4 The Cosine Power and Gaussian Distributions for 40° and 60° FWHM

The light sources also have a Gaussian spatial intensity distribution:

$$I(x,y) = I_0 \exp\left[-2\left(\left(\frac{x}{s_x}\right)^{2H_x} + \left(\frac{y}{s_y}\right)^{2Hy}\right)\right] \tag{4.14}$$

$$-W_{x,y} < x, y < W_{x,y} \tag{4.15}$$

- s_x, s_y are the Gaussian width of the spatial distribution in the X,Y directions
- H_x, H_y are X,Y direction spatial distribution super Gaussian factor
- W_x, W_y are X,Y direction half widths of the rectangular region LEDs are emitting light arrays

The light sources with Gaussian distribution are suitable to model LEDs in the display optical simulation and analysis.

4.2 Plane of Elliptical Diffusing Screen and Viewer

4.2.1 Elliptical Diffusing Screen

In order to model the elliptical diffusing screen that diffuses the incoming light with a narrow angle in horizontal direction and with a wide angle in vertical direction; a plane surface is generated having a scattering function realizing the requirements of the elliptical diffuser. Two different scattering functions, Gaussian and uniform are generated. For generating a pair of independent standard normally distributed (zero expectation, unit variance) random numbers from uniformly distributed random numbers, Box-Mueller transform is used. According to Box-Mueller transform, if U_1, U_2 are two independent, uniformly distributed random numbers in the interval of [0, 1), two independent standard normally distributed random numbers ($Z_0^{'}$, $Z_1^{'}$) can be generated as follows **[53]**:

$$Z_0^{'} = \sqrt{-2\ln(U_1)}\cos(2\pi U_2) \tag{4.16a}$$

$$Z_1^{'} = \sqrt{-2\ln(U_1)}\sin(2\pi U_2) \tag{4.16b}$$

The two random numbers $Z_0^{'}$, $Z_1^{'}$ are multiplied with separate parameters (α_x, α_y) that can be controlled by the user externally to specify the divergence angles in wide angle and narrow angle diffusing directions to determine the final scattering amounts Z_0, Z_1:

$$Z_0 = \alpha_x\sqrt{-2\ln(U_1)}\cos(2\pi U_2) \tag{4.17a}$$

$$Z_1 = \alpha_y\sqrt{-2\ln(U_1)}\sin(2\pi U_2) \tag{4.17b}$$

The diffuser is assumed to be "z = k" plane and Z_0, Z_1 are added onto the specular ray's x (narrow angle diffusing direction) and y (wide angle diffusing direction) components in

the diffuser plane respectively and the scattered ray projected into the diffuser plane is obtained. The magnitude of the new scattered ray in the diffuser plane is compared with 1.0 to validate that the scattered ray is in unit circle. If it is not in the unit circle, new random numbers are generated and a new scattered ray is constituted. If it is in the unit circle than with magnitude M, it is completed to unit vector by adding the vector normal to the diffuser plane with magnitude $\sqrt{1-M^2}$.

$$s_i = s_x\vec{x} + s_y\vec{y} + s_z\vec{z} \tag{4.18}$$

$$M_G = \sqrt{(Z_0 + s_x)^2 + (Z_1 + s_y)^2} \tag{4.19}$$

$$s_o = (Z_0 + s_x)\vec{x} + (Z_1 + s_y)\vec{y} + (\sqrt{1 - M_G{}^2})\vec{z} \tag{4.20}$$

The same methodology is used in the case of uniform distribution and instead of adding two independent standard normally distributed random numbers (Z_0, Z_1), (U_1, U_2) are added to X and Y components of the specular ray.

$$M_U = \sqrt{(\alpha_x U_0 + s_x)^2 + (\alpha_y U_1 + s_y)^2} \tag{4.21}$$

$$s_o = (\alpha_x U_0 + s_x)\vec{x} + (\alpha_y U_1 + s_y)\vec{y} + (\sqrt{1 - M_U{}^2})\vec{z} \tag{4.22}$$

4.2.2 Plane of the Viewer

There are literally many different eye models that are published since mid 19th century from very complex ones consisting of more than 4000 refracting surfaces to very simple reduced ones consisting of only single refracting surface. It should be mentioned that a more complex model is not always a better one and different eye models can be more appropriate for different purposes. Vertical cross section of a quite accurate eye model developed for non sequential mode analysis of ZEMAX™ can be seen in Figure 4-5.

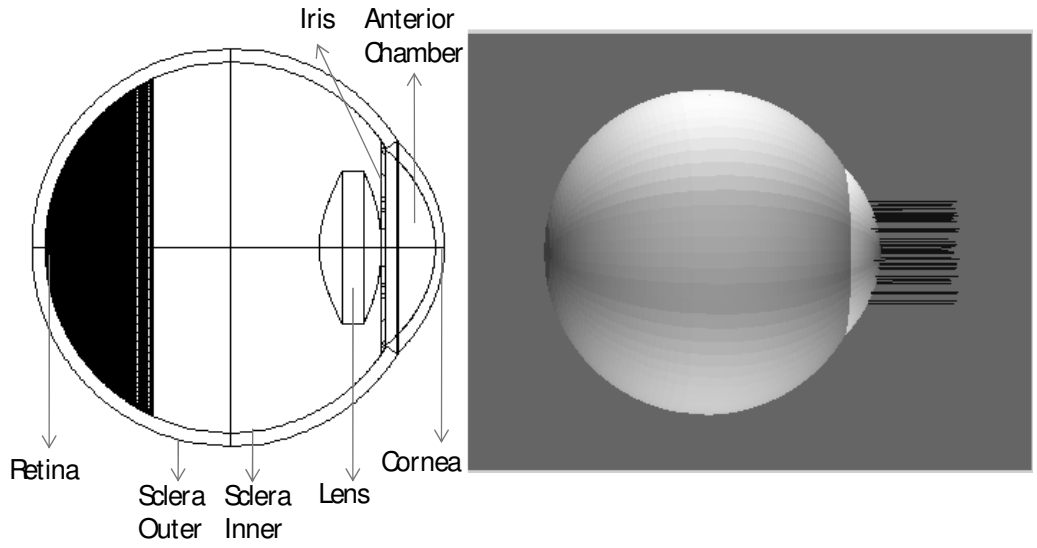

Figure 4-5 Vertical Cross-Section of the Eye

The model includes all the key biological components along the optical axis. The first part on the optical axis that the light enters through is the cornea with a refractive index of 1.376. The sudden change of refractive index from 1.0 to 1.376 when the light bundles are entering the cornea, results in high amount of bending. Actually the cornea provides approximately, %73 of the total refractive power of the eye **[54]**. The next surface behind the cornea is anterior chamber providing the essential nutrients for the cornea. Anterior chamber has a close refractive index (1.336) to the refractive index of cornea so that little bending occurs when the light moves *from* cornea to anterior chamber. The next part is the iris including the pupil with adjustable diameter – 2 mm under high brightness conditions and 8 mm under low brightness conditions, controlling the amount of light entering to the eye. The light passing through the eye pupil enters to the crystalline lens that fine-tunes the light bending to form a sharp image on the retina. The crystalline lens changes its shape according to the tension amount of the ciliary muscle connected to its periphery by fibers.

Tenser muscles result in a more curved lens with higher bending power and the eye forms a sharper image of the closer objects. The relaxed muscles results in a less curved lens with lower bending and the eye forms a sharper image of the distant object **[54]**. After the crystalline lens, the light enters to the posterior chamber with a refractive index of 1.336. On the back wall of the sclera inner, behind the posterior chamber the retina is positioned. Retina converts the optical energy into electrochemical energy.

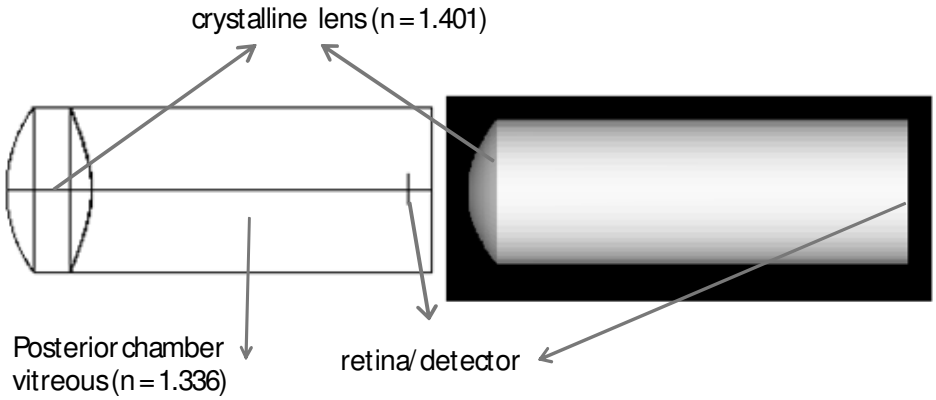

Figure 4-6 The reduced eye model including the crystalline lens

In the current design, a reduced version of the eye model only including the crystalline lens is used as illustrated in Figure 4-6. The crystalline lens' first surfaces has radius of 10 mm and second surface has radius of -6 mm with a conic value of -3.25 in relaxed mode. When the eye tries to focus to different depths, the changing parameters in the eye model are the radius of the first surface, the conic value of the second surface, the thickness of the crystalline lens and the distance of the second surface to the eye retina.

4.3 Optical Design of a Single Scanning Module

As mentioned in Chapter 3, the LEDs mounted onto the scanners are simply imaged onto the screen and each LED constitutes of the display pixels on the scan path of the scanner it is placed on. There are some critique requirements in the imaging properties of the single lens imaging system:

- The pixel sizes – LED images should be smaller than 1 mm for all the pixels. This is a condition that should be satisfied independent of the LED pitches which means that with changing LED sizes, the magnification of the system should be changed. As the scanners are scanning with fairly high scan angles, LEDs are imaged onto an arc that results in different image planes for different scan angles. The deviation amount can be simply formulated with the following equation:

$$D = r - r\cos(\frac{\theta_{TOSA}}{2}) = r(1-\cos(\frac{\theta_{TOSA}}{2})) \tag{4.23}$$

For small angles:

$$D \cong \frac{r\theta_{TOSA}^{\ 2}}{8} = \frac{d_{lens}^{\ 2}}{8r} \tag{4.24}$$

For a system with 50º FOV, the scanners should have 50º total optical scan angle (TOSA) and corresponding deviation between image planes for 0º and 25º scan angles at a distance of 300 mm would be approximately 28 mm. The screen should be placed in an optimum distance in this 28 mm range.

- The emission angle of the display pixels should not surpass the angular resolution (R_A) of the display. This critique condition should be satisfied in order to prevent the cross talk between different emission directions. As mentioned in 3.1, the emission direction divergence before the diffuser is directly related with the imaging lens diameter and screen distance.

As each scanner module has an LED array for each primary color, the screen distance, the lens shape and the lens material (with high Abbe number) should be specified to minimize the chromatic aberrations. An achromatic doublet lens is also designed as an alternative lens with minimized chromatic aberration.

4.3.1 Single Spherical Lens Design

The first lens design is realized for a candidate system with 1° angular resolution (R_A) and 50 different light directions from each pixel. The screen pixels are the images of LEDs having 80 μm pitches with 20 μm spacing between each other which necessitates 10X magnification. For different display resolutions, the critical system parameters are shown in below Table 4-3:

Voxels	$2x10^6$	$20x10^6$	$65x10^6$	
N_H	240	720	1440	Unitless
N_v	160	576	900	Unitless
n_h	48	144	288	Unitless
n_v	5	18	30	Unitless
d_m	**5**	**5**	**5**	Mm
d_p	**1**	**1**	**1**	Mm
r	**50**	**50**	**50**	Degree
R_A	**1**	**1**	**1**	Degree
L_D	**4**	**4**	**4**	Mm
led_p	**80**	**80**	**80**	μm
Display Thickness	**268**	**268**	**268**	Mm

Table 4-3 Candidate System Parameters

The lens diameter (L_D) is chosen as 4 mm, as the distance between adjacent modules (d_m) is 5 mm. The display thickness is 268 mm to provide the essential angular resolution

of 1º so that in the imaging system the distance between object plane (plane of scanner modules) and image plane (display screen plane) should be 268 mm. This is one of the critical constraints used in the optimization step. For a 10X system with 268 mm thickness, the focal length of the imaging lens should be approximately 25 mm which constraints the f/# of the system approximately to 6.

The lens thickness is also critical as the thicker lenses with more mass would degrade the scanner performance dramatically. The lens edge thickness corresponding to the minimum lens thickness can be easily calculated from:

$$t_{lens} \cong \frac{d_{lens}{}^2}{8r} \cong \frac{d_{lens}{}^2}{8}\left(\frac{1}{R_1}-\frac{1}{R_2}\right) \cong \frac{d_{lens}{}^2}{8 f_\lambda (n_\lambda - 1)} \tag{4.25}$$

For a lens with 25 mm focal length, 4 mm diameter and 1.5 refraction indexes, the edge thickness of the lens would be approximately 0.16 mm. During the optimizations, the lens thickness is limited with 2 mm.

Optimizations are done with sequential mode of commercial ray tracing tool ZEMAX^{TM} using three different wavelengths – 486, 588, 656 (F, d, C – Fraunhofer notation) nanometers (nm) for three different configurations specified with changing positive scan angles 0º, 12.5º, and 25º. 10 field points are used with 200 μm spacing from 0.05 mm to 1.85 mm. As the system is circular symmetric, only positive scan angles and positive field points are enough to use in optimizations. The optimized imaging lens can be seen in Figure 4-7. BK7 is chosen as the glass type. The thickness of the lens is smaller than 1 mm.

Surf:Type		Comment	Radius		Thickness		Glass		Semi-Diameter		Conic
OBJ	Standard	239	Infinity		0.000000				1.890000		0.000000
1	Standard		Infinity		27.139074	V			1.890000		0.000000
STO*	Standard	LA1289	144.726565	V	0.898821	V	BK7		2.000000	U	0.000000
3*	Standard		-14.285058	V	0.000000				2.000000	U	0.000000
4	Coordinate B..				0.000000		-		0.000000		
5	Standard		Infinity		241.960363	V			1.874053		0.000000
IMA	Standard		Infinity		-				250.000000	U	0.000000

Figure 4-7 The optimized single imaging lens properties

The spot diagrams for the three different wavelengths at the three different configurations for the field points of 0.05, 0.65, 1.25 and 1.85 mm can be seen in the below Figure 4-8. As the 586 nm is the central wavelength, the optimization results are closer to the ideal solution for 586 nm wavelength. At the configurations where the spot diagrams for 656 nm are larger, the spot diagrams for 486 are smaller. The corresponding RMS spot radius values for each spot are listed in Table 4-4.

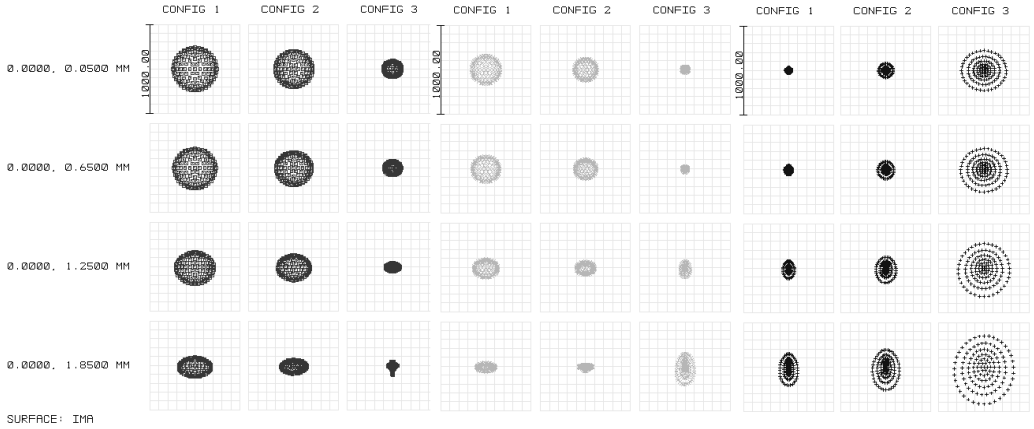

Figure 4-8 The Spot Diagrams of 4 different field points at each primary wavelength and scan angle

In the current system, diffraction limited radius are 57.93, 51.87 and 42.91 μm for red (656 nm), green (588 nm) and blue (486 nm) wavelengths respectively. According to the

optimization results, for each wavelength there are specific field points with a specific scan angle which the spot radius approach to the diffraction limited radius of the imaging system.

	RMS Radius of Field Points at Different Scan Angles								
Field Position	**486 nm**			**588 nm**			**656 nm**		
	0 º	12.5 º	25 º	0 º	12.5 º	25 º	0 º	12.5 º	25 º
0.05 mm	21.7	46.0	160.6	140.1	111.5	25.5	203.8	177.3	87.2
0.65 mm	27.0	55.4	171.5	130.7	101.9	24.8	194.4	167.6	77.2
1.25 mm	50.1	82.6	201.7	106.0	77.5	43.2	169.1	141.9	53.2
1.85 mm	94.3	128.9	251.8	71.3	103.7	90.5	130.2	103.5	44.3

Table 4-4 RMS Spot Radius for 4 different field points, three different wavelengths and three different scan angles

The Table 4-5 shows the RMS direction cosine values for each wavelength with 0 º, 12.5º and 25º scan angles at 4 different field points. The direction cosines provide critical information about the emission angle of the rays from the pixels which should be smaller than the R_A of the display. RMS direction cosine values in Table 4-5 satisfy the 1º requirement for R_A.

	Angles corresponding to Direct Cosines of Field Points at Different Scan Angles								
Field Position	**486 nm**			**588 nm**			**656 nm**		
	0 º	12.5 º	25 º	0 º	12.5 º	25 º	0 º	12.5 º	25 º
0.05 mm	0.331	0.328	0.316	0.297	0.294	0.284	0.281	0.279	0.269
0.65 mm	0.334	0.330	0.318	0.299	0.296	0.286	0.284	0.281	0.271
1.25 mm	0.340	0.335	0.324	0.305	0.302	0.292	0.289	0.286	0.277
1.85 mm	0.350	0.345	0.334	0.314	0.310	0.300	0.300	0.296	0.286

Table 4-5 Angles corresponding to RMS Direction Cosines for 4 different field points, three different wavelengths and three different scan angles

The largest direction cosine is 0.08356 corresponding to 0.478º between all the wavelengths, configurations and field points, is for the 486 nm wavelength at 1.85 mm field point and 25 º scan angle.

It can be informative to look at the spot diagrams of different fields – four at the middle of 80 µm X 80 µm square LED's edges and one at the center of the LED, relative to the chief ray from the center field point in order to have an idea about RMS radius of pixels on the screen with changing wavelengths. The results can be seen in below figures for two different LEDs, one positioned at 0.05 mm and the other positioned at 1.85 mm.

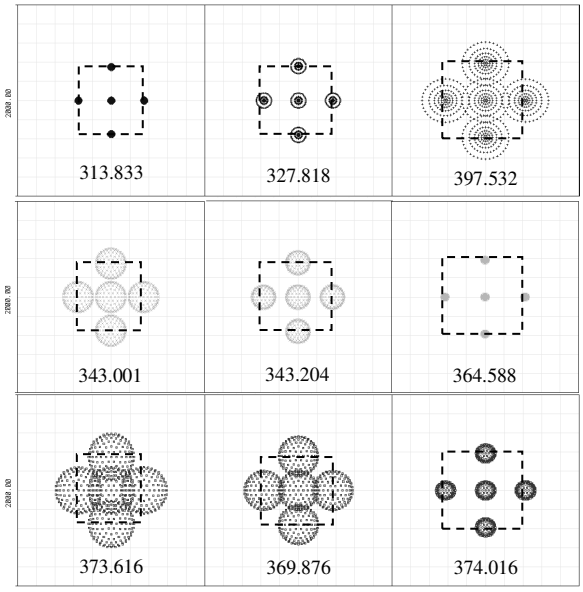

Figure 4-9 The spot diagrams of 4 fields at the middle of LEDs' edges and a field at the center of LED located on 0.05 mm on the same reference system at each primary wavelength and scan angle

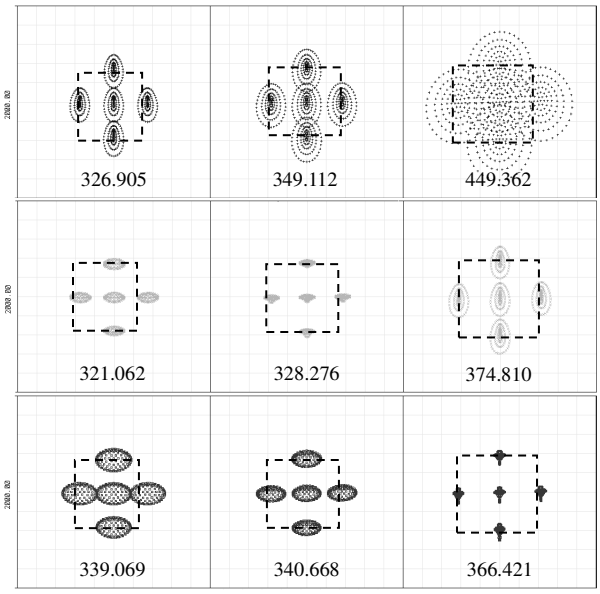

Figure 4-10 The spot diagrams of 4 fields at the middle of LEDs' edges and a field at the center of LED located on 1.85 mm on the same reference system at each primary wavelength and scan angle

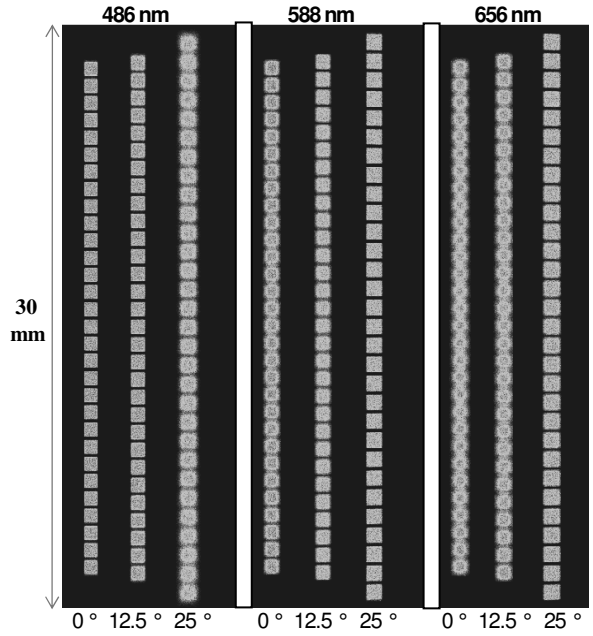

Figure 4-11 The Screen Pixels for each wavelength at 0 º, 12.5 º and 25 º scan angles

The total RMS radius for five field points is varying most at 486 nm wavelength. For 0.05 mm field point RMS radius varies between 313.833 μm and 397.532 μm and for 1.85 mm field point RMS radius varies between 326.905 μm and 449.362 μm. In Figure 4-11, the images of 80 μm X 80 μm LEDs on the screen can be seen for each wavelength at 0 º, 12.5 º and 25 º scan angles.

For qualitative measure of the LED images on the screen it is quite insightful to investigate using "Geometrical Image Analysis" of ZEMAX^{TM}. In geometrical image analysis, the light sources are defined with definite sizes instead of dimensionless point sources and a certain amount of rays are traced to the image plane from the region the light source is occupying. The image of 30 LEDs scanning on a scanner module can be seen in Figure 4-11 for each wavelength at 0 º, 12.5 º and 25 º scan angles. The imaging quality variations for different wavelengths, for different scan angles and also for different spatial coordinates can be seen in the figure. Actually, the variations are in a small range and all the LED images are resolvable. The important problem appearing in the analysis is the varying magnification for different scan angles as expected. In the system as different modules illuminate the same pixel with different scan angles, the different directions of a pixel will not overlap in the vertical direction. However, such problems are common in scanning displays such as Cathode Ray Tube (CRT) and projectors and they can be corrected electronically.

4.3.2 Achromatic Doublet Lens Design

The spot radius variance between different wavelengths stemming from the variation of refraction index with wavelength is acceptable for the current system requirements. However by using achromatic doublet lenses consisting of a convex and concave lens of different glasses cemented to each other, the spot size variations depending on wavelength can be minimized. The first glass in the achromatic doublet is generally is a convex lens

with higher Abbe number – has lower dispersion while the second glass is a concave lens with lower Abbe number – higher dispersion. An achromatic doublet lens design for the same system requirements can be seen in Figure 4-12. The first glass of the lens is chosen as BK7 (Abbe number = 64.2 – crown glass) and the second one as SF2 (Abbe number = 33.8 – flint glass).

Surf:Type		Comment	Radius		Thickness		Glass		Semi-Diameter		Conic
OBJ	Standard	239	Infinity		0.000000				1.850000		0.000000
1	Standard		Infinity		27.999364	V			1.850000		0.000000
STO*	Standard	LA1289	20.474816	V	0.501231	V	BK7		2.000000	U	0.000000
3*	Standard		-9.610345	V	0.289529	V	SF2	S	2.000000	U	0.000000
4*	Standard		-23.412817	V	0.000000				2.000000	U	0.000000
5	Coordinate B..				0.000000		-		0.000000		
6	Standard		Infinity		241.209880	V			2.012883		0.000000
IMA	Standard		Infinity		-				250.000000	U	0.000000

Figure 4-12 The optimized single achromatic imaging lens properties

The spot diagrams for three wavelengths shows quiet similar aberrations and very close RMS radius at the same configurations and field points as shown in Figure 4-13 and Table 4-6.

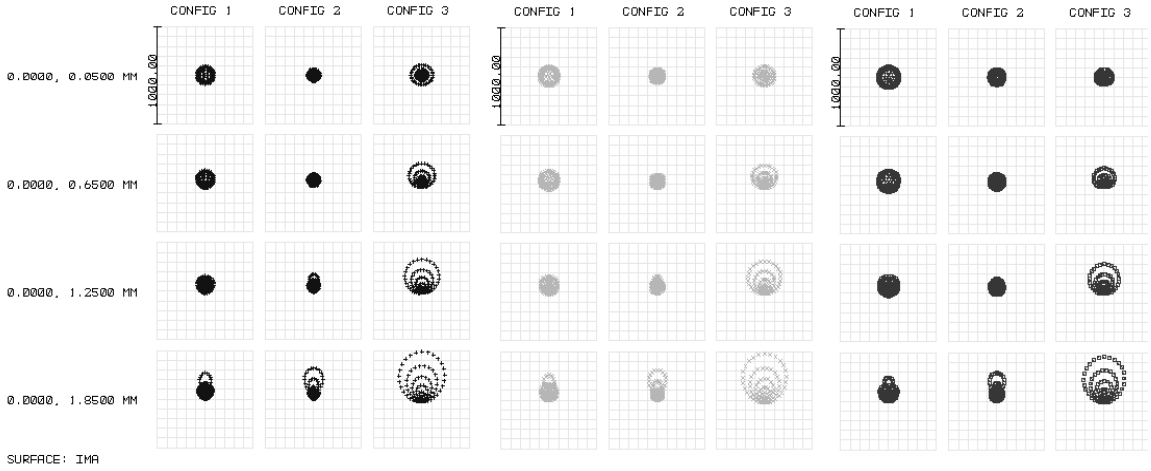

Figure 4-13 The Spot Diagrams of 4 different field points at each primary wavelength and scan angle for the achromatic lens

	RMS Radius of Field Points at Different Scan Angles								
Field Position	**486 nm**			**588 nm**			**656 nm**		
	0 º	12.5 º	25 º	0 º	12.5 º	25 º	0 º	12.5 º	25 º
0.05 mm	79.8	50.7	65.7	85.8	56.7	59.5	96.9	67.8	48.0
0.65 mm	79.8	56.7	86.0	84.9	60.8	80.1	94.9	69.5	69.9
1.25 mm	85.9	77.5	130.3	88.3	77.7	124.3	94.8	80.7	114.5
1.85 mm	110.2	117.8	191.4	109.0	114.8	184.9	109.8	112.0	174.7

Table 4-6 RMS Spot Radius for 4 different field points, three different wavelengths and three different scan angles

4.4 Full System Image Analysis

4.4.1 Single Screen Pixel Analysis

A single pixel on the screen will be illuminated by as many different polymer scanner modules as the number of different ray directions from the pixel which is at least 40. It is vital to prevent crosstalk or unlit regions between the neighbor ray directions. As mentioned in the system level calculations in Chapter 3, for a non-diffusing screen in the horizontal direction, there will be always an unlit or crosstalk regions whether constant or enlarging with a specific small angle that can be controlled by the lens diameter choice. In the below Figure 4-14, the light distribution after the elliptical diffuser can be seen for a single pixel illuminated by 11 different modules with 5 mm distance to each other (d_m) for 3 different horizontal diffusing values of the elliptical diffuser. In each case $L_D = 4$ mm.

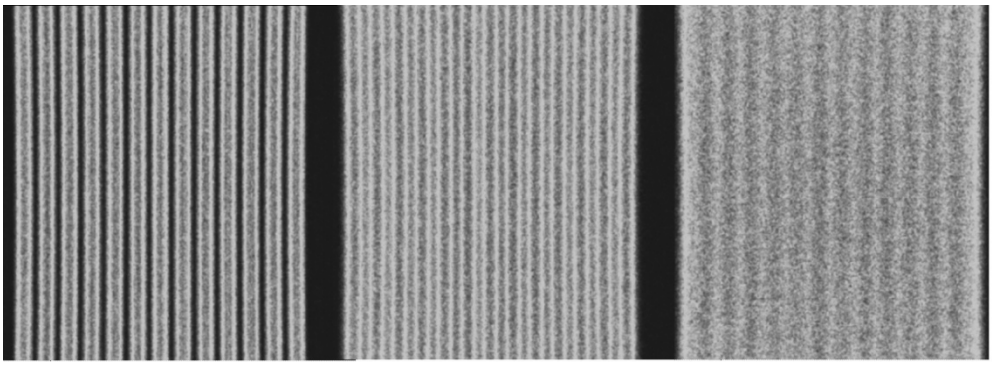

Figure 4-14 The emission of different ray directions from a single pixel without horizontal diffusing, with approximately 0.286° and 0.572° horizontal diffusing

In the case of no horizontal diffuser as illustrated in Figure 4-14(a) (same with using a cylindrical lens array diverging light only in vertical direction), two neighbor emission directions from the single pixel nearly fill the space between their emission directions. There are very narrow vertical regions that are not illuminated. As it is illustrated in Figure 4-14(b), by using an elliptical diffuser, diffusing approximately 0.286° in horizontal direction, these vertical regions are almost illuminated. Diffusing more (approximately 0.572°) in horizontal direction results in crosstalk between neighbor emission directions as shown in Figure 4-14(c).

4.4.2 Multiple Screen Pixel Analysis

The LED array modules are modulated at proper scanning directions with right intensity level according to the image that would be constituted on left and right eye retina. Actually there is a simple mapping from plane of LED modules to the plane of display screen and from the plane of display screen to the plane of the viewer. When each module could be stopped at the scan angle or scan angles that they are illuminating a specific viewer, than

the same image appearing in the eye retina would be on the plane of display and on the plane of LED array modules.

As an example, in order to write “LEFT” to the left eye retina end “RIGHT” to the right eye retina, the same 13 modules located between -30 mm and 30 mm with 5 mm interval between each other in horizontal direction, write “LEFT” and “RIGHT” to the screen at a different “direction set” of the scanning modules. The left eye is located at “-30” mm in horizontal direction and 1000 mm away from the screen while the right eye is located at “30” mm in horizontal direction and again right eye is 1000 mm away from the screen. As illustrated in Figure 4-15, “LEFT” is located at left hand (-30 to 18 mm) relative to “RIGHT” (-18 to 30 mm) as they are sent to a left and right hand location respectively.

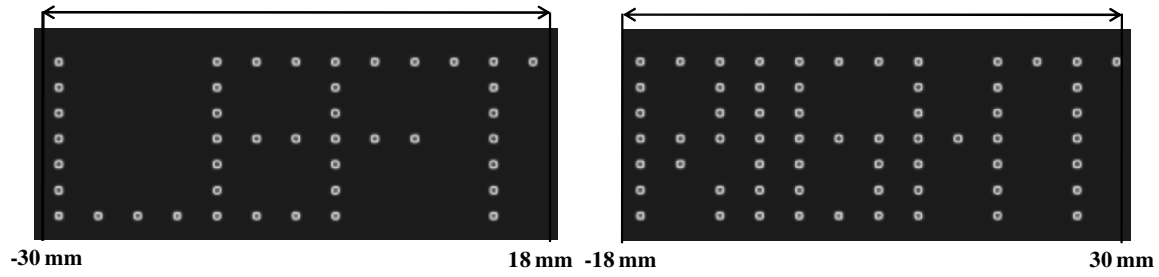

Figure 4-15 “LEFT” and “RIGHT” is written to the screen with different direction set of same scanning modules.

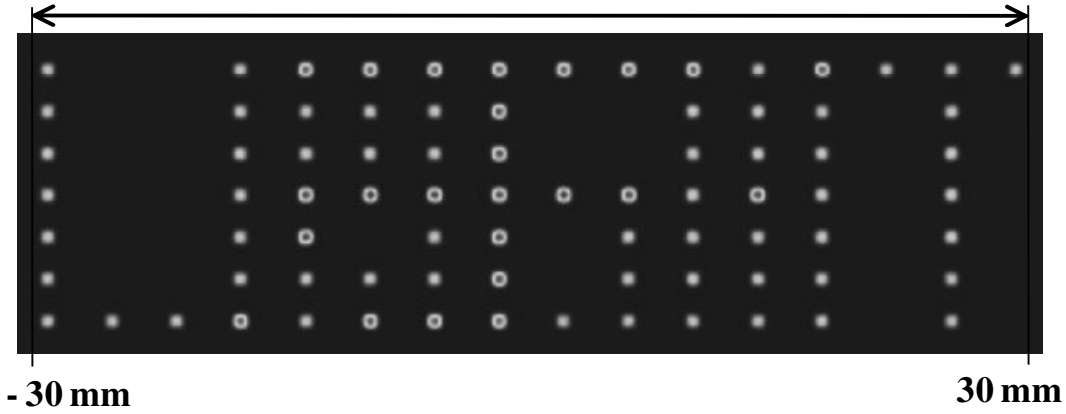

Figure 4-16 "LEFT" and "RIGHT" are on the screen at the same time. The brighter pixels are the ones that are sending information both to the left and right eye

If "LEFT" and "RIGHT" are observed at the same time on the display screen, it can be easily realized that some of the screen pixels will emit light to both left and right eye as shown in Figure 4-16. In Figure 4-16, the screen pixels that are brighter than the others are the ones that are illuminating both eyes.

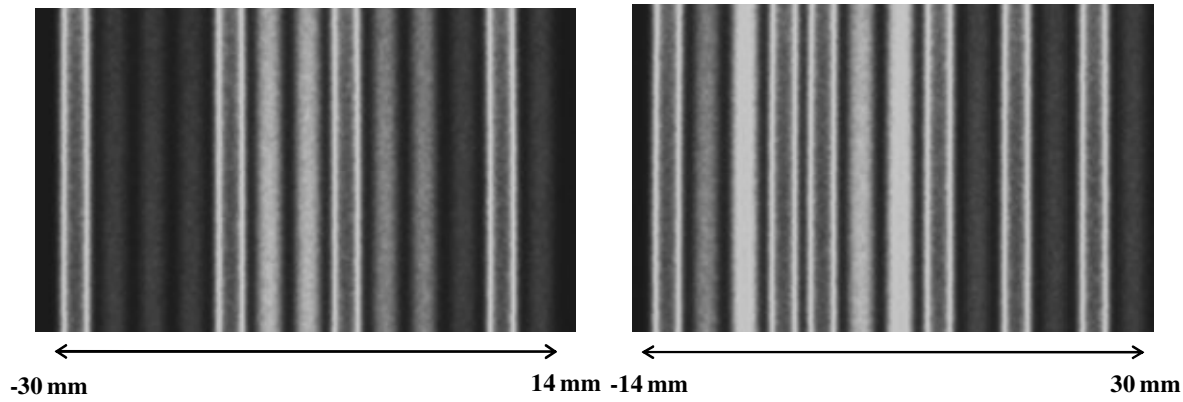

Figure 4-17 "LEFT" to the left eye and "RIGHT" to the right eye after diffused by the elliptical diffusing screen

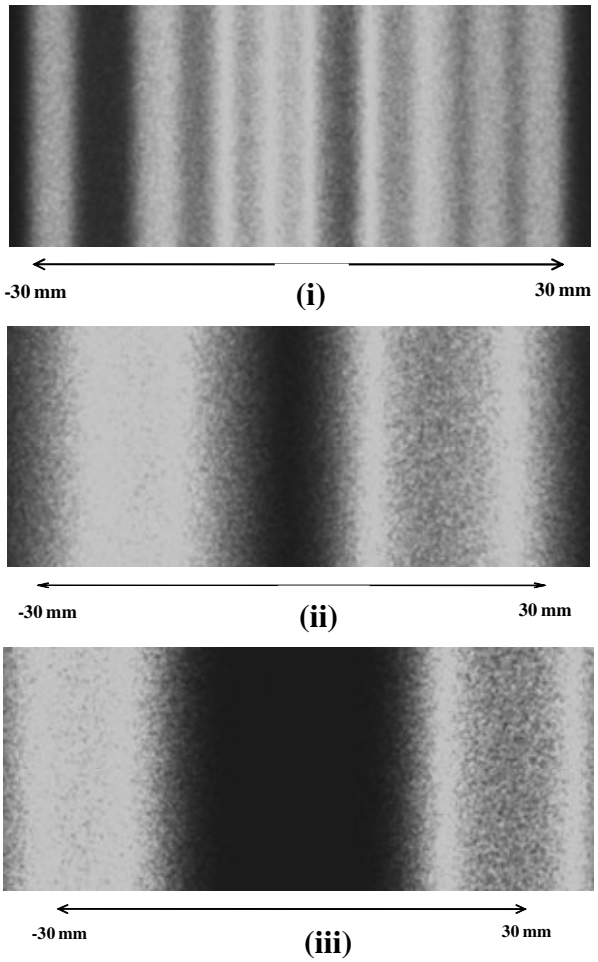

Figure 4-18 "LEFT" and "RIGHT" together after diffused by the elliptical diffuser (i) at 250 mm from the screen (ii) at 600 mm from the screen (iii) at the viewer plane 1000 mm from the screen

The screen would diffuse the directional rays elliptically with wide angle (60°) in vertical direction and very narrow angle (0.5°) in horizontal direction. The Figure 4-17 shows the "LEFT" and "RIGHT" after diffused with the elliptical diffusing screen at 50 mm distance from the screen. There will be intensity differences between different elliptically diffused strips changing according to the number of screen pixels diffused to the

same vertical strip. It is expected that the vertical strips of the "LEFT" and "RIGHT" will converge to one wider strip at left eye and right eye position respectively as illustrated in Figure 4-18. The size of the vertical strips is determined by the distance from the screen and the amount of horizontal diffusing. In Figure 4-17, the strip for left and right eye have a width of 20 mm approximately.

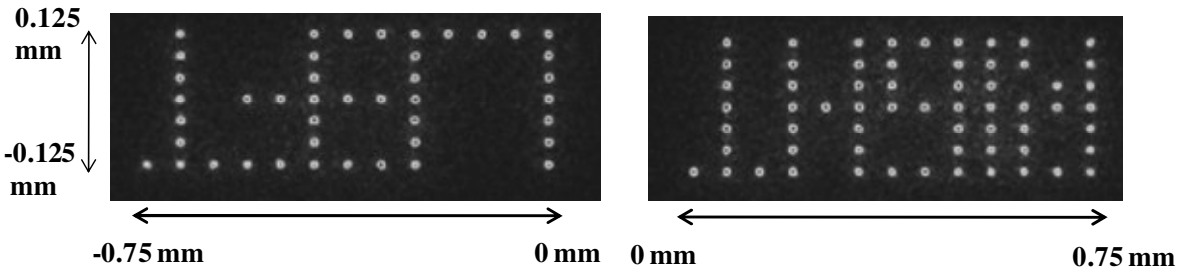

Figure 4-19 Inverted "LEFT" and "RIGHT" at the left eye and right eye retina of the viewer

The vertical strips representing "LEFT" and "RIGHT" at the left eye and right eye position of the viewer respectively are imaged to the left and right eye retina of the viewer as illustrated in Figure 4-20.

4.5 Experimental Demonstrations

A 1D LED array integrated FR4 scanner module is fabricated using standard PCB technology on FR4 substrate. The scanner has a rectangle frame with 13 mm X 13.5 mm area and flexures with 3.95 mm length, 1.85 mm width as mentioned in Section 3.2. The thickness of the scanner is 200 μm. It has 10 LEDs mounted on it as a 1D array with 1.137 mm distance between two adjacent ones. Different color LEDs are received from OSRAM and have a size of 220 x 220 x 170 μm. The bottom and the side surfaces of the LEDs are the anode and the cathode is a circular area of 70 μm diameter at the center of the top surface. The LEDs are emitting from around the cathode region at the top surface.

There is a common anode line on the polymer scanner in the middle and LEDs are mounted on it from their bottom surface by conducting epoxy. As seen in Figure 4-20, the cathode contacts of the LEDs are wire bonded to separate cathode connections on the scanner. The LEDs are controlled independently by changing the voltage level at these cathode connections. The voltage level of all the cathode connections are controlled by the output pins of the FPGA via the driving circuitry as shown in Figure 4-20. The voltage level of the common anode connection is controlled by the external DC voltage source. The cathode and anode connections are carried to the LEDs through the flexures of the scanner.

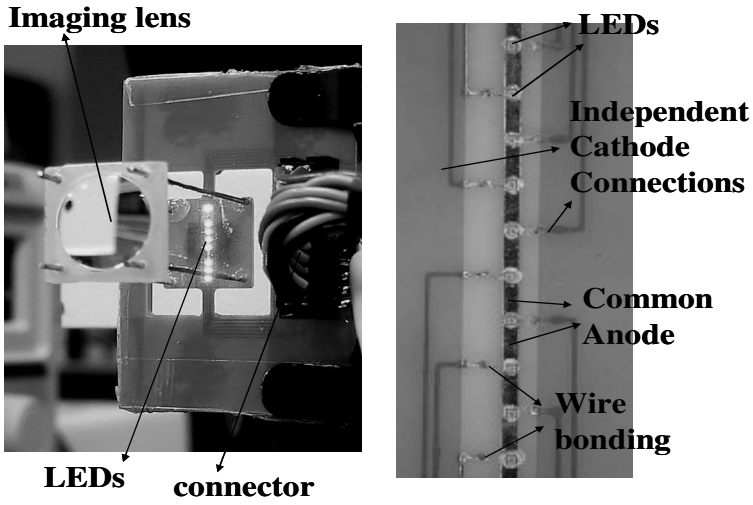

Figure 4-20 1D LED Array integrated FR4 module

4.5.1 Determination of Object/Image Plane Locations the Thorlabs Lens

A Plano-convex lens made from BK7 with 12.7 mm diameter and 30 mm effective focal length (0.486 μm – 29.576 mm, 0.588 μm – 29.896 mm, 0.656 μm – 30.040 mm) is used as the imaging lens as shown Figure 4-20. The lens thickness is 3.16 mm. As the LED

sizes are 220 µm, the pixel edge sizes on the display are approximately 1.8 mm. The only optimization parameters for the system design are object plane and image plane positions. As the lens diameter is 12.7 mm, the distances between adjacent modules (d_m) are assumed to be 13.5 mm which corresponds to a total distance of 280 mm between object plane – scanners and image plane – diffuser screen resulting in 2.75º angular resolution (R_A). In order to decrease R_A, d_m and as a result lens diameter should be decreased in horizontal direction. As a possibility, the lens can be cut in vertical direction from its edges to decrease its size in horizontal direction. The features of the lens and optimized object and image distances can be seen in Figure 4-21

	Surf:Type	Comment	Radius	Thickness		Glass		Semi-Diameter	
OBJ	Standard		Infinity	0.000000				5.175000	
1	Standard		Infinity	30.044113	V			5.175000	
STO*	Standard	LA1289	Infinity	3.160000		BK7		6.350000	U
3*	Standard		-15.450000	0.000000				6.350000	U
4	Coordinate B..			0.000000		-		0.000000	
5	Standard		Infinity	249.847308	V			5.699085	
IMA	Standard		Infinity	-				120.000000	U

Figure 4-21 The single imaging lens of the first prototype

During the optimizations, the same three configurations – 25º, 12.5º and 0º scan angles and three wavelengths (486 nm, 588 nm, 656 nm) are used. Five field points are used that are placed with 1.150 mm distance between each other starting from 0.575 mm and ending at 5.175 mm on the x-axis. As the lens diameter is relatively large and has f/# of 2.35, the aberrations are much higher than the ideal case lens. In Figure 4-22, the spot diagrams for the five field points at three different wavelengths and three different configurations can be seen.

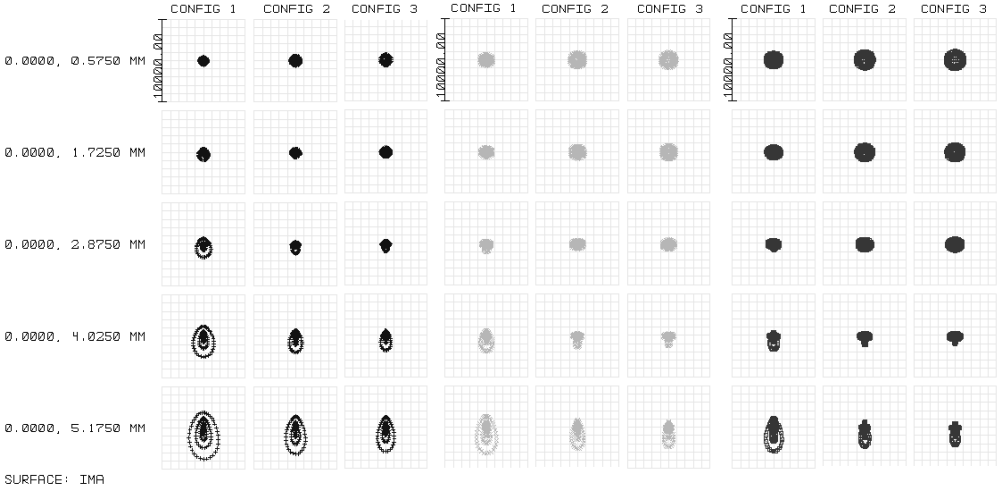

Figure 4-22 The Spot Diagrams of 5 different field points at each primary wavelength and scan angle

	RMS Radius of Field Points at Different Scan Angles								
Field Position	**486 nm**			**588 nm**			**656 nm**		
	0 º	-12.5 º	-25 º	-0 º	-12.5 º	-25 º	-0 º	-12.5 º	-25 º
0.575 mm	477.86	430.79	372.46	777.07	721.16	550.03	923.28	869.81	696.88
1.725 mm	422.71	392.20	420.41	689.57	635.61	485.54	830.70	777.18	611.12
2.875 mm	410.30	430.25	606.97	550.91	511.92	460.63	669.34	622.11	506.63
4.025 mm	619.80	691.75	977.83	515.44	532.65	681.21	547.96	539.38	600.87
5.175 mm	1062.7	1164.8	1527.3	806.91	881.33	1161.9	727.79	785.43	1026.1

Table 4.5-1 RMS Spot Radius for 5 different field points, three different wavelengths and three different scan angles

The RMS radiuses of the spot diagrams are changing between 400 µm to 1500 µm as shown in Table 4.5-1. The smallest and largest RMS spot radiuses are both for -25º scan angle at 486 nm wavelength for the field point at 0.575 mm and 5.175 mm respectively.

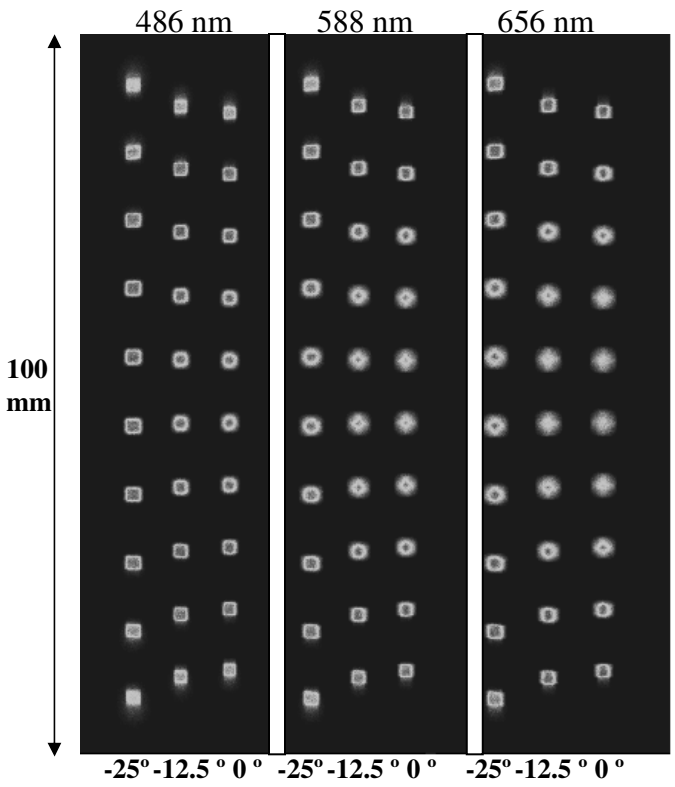

Figure 4-23 The Screen Pixels for each wavelength at 0 º, 12.5 º and 25 º scan angles

The geometric image analysis for different scan angles at different wavelengths can be seen in Figure 4-23. Here and in the ideal lens design, the most important problem is the different magnifications for different scan angles.

4.5.2 Experimental Results

The scanner is actuated electromagnetically by fixing a permanent magnet to the back surface of the scanner and forcing it with an external electro coil, illustrated in Figure 4-24, driven with a sinusoidal wave.

1D LED array integrated polymer scanner with permanent magnet has a resonant frequency of 70 Hz which is consistent with the FEM analysis. The inertial load of the

glass lens with long pins reduces the resonant frequency to 12.7 Hz. Achieving the desired 60Hz loaded resonant frequency is not difficult with plastic optics and shorter focal lengths and changing the scanner flexure dimensions. The scanning system behavior is linear and has a mechanical quality factor of 20, which makes it relatively easy to control even with open-loop driver. The total optical scan angle (TOSA) of the scanner, which corresponds to the FOV (field of view) of the display, is desired to be 40º or larger. With the current design, 40 TOSA, i.e., 300 mm scanline at 425 mm distance, is achieved only by dissipating about 100mW at the coil with a suboptimal magnetic design.

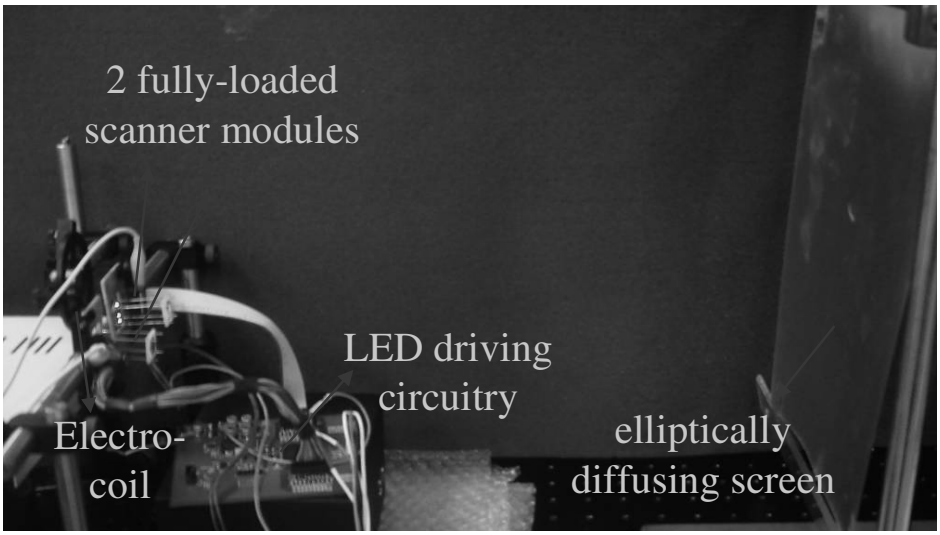

Figure 4-24 The total display setup consisting of the scanner module driven by LED driving circuitry and elliptical diffusing screen

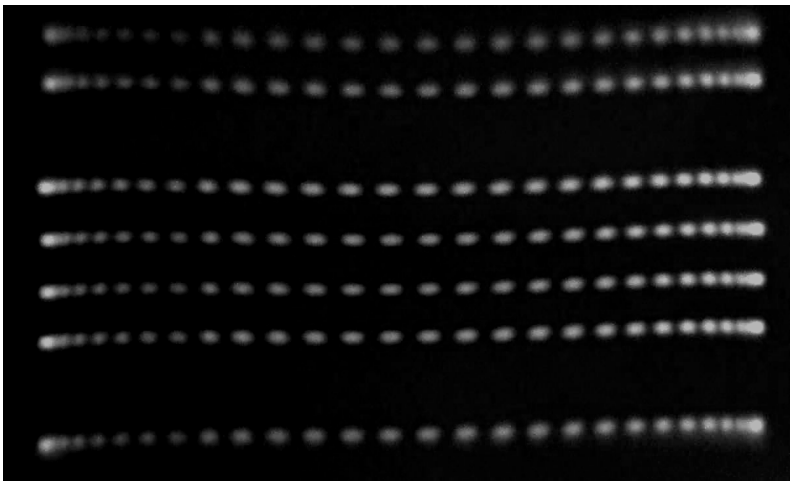

Figure 4-25 25 separate LED images are obtained on the horizontal scan line of 7 different LEDs

Figure 4-25 illustrates scanning and LED modulation concepts. In the experiment, the LEDs are modulated at 732 Hz with %50 duty cycles and the scanner is actuated at its loaded resonant frequency of 12.7 Hz. One can see 25 separate LED images on the horizontal scan line and turning on only 7 different vertical LEDs. The horizontal lines appear bended due to poor mounting of the elliptical diffusing screen during the experiment. The scanning module design is capable of addressing 10 vertical lines and 150 horizontal pixels per module for a 40^0 FOV display system. The number of horizontal pixels addressed by the module will increase by using smaller LEDs.

The 3D display concept is proven by using 3 scanner modules placed side by side and single LED from each module. The display setup that is used in the experiments is shown in Figure 4-24. One of the LEDs is always turned on and emits light to the left eye of the viewer. The other two LEDs are directed to the viewer's right eye and are in reverse states. When one of the LEDs is turned on the other one is turned off. The viewer integrates the two LED images coming to his/her left and right eye and focuses in a different depth than

the depth of elliptically diffusing screen. The perceived depth changes by switching ON different LEDs. The viewer's eyes indeed perceive a light source at different depths.

Chapter 5 CONCLUSIONS

In this research, a novel scanning LED array based 3D display that can be categorized in quasi-holographic type displays is introduced and conceptually designed. The display offers a possibility of eliminating accommodation-vergence rivalry and providing smoother motion parallax. The basic module of the display concept with 10 independently controllable LEDs is designed and fabricated together with an external LED driving circuitry. The display concept is proven successfully by using 3 of these modules and showing the viewer different points at different depth levels. System level simulations and module level optimizations are realized to explore the concept more in detail.

A unique feature of the system is the integration of LEDs with PCB electronics and magnetic actuation directly on the scan modules. The display has 1D LED array mounted FR4 scanners scanning in torsion mode as the main building block. The scan modules are easy and low-cost to fabricate using the standard PCB fabrication techniques. Using LEDs is quite advantageous as they are available at various pitch sizes, colors and have high light efficiency. Even though LEDs are turned on only while traversing a screen pixel, high brightness can be achieved by overdriving LEDs with a short current pulse. The display is easily scalable for different vertical and horizontal resolutions by integrating FR4 scan modules in vertical and horizontal direction respectively in a way similar building LEGO™ blocks. The brightness calculations showed that the display can provide enough brightness levels (200 nits) similar to conventional display technologies such as LCD Displays.

Future work will focus on building more complex systems including many modules for more sophisticated demonstrators. The modules will be reduced in size using small LEDs and decreasing the distance between two adjacent LEDs. New modules will be produced

with LED drivers on for more compact units and for driving more LEDs on the same scanner. More experimental results are needed to verify the important performance advantages offered by the quasi-holographic displays.

Appendix A Scanning LED Array Based 3D Display (Submitted to J. of Display Technology)

Murat Sayinta, Hakan Urey, *Member IEEE*
Koç University, Electrical Engineering, Optical Microsystems Laboratory, Istanbul, Turkey
E-mail: hurey@ku.edu.t

Abstract—A new three dimensional (3D) display technology using scanning Light Emitting Diode (LED) array modules is developed. The method is based on creating multiple light emission directions from each screen pixel using scanning LED modules behind a screen. The system architecture is scalable and provides a possibility of solving or relieving the accommodation-vergence rivalry particularly when multiple views are provided to each eye pupil. LEDs are mounted on a torsional scanner made using standard PCB technology, allowing the integration of photonics, mechanics, and electronics on the same platform. Operation principles of the system, LED drivers, and the proof of principle experimental results are presented.

Index Terms—3D Displays, electromagnetic actuation, polymer scanners, LED arrays, LED drivers

1. INTRODUCTION

3D displays seem to be the next step in the evolution of displays from monochrome to color and high definition displays. With the rapid developments in the digital video processing and visualizing technologies, first commercial 3D display products are already available in the market. 3D displays can be classified as holographic displays, volumetric displays and auto-stereoscopic displays [1].

The display system proposed in this article can be classified as a quasi-holographic type display. This type of display is capable of providing sufficient multi views that single eye perceives at least two different parallax views. This region is called the super-multiview region (SMV). It is claimed that in the SMV region the accommodation-vergence problem can be solved and smoother motion parallax is provided [2], [3], [4] which are the two major problems associated with auto-stereoscopic displays [1], [5]. There are a few examples of quasi-holographic displays that use micro display array and collimated light source [6], [7], a laser or array of laser diodes and 2D scanners [3], [4]. The basic concept is similar to a two dimensional (2D) display where pixels can emit light with different color and intensity to different directions [3], [4], [6], [7]. One example of the quasi-holographic displays realizes the basic concept by 1D array of 2D micro displays placed in horizontal direction behind the screen that are illuminated by collimated light [6], [7]. The modulated light through each micro display is focused to a point light source that is emitting different color and intensity light to different directions as much as the number of pixels on the micro display. Each generated point light source provides a specific emission direction for each pixel on the part of the screen that they are illuminating. By the help of a holographic screen, the modulated light beams are asymmetrically diffused to the viewing zone [6], [7].

The system proposed in this article is similar to the above quasi-holographic concept and the unique feature of the system is replacing the light sources illuminating the 2D micro displays, collimating optics and 2D micro displays with 1D independently modulatable vertical LED arrays mounted on polymer scanners. Individual modules appear as rotating horizontal lines of light emanating from the LED light sources, providing different emission angles. The use of the LEDs is a key advantage as they are widely available in different colors at low-cost and

modulatable at several MHz rates. Furthermore, scanning platform is fabricated directly on the printed circuit board (PCB) using the technology developed in our group [8].

The paper is organized as follows: The 3D display concept and the scanning LED module as a building block are introduced in Section 2. The LED driving circuitry and driving principles of LEDs are discussed in Section 3. Scanner module prototypes and the proof-of-concept experimental results are discussed in Section 4.

2. SCANNING LED ARRAY CONCEPT

A one-dimensional (1D) LED array per color and the LED driver IC integrated on a scanning module can be seen in Fig. A-1(a) which constitutes the basic functional unit of the display system. Scanner is made on FR4 substrate, a fiber-glass epoxy composite, using standard PCB technology [8]. Depending on the number of LEDs per module, the driver IC can be mounted ON or OFF the moving platform. 2D array of such modules are tiled behind a special screen for full system operation [9].

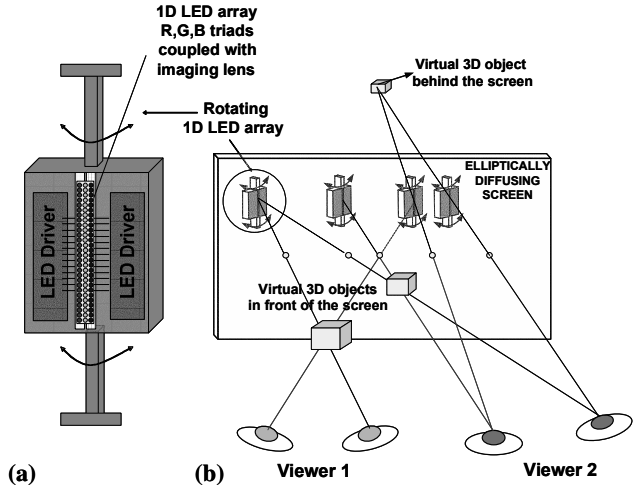

Fig. A-1 (a) 1D LED arrays in RGB colors and driver IC mounted on FR4 scanner platform; (b) Scanner modules as the basic unit of the 3D display.

Each scan module creates a horizontal scan line by way of electromagnetic actuation [10]. In order to realize the screen capable of emitting different color and intensity light to different directions from its pixels, red, green, and blue LEDs are modulated individually during scan. As R, G, B 1 D LED arrays are slightly shifted on the scan module, their images on the screen are also shifted by a few screen pixels. However, the images for each color LED can be overlapped on the screen by introducing slight time-shifts in between R, G, B LED drive signals during the scan. As an example, if we assume a spatial shift of 3 pixels in between R, G, B LEDs, while the middle color LED is fed with the information of pixel N, the other color LEDs on either side will be fed with the information of pixels N+3 and N-3.There will be also slight angular displacement between ray angles of different color LEDs illuminating the same pixel on the screen and generating the same ray angle. However, the angular displacement is small enough to ignore (~0.02º for 0.1 mm distant LEDs illuminating a screen at 250 mm distance from the LED arrays). Synchronization of modules to each other can be done but not essential. Each module should complete a full rotation within the frame time and the video data fed to each module need to be synchronized with the position of the scanner. The position feedback is obtained using the back-emf signal from the rotation of the magnet mounted on the scanner. The back-emf coil is simply machined on the FR4 scanner using standard PCB technology.

As illustrated in Fig. 1(b), each module address an array of pixels on the special screen and provide different particular ray angles for each screen pixel. Screen pixels are illuminated by a number of such scan modules with different ray angles to convert them into pixels capable of emitting different color and intensity light to different directions. The number of pixel emission directions is equal to the number of modules illuminating the pixel. Placing mirrors at the sides of the display would create virtual modules and create the missing illumination directions for the screen pixels near the edge of the display as illustrated in Fig. A-2 [6], [7]. A virtual source point or voxel is perceived at the intersection of two properly modulated ray bundles received by the left and right eyes of a viewer. As illustrated in Fig. A-3, voxels can be rendered at different depths. Note that the viewer's focus and vergence may be in coordination and different for each voxel depth and the binocular rivalry may be

eliminated by working the system in super-multi view region. Two viewers observing from two different horizontal positions would see different virtual source positions and perceive different 3D images [6], [7], and [9].

The screen is capable of diffusing light into a narrow angle in the horizontal direction and into a wide angle in the vertical direction – i.e., elliptically diffusing screen. A narrow angle is required in the horizontal direction as each pixel on the screen should emit light with different color and intensity to separate horizontal directions without any crosstalk between neighboring directions. The wide angle in the vertical direction is required as the display is designed to provide motion parallax only in the horizontal direction (i.e., the same image is received by the viewer at the same horizontal position and different vertical positions of the eye pupils.

The number of different views for the display is the same with the number of independently controllable horizontal emission directions from the screen pixels. Actually the number of screen pixels in horizontal and vertical direction gives the resolution of each view the viewer will perceive. As an example, there are 40 different views using 1º divergence for each emission direction and 40º scan angle. When mirrors are assumed on the sides of the display as Fig. A-2, the resolution of the display – the resolution of each view can be calculated using the following relationship:

$$N_H = \frac{n_h \times p}{r} \quad (1)$$

$$N_V = n_v \times l \quad (2)$$

N_H , N_v: number of screen pixels in the horizontal and vertical directions,
n_h, n_v: number of scanner modules in the horizontal and vertical directions,
p: number of horizontal screen pixels addressed by each scanning module
r: number of different ray directions through each screen pixel
l: number of LED color triads on a line in each scanner module

In Fig. A-2, n_h=4, p=6, and r=3, resulting in N_H=8 using Eq. 1. It should be mentioned that equation 1 should be treated together with the subsequent equations to result in a reliable display system.

Number of voxels-perceived-by-a-single-eye is equal to the number of screen pixels. However, unlike FPDs, the voxels are not perceived on the screen, they would appear to come from a virtual source point when combined with the view of the other eye. The total number of voxels (N_T) is defined as a product of voxels-perceived-by-a-single-eye and the number of views:

$$N_T = N_h N_v r \quad (3a)$$

Equivalently, N_T can also be calculated by the product of total number of LEDs and p using the total number of screen pixels and ray directions:

$$N_T = n_h n_v l p \quad (3b)$$

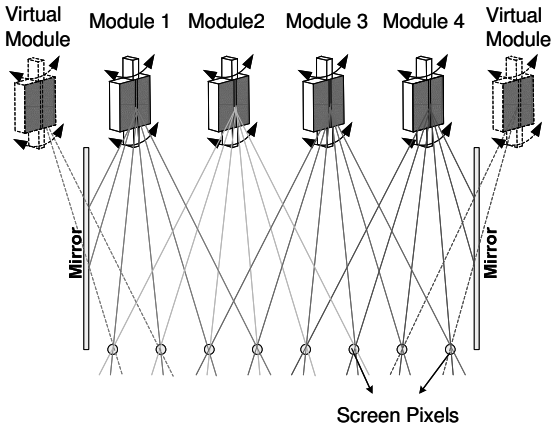

Fig. A-2 Placing mirrors at the sides of the display would create virtual modules generating the missing illumination directions for the side pixels.

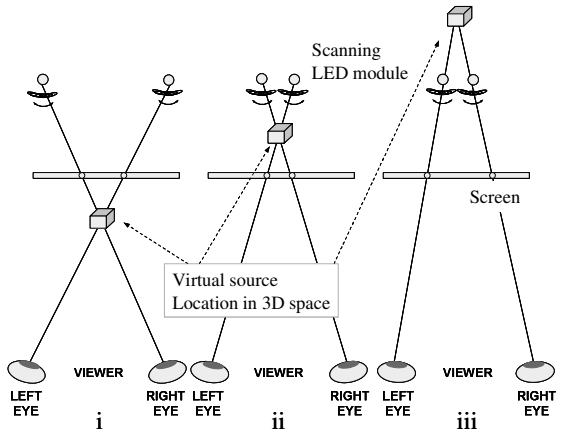

Fig. A-3 Voxels rendered (i) in front of the screen, (ii) between the screen and the LED modules, (iii) behind the LED modules.

Table 2 provides an exemplary system design parameters for 2 million and 20 million voxels with different display depths. The table implies that the resolution of the system can be increased by increasing the number of scan modules without altering the scan module design or the screen depth, resulting in a scalable architecture. Another implication of the table is that the screen depth can be reduced by reducing p and increasing n_h.

Voxels	$2x10^6$	$2x10^6$	$20x10^6$	$20x10^6$
N_H	240	240	720	720
N_v	160	160	576	576
n_h	80	48	240	144
n_v	5	5	18	18
p	150	250	150	250
l	32	32	32	32
r	50	50	50	50
FOV	50	50	50	50
Display Thickness	160 mm	268 mm	160 mm	268 mm

Table 2 Exemplary system design parameters for 2 Million and 20 Million voxels in 3D space for two different system sizes.

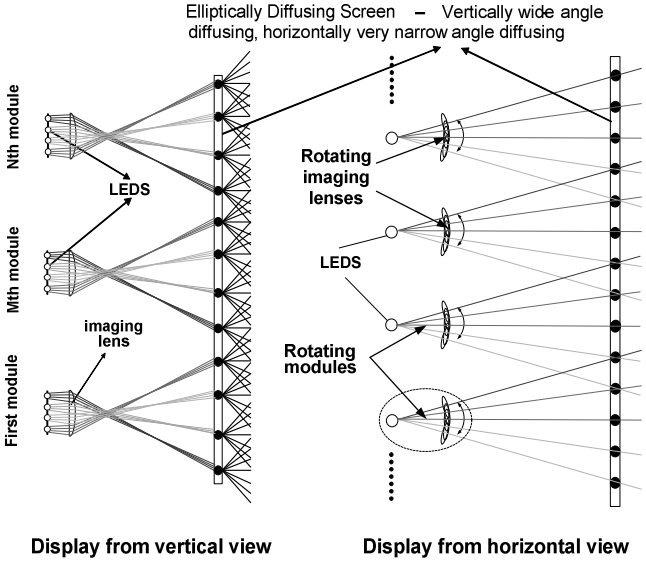

Fig. A-4 The optical behavior of the system in vertical and horizontal directions.

The optics for the system is rather simple and illustrated in Fig. A-4. Each scan module has a lens that rotates together with the module and provides imaging of LEDs onto the screen with some magnification. The focal length of the lenses and the distance of the lenses to the LEDs are determined by the distance of the screen to the scanners and the emission area of the LEDs. The vertical cross section of the display shows an array of 1D LED arrays and the horizontal cross section shows an array of single LEDs. Each LED on a module provides illumination to a fraction of one row of the screen in a light efficient manner by turning the LED ON only while traversing a screen pixel. The vertical resolution is increased by tiling modules in the vertical axis and number of ray angles from each screen pixel is increased by tiling modules in the horizontal axis.

3. LED DRIVING CIRCUITRY

An external LED driving 4-layer PCB circuitry with a Field Programmable Gate Array (FPGA) is designed for driving the LEDs on each module as can be seen in Fig. A-5.

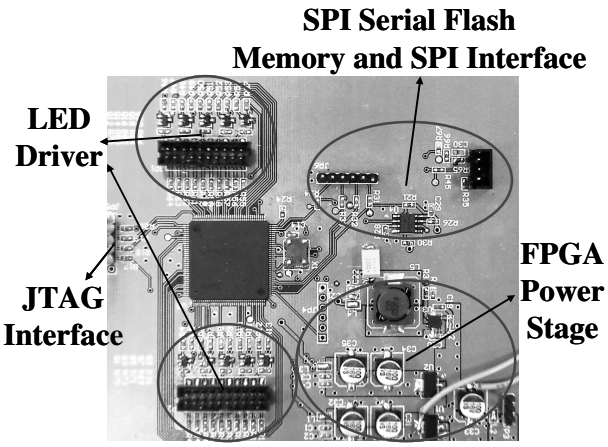

Fig. A-5 LED driving circuitry with Spartan 3E FPGA

The FPGA on the external circuitry is XC3S100E device from Xilinx Spartan-3E FPGA family having 108 pins available as user I/Os. The PCB circuitry can be divided into three parts. The first part is the FPGA power stage. This part takes 5 volt as input voltage and regulates it with 3 different regulators to V_{CCO} = 3.3 V, V_{CCAUX} = 2.5 V and V_{CCINT} = 1.2 V which are supply voltages of the FPGA. The second part is the FPGA configuring stage. The circuitry provides two different methods of programming the FPGA. The first method is programming in boundary scan mode through the Joint Test Action Group (JTAG) interface and the second method is programming through serial peripheral interface (SPI) from an SPI serial flash. In this circuitry, a 4 mega-bit flash memory "25P40" is used.

The third part is the LED driver, which is outside the scan module, and is capable of driving 40 LEDs from 40 different output pins of the FPGA. Two different driving circuits illustrated in Fig. A-6 are tried for the prototypes. 20 LEDs are directly driven from the output pins through 100Ω resistors. The other 20 LEDs are driven through a general purpose NPN BJT transistor – 2N3904. The output pins of FPGA are connected to the bases of the transistors through 2.2 kΩ resistors. All LED cathodes are connected to the collectors of the transistors through 100Ω resistors while anodes are connected to a controllable DC voltage source in order to control the amount of current conducting through the LEDs. The emitter of the transistor is connected to the ground. When the output pin of the FPGA is set to zero, the transistor and the LED are off. When the FPGA is set to 3.3V, LED conducts current according to the voltage level of the controllable DC voltage source. The I/O pins of Spartan 3E family devices are capable of driving maximum 16 mA so that the above configuration prevents damage to the I/O pins of the FPGA from excessive current flow and as a result increase the current flow limitation through the LED from 16 mA to 200 mA, the maximum rating for the collector current of the transistor.

The LEDs are driven by pulse width modulation (PWM) method. N bit depth level PWM provides 2^N different intensity levels. A counter is synthesized within FPGA whose output value is compared with a reference value for each single output pin and produces PWM LED drive signal as shown in Fig. A-7. N-bit video input determines the LED drive pulse width.

The input video data frequency at which the data will be fed into the FPGA will be:

$$f_V = \frac{3l\, n\, 2p\, f_{\mathrm{D}}\, d_{PWM}}{\mathrm{d_w}} \qquad (4)$$

f_v: the frequency of the input video data
l: number of LEDs per color on a line on each scanner module
n: the number of scanners driven with the same driver
p: number of horizontal screen pixels addressed by each scanning module
f_D: display refresh rate
d_{PWM} : PWM bit depth
d_W : input video data line width

As an example, assume f_{D}=60 Hz scan frequency– typical refresh rates of displays and l=30 (or 90 LEDs per module), d_{PWM}=10-bit, n=1 (scanners controlled by each driver), p=100 pixels/LED (=200 modulations per cycle due to bidirectional scanning). In such a case, if 1 bit per color (d_W = 3) serial input video data is fed into the FPGA then 3.6 MHz clock frequency would be required. This average data rate varies by about a factor of 2 from the center to the edge of the scan line due to sinusoidal speed variation of the scanner.

There is a 4 MHz oscillator on the PCB board whose frequency can be modified by FPGA's DCM blocks for different scanner and system designs according to the above calculation.

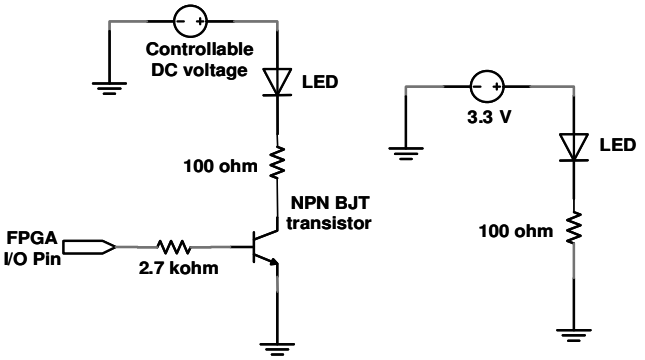

Fig. A-6. Two different configurations to drive LEDs

The other method of driving LEDs will be an LED driving IC placed directly on the backside of the scanner, which is planned to be an FPGA or a complex programmable logic device (CPLD) as illustrated in Fig. A-1(a). It is better to place an ASIC in the long run as it will be much smaller than an FPGA or CPLD and give the opportunity of designing smaller scanner modules.

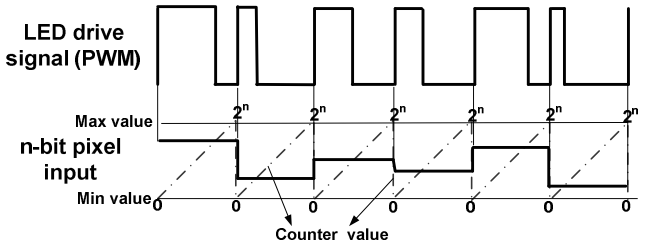

Fig. A-7 LEDs are driven with PWM by using a counter synthesized in FPGA. LED remains ON until dashed-red line reaches the n-bit pixel input level and turned OFF for the rest of the pixel time

Placing the LED driving IC on top of the scanner provides a more compact design and gives the opportunity of increasing the number of LEDs on a single FR4 scanner as fewer electrical signals should be carried through the flexures of the scanner. These signals would be limited, in the case of an FPGA, with the FPGA supply voltages V_{CCO}, V_{CCAUX} and V_{CCINT}, JTAG programming interface signals, 1 bit clock signal and 1 bit serial input data that would modulate the LEDS connected to the FPGA I/O pins. In this case, the number of the LEDs that can be driven will be limited with the number of I/O pins of the FPGA which can be quiet high; more than four hundred with an I/O optimized FPGA.

4. EXPERIMENTAL RESULTS

A 1D LED array integrated FR4 scanner module is fabricated using standard PCB technology on FR4 substrate [8]. The scanner has a rectangle frame with 13 mm X 13.5 mm area and flexures with 3.95 mm length, 1.85 mm width. The thickness of the scanner is 200 µm. It has 10 LEDs mounted on it as a 1D array with 1.137 mm distance between two adjacent ones. Different color LEDs are received from OSRAM and have a size of 220 x 220 x 170 µm. The bottom and the side surfaces of the LEDs are the anode and the cathode is a circular area of 70 µm diameter at the center of the top surface. The LEDs are emitting from around the cathode region at the top surface.

There is a common anode line on the polymer scanner in the middle and LEDs are mounted on it from their bottom surface by conducting epoxy. As seen in Fig. A-8, the cathode contacts of the LEDs are wire bonded to separate cathode connections on the scanner. The LEDs are controlled independently by changing the voltage level at these cathode connections. The voltage level of all the cathode connections are controlled by the output pins of the FPGA via the driving circuitry as shown in Fig. A-5 and Fig. A-8. The voltage level of the common anode connection is controlled by the external DC voltage source. The cathode and anode connections are carried to the LEDs through the flexures of the scanner.

As illustrated in Fig. A-8(a), a plano-convex lens is fixed on top of the scanner. The lens has a focal length of 30 mm and diameter of 12.7 mm to cover the 1D LED array that has total length of 9 x 1.137 – 10.233 mm. The lens is fixed at a distance slightly more than the focal length of the lens to image the LEDs to 400 mm distance at an elliptically diffusing screen as illustrated in Fig. A-9.

The scanner is actuated electromagnetically by fixing a permanent magnet to the back surface of the scanner and forcing it with an external electro coil, illustrated in Fig. A-9, driven with a sinusoidal wave,.

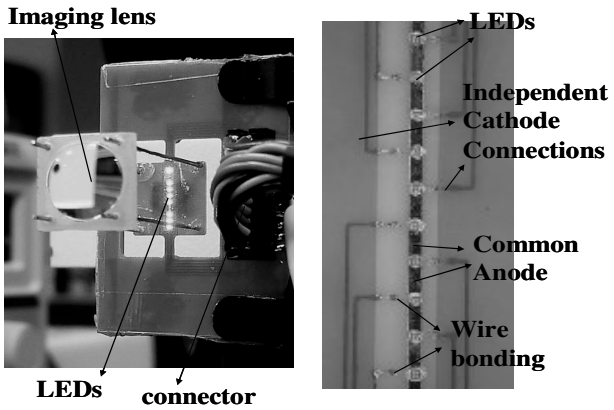

Fig. A-8 1D LED Array integrated FR4 module

1D LED array integrated polymer scanner with permanent magnet has a resonant frequency of 70 Hz. The inertial load of the glass lens with long pins reduces the resonant frequency to 12.7 Hz. Achieving the desired 60Hz loaded resonant frequency is not difficult with plastic optics and shorter focal lengths and changing the scanner flexure dimensions. The scanning system behavior is linear and has a mechanical quality factor of 20, which makes it relatively easy to control even with open-loop driver. The total optical scan angle (TOSA) of the scanner, which corresponds to the FOV (field of view) of the display, is desired to be 40º or larger.

With the current design, 40 TOSA, i.e., 300 mm scanline at 425 mm distance, is achieved only by dissipating about 100mW at the coil with a suboptimal magnetic design.

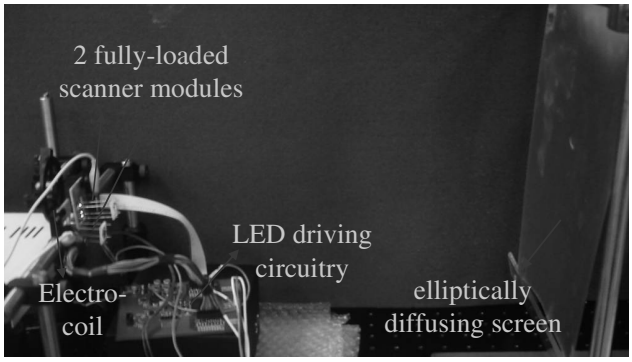

Fig. A-9 The total display setup consisting of the scanner module driven by LED driving circuitry and elliptical diffusing screen

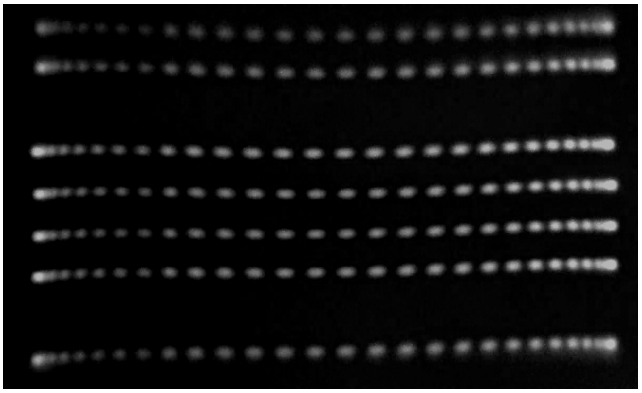

Fig. A-10 25 separate LED images are obtained on the horizontal scan line of 7 different LEDs

Fig. A-10 illustrates scanning and LED modulation concepts. In the experiment, the LEDs are modulated at 732 Hz with %50 duty cycles and the scanner is actuated at its loaded resonant frequency of 12.7 Hz. One can see 25 separate LED images on the horizontal scan line and turning on only 7 different vertical LEDs. The horizontal lines appear bended due to poor mounting of the elliptical diffusing screen during the experiment. The scanning module design is capable of addressing 10 vertical lines and 150 horizontal pixels per module for a 40^0 FOV display system. The number of horizontal pixels addressed by the module will increase by using smaller LEDs.

The 3D display concept is proven by using 3 scanner modules placed side by side and single LED from each module. The display setup that is used in the experiments is shown in Fig. A-9. One of the LEDs is always turned on and emits light to the left eye of the

viewer. The other two LEDs are directed to the viewer's right eye and are in reverse states. When one of the LEDs is turned on the other one is turned off. The viewer integrates the two LED images coming to his/her left and right eye and focuses in a different depth than the depth of elliptically diffusing screen. The perceived depth changes by switching ON different LEDs. The viewer's eyes indeed perceive a light source at different depths without accommodation-vergence rivalry.

CONCLUSIONS

A novel scanning LED based 3D display that can be categorized as quasi-holographic is introduced. It offers a possibility of eliminating accommodation-vergence rivalry and providing smoother motion parallax. More experimental results are needed to verify the important performance advantages offered by the quasi- holographic displays. A unique feature of the system is the integration of LEDs with PCB electronics and magnetic actuation directly on the scan modules. The display has 1D LED array mounted FR4 scanners scanning in torsional mode as the main building block. The scan modules are easy and low-cost to fabricate using the standard PCB fabrication techniques. Using LEDs is quite advantageous as they are available at various pitch sizes, colors and have high light efficiency. Even tough LEDs are turned on only while traversing a screen pixel, high brightness can be achieved by overdriving LEDs with a short current pulse. The display is easily scalable for different vertical and horizontal resolutions by integrating FR4 scan modules in vertical and horizontal direction respectively in a way similar building LEGO™ blocks.

The first 1D LED array integrated scan modules are fabricated and imaging lenses are mounted on them. They are capable of providing sufficient TOSA values for large FOV that is >40º. The display concept is proven successfully by using 3 of these modules and showing the viewer different points at different depth levels.

ACKNOWLEDGMENT

This work was supported by EC within FP6 under grant 511568 with the acronym 3DTV NoE and by the Network of Excellence in Micro-Optics (NEMO). TÜBA-GEBİP Award to H. Urey is gratefully acknowledged. We thank OSRAM for LEDs, Necmiye Genc from Vestek Electronics, Serbulent Aydinoglu and Sercan Kibar from Vestel Defense & Security for help with LED driving circuitry design and integration, and Engin Ufuk Temucin (Aselsan) for wire bonding, and Serhan Isikman for FR4 mechanical designs.

REFERENCES

[1] P. Benzie, J. Watson, P. Surman, I. Rakkolainen, K. Hopf, H. Urey, V. Sainov, C. Von Kopylow, "A survey of 3DTV Displays, Techniques and Technologies", *IEEE Transactions on Circuits and Systems for Video Technology* , vol.17, no. 11, Nov 2007

[2] J. Y. Son, B Javidi, "Methods for Displaying 3 Dimensional Images", Proceedings of the IEEE, Special Issue on: 3-D Technologies for Imaging & Display, vol. 94, no. 3, pp502-523, 2006

[3] Y. Takaki, "High-Density Directional Display for Generating Natural Three-Dimensional Images," Proc. of the IEEE, vol.94, no.3, pp.654-663, 2006.

[4]Y. Kajiki, H. Yoshikowa, T. Honda, "Auto Streoscopic 3-D Video Display Using Multiple Light Beams with Scanning", IEEE Transactions on Circuits and Systems for Video Technology, Vol. 10, No. 2, March 2000

[5] J. Y. Son, B. Javidi, "Three Dimensional Imaging Methods Based on Multiview Images", IEEE Journal of Display Technology, vol. 1, no. 1, pp. 125-140, September 2005

[6] T. Balogh, Method and Apparatus for Displaying 3D Images, US Patent Office-6,999,071, 14 February 2006

[7] T. Balogh, T. Forgacs, T. Agocs, O. Balet, E. Bouvier, F. Bettio, E. Gobbetti, G. Zanetti, "A Scalable Hardware and Software System for the Holographic Display of Interactive Graphics Applications", Eurographics 2005

[8] H. Urey, S. Holmstrom, A. D. Yalcinkaya, "Electro magnetically actuated FR4 Scanners," Phot. Tech. Lett., Vol. 20, p. 30-32, 2008

[9] M. Sayinta, H. Urey, "Scanning LED Array Based Volumetric Display", IEEE 3DTV-CON, Kos Island-Greece, 2007

[10] Serhan O. Isikman, Olgac Ergeneman, Arda D.

Yalcinkaya, Hakan Urey**,** "Modeling and Characterization of Soft Magnetic Film Actuated 2D Scanners," J. Sel. Top. Quantum Elect., Vol. 12, pp.283-289, Mar/Apr. 2007

Murat Sayinta was born in Izmir, Turkey, in 1981. He received the B.S. degree in microelectronics engineering from Sabanci University, Istanbul, Turkey in 2004. Currently, he is working toward the M.Sc degree in Koc University, Istanbul, Turkey. He is also working as a design engineer in Vestek Research and Development Company in Istanbul.

Hakan Urey received the BS degree from Middle East Technical University, Ankara, Turkey in 1992, and MS and Ph.D. degrees from Georgia Institute of Technology, Atlanta, Georgia, USA in 1996 and in 1997, all in electrical engineering. He is currently an Associate Professor of Electrical Engineering at Koç University, Istanbul, Turkey. He joined Microvision Inc.-Seattle in 1998 and he was the Principal System Engineer when he left and has been consulting for the company since 2002. He has published more than 70 journal and conference papers, 6 edited books, 2 book chapters, and has 21 issued and several pending patents. He received the Werner Von Siemens Faculty Excellence Award in 2006 and the TÜBA-GEBİP Distinguished Young Scientist Award from Turkish Academy of Sciences in 2007. His research interests are in scanning systems, micro-optics, optical MEMS, optical system design, and display and imaging systems. Dr. Urey is a member of SPIE, OSA, IEEE, and president of the IEEE-LEOS Turkey chapter.

Appendix B PCT Patent Application: “AN APPRATUS FOR DISPLAYING 3D IMAGES”

Summary of the Invention

In this invention, the above 3D visualization concept, approaching 3D displays as 2D displays that have pixels emitting different color and intensity light to different directions, is realized by using an array of scanners that images properly modulated light to the proper screen pixels on their scanning path.

In a preferred embodiment of the system, 1D array of light sources per each main color are integrated with 1D modules scanning in torsion mode together with imaging lenses. The light sources are modulated by a driving circuitry which is mounted ON or OFF the scanning platform. There is 2D array of these scanning modules behind the screen placed with a specific periodicity to a specific distance according to the resolution requirements of the display and the number of different views the display requires to provide. The precisely controlled intersections of rays coming from several scanning modules correspond to a complete set of voxels and the viewers looking from different perspectives will see different 3D images. In the system, light sources are preferably LEDs or organic LEDs and scanners are preferably made from polymer or silicon materials.

Another preferable scanning mode can be in-plane mode but in this mode the imaging lens will not be connected to the scanning platform. The module will scan behind a motionless lens and according to scanner’s relative position to the lens; the ray bundles emitted from the light sources on the scanner will be directed to different screen pixels.

In a further advantageous implementation, the light sources can be motionless and the lens is scanned in in-plane mode in front of the light sources to image them to different screen pixels.

Different actuation mechanisms such as electrostatic or electromagnetic actuation can be used for realizing the scanning. In a preferred system, electromagnetic actuation with a magnet placed on top of the scanner interacts with an external electro coil driven with alternating current. In a further preferred system, the electro coil can be printed or fabricated on to the scanner and actuation can be realized by an external magnet.

In another implementation of the system, instead of using 1D array of light sources per each main color coupled with 1D scanner, a single light source per each main color coupled with 2D scanners is used. Here the light source can be preferably laser diodes, vertical cavity surface emitting diodes (VCSELs). Scanners are preferably made from polymer or silicon materials or from both of them. The light sources can be on top of the scanners or they can be external and their light can be reflected to the screen pixels by a mirror placed on top of the 2D scanners.

In all configurations, the scanning angle of the scanners can be limited to a specific narrow angle with a specific offset if only limited numbers of viewers are viewing the display from a limited viewing angle. This embodiment of the system is quiet advantageous as it will increase the efficiency and as a result brightness of the display.

In another system, a special screen that can move left and right directions according to the position of the viewers constituted from an array of cylindrical lenses that have modulatable pitch sizes can be used together with a head tracking system to send 3D information only to the specific region where viewers are standing. This system can be preferably used with personal devices. This special screen can be used either in front of displays having light sources located at the pixel positions including liquid crystal displays

(LCD) or displays that have pixels scanned with at least one scanner coupled with at least one light source in a certain depth.

REFERENCES

[1] Wheatstone C. “On Some Remarkable, and Hitherto Unobserved, Phenomena of Binocular Vision”. Philosophical Transactions of the Royal Society of London, 1838.

[2] The Turing Institute, “The History of Stereo Photography”, 31 July 1996. http://www.arts.rpi.edu/~ruiz /stereo_history/text/historystereog.html, (10 May 2008)

[3] Swiss Federal Institute of Technology Zurich, “Lecture Notes on Stereoscopic Imaging”, http://www.lst.inf.ethz.ch/teaching/lectures/ss05/230/slides/2005/Lecture% 201.pdf, (10 May 2008)

[4] Lipton, L. Foundations of the Stereoscopic Cinema – A Study in Depth Van Nostrand

Reinhold, New York, NY, USA, 1982

[5] C. Fehn, “3DTV Broadcasting”, 3D Video Communication, John Wiles & Sons Ltd., 2001

[6] Sand R. 3-DTV – A Review of Recent and Current Developments. IEE Colloquium on Stereoscopic Television, pp. 1–4, London, UK, 1992.

[7] Holliman N., “3D Display Systems”, University of Durham, 2 February 2005.

[8] Ince S., “Correspondence Estimation and Intermediate View Reconstruction”. Technical Report No. ECE-2004-01, January, 2004.

[9] McAllister D. F., “Display Technology: Stereo & 3D Display Technologies”, North Caroline State University.

[10] Hill L., Jacobs A., “3D Liquid Crystal Displays and Their Applications”, Proceedings of IEEE, Vol. 94, No. 3, 2006

[11] Thomas E. “Depth Perception”. Psychology 159 Course, Psychology Department of University of California, San Diego.

[12] Wikipedia Foundation Inc., 23 June 2008, “Parallax”. <http://en.wikipedia.org/wiki/Parallax>, (24 June 2008)

[13] Qian N., “Binocular Disparity and Perception of Depth”, Neuron Vol. 18, 359-368, March, 1997.

[14] Benzie P., Watson J., Surman P., Rakkolainen I., Hopf K., Urey H., Sainov V., Von Kopylow C., “A survey of 3DTV Displays, Techniques and Technologies”, *IEEE Transactions on Circuits and Systems for Video Technology* , vol.17, no. 11, Nov 2007

[15] Gabor D., “Microscopy by Recorded Wavefronts”, Proceedings of the Royal Society (Lond), B, 64, 446-469, 1949

[16] Joseph W. Goodman, “Introduction to Fourier Optics”, Roberts & Company Publishers, 2005

[17] Enloe L. H., Murphy J. A., and Rubinstein C. B., “Hologram Transmission via Television,” *Bell Syst. Tech. J.*, vol. 45, no. 2, pp. 225–339, 1966

[18] Wernicke G., “Dynamic System for Recording and Optical Reconstruction of Digital Holograms”, Diffractive Optics, Warsaw, 2005

[19] Hashimoto N., Morokawa S., "Real-time electro holographic system using liquid crystal television spatial light modulators" *Journal of Electronic Imaging*, 2(2) pp 93-99, (1993).

[20] Poon T. C., "Three-dimensional television system using optical scanning holography and spatial light modulator," *J. Inf. Displ.*, vol. 3, no.12, 2002.

[21] Moore G. E., "Cramming more Components onto Integrated Circuits," *Electron.*, vol. 38, no. 8, Apr. 19, 1965.

[22] Sato, K., "Animated Color 3-D Image Using Kinoforms by Liquid Crystal Devices," *J. Inst. Telev. Eng. Jpn.*, vol. 48, pp. 1261–1266, 1994.

[23] Shimobaba, T. and Ito, T. "A color holographic reconstruction system by time division multiplexing with reference lights of laser," *Opt. Rev.*, vol. 10, pp. 339–341, 2003.

[24] Ahrenberg, L., Benzie, P., Magnor, M. and Watson, J., "Computer generated holography using parallel commodity graphics hardware," *Opt. Exp.*, vol. 14, no. 17, pp. 7636–7641, 2007.

[25] Yoshikawa H. and Tami J., "Holographic image compression by motion picture coding," in *Proc. SPIE, Practical Hologr. X*, 1996, vol. 2652.

[26] Favalora G. E., "Volumetric 3D Displays and Application Infrastructure," *IEEE Computer Society*, vol.38, pp. 37- 44, August 2005

[27] Actuality Systems, "Homepage of Actuality Systems", 13 December 2006 http://www.actuality-medical.com/indexAS.html, (24 June 2008)

[28] LightSpace Technologies Inc., "Homepage of LightSpace Technologies", 2006 http://lightspacetech.com/, (24 June 2008)

[29] Blundell B. G., Schwarz A. J., "The Classification of Volumetric Display Systems: Characteristics and Predictability of the Image Space", *IEEE Transactions on Visualization and Computer Graphics*, vol. 8, no.1, January 2002

[30] Dodgson N. A., Moore J. R., Lang S. R., "Multiview Autostreoscopic 3D Display", IBC99 (Invited Paper), 10-14 September 1999, pp 497-502

[31] I. Sexton, P. Surman, "Stereoscopic and Auto Stereoscopic Display Systems," *IEEE Signal Processing Magazine*, vol.99, pp. 85-99, May 1999

[32] J. Y. Son, B. Javidi, "Three Dimensional Imaging Methods Based on Multiview Images", *IEEE Journal of Display Technology*, vol. 1, no. 1, pp. 125-140, September 2005

[33] J. Y. Son, B Javidi, "Methods for Displaying 3 Dimensional Images", Proceedings of the IEEE, Special Issue on: 3-D Technologies for Imaging & Display, vol. 94, no. 3, pp502-523, 2006

[34] Van Berkel C., Clarke J. A., "Characterization and Optimization of 3D LCD Module Design", Proc. SPIE vol. 3012, pp. 179-187, 1997

[35] Y. Takaki, "High-Density Directional Display for Generating Natural Three-Dimensional Images," Proc. of the IEEE, vol.94, no.3, pp.654-663, 2006.

[36] Y. Kajiki, H. Yoshikowa, T. Honda, "Auto Streoscopic 3-D Video Display Using Multiple Light Beams with Scanning", IEEE Transactions on Circuits and Systems for Video Technology, Vol. 10, No. 2, March 2000

[37] Kajiki Y., "Hologram Like Video Images by 45-view Stereoscopic Display", SPIE. Vol. 3012, 0212-786, 1997

[38]T. Balogh, Method and Apparatus for Displaying 3D Images, US Patent Office-6,999,071, 14 February 2006

[39] T. Balogh, T. Forgacs, T. Agocs, O. Balet, E. Bouvier, F. Bettio, E. Gobbetti, G. Zanetti, "A Scalable Hardware and Software System for the Holographic Display of Interactive Graphics Applications", Eurographics 2005

[40] Holografika Inc., "Homepage of Holografika Inc", <http://www. holografika.com>, (21 June 2008)

[41] H. Urey, S. Holmstrom, A. D. Yalcinkaya, "Electro magnetically actuated FR4 Scanners," Phot. Tech. Lett., Vol. 20, p. 30-32, 2008

[42] M. Sayinta, H. Urey, "Scanning LED Array Based Volumetric Display", IEEE 3DTV-CON, Kos Island-Greece, 2007

[43] Serhan O. Isikman, Olgac Ergeneman, Arda D. Yalcinkaya, Hakan Urey, "Modeling and Characterization of Soft Magnetic Film Actuated 2D Scanners," J. Sel. Top. Quantum Elect., Vol. 12, pp.283-289, Mar/Apr. 2007

[44] A.D. Yalcinkaya, O. Ergeneman, H. Urey, "Polymer Magnetic Scanners for Barcode Applications", Sens. Act. A, Vol. 135, pp 236-243, 2007

[45] Wikipedia Foundation Inc., 1 July 2008, "Luminance". http://en.wikipedia.org/wiki/ Luminance, (08 July 2008)

[46] Ashdown I., "Photometry and Radiometry – A Tour Guide for Computer Graphics Enthusiasts", Tutorial, byHeart Consultants Limited, October 2002

[47] Wolfram Research Inc., 27 June 2008, "Solid Angle" http://mathworld.wolfram.com/ SolidAngle.html, 1 July 2008

[48] Jannson T., Arik E., Bennahmias M., Nathan N., Wang S., Lee K., Yu K., Poliakov E., "Performance Metrics for Integrated Lighting Systems", Defense Security, Cockpit, and Future Displays I, Proc. of SPIE Vol 62251E, (2006)

[49] Davis A., "Light Emitting Diode Source Modeling For Optical Design", Reflexite Display Optics, October 2004

[50] Rieke G. H., "Detection of Light: From the Ultraviolet to the Sub millimeter", Cambridge University Press, Second Edition

[51] Wikipedia Foundation Inc., 27 June 2008, "Solid Angle". http://en.wikipedia.org/wiki/ Solid_Angle, (20 April 2008)

[52] Zemax Development Corporation of Bellevue "ZEMAX Optical Design Program, User's Guide", July 2002

[53] Wikipedia Foundation Inc., 23 June 2008, "Box-Mueller Transform", http://en. wikipedia.org/wiki/ Box-Muller_transform, (20 April 2008)

[54] Frank L. Pedrotti, Leno M. Pedrotti, Leno S. Pedrotti, "Introduction to Optics", Pearson International Edition, 2007